The influence of heat treatments on the damping behaviour of magnesium-aluminium-zinc alloys

Dissertation

zur Erlangung des Doktorgrades

der Ingenieurwissenschaften

vorgelegt von

Msc Rodolfo González Martínez

aus Mexiko-Stadt

genehmigt von der Fakultät für Natur- und Materialwissenschaften

der Technischen Universität Clausthal,

Tag der mündlichen Prüfung

29.11.2011

Vorsitzender der Promotionskommission:	Prof. Dr. K. -H. Spitzer
Hauptberichterstatter:	Prof. Dr. rer. nat. Dr.-Ing. habil. W.Riehemann
Mitberichterstatter:	Prof. Dr.-Ing. Karl Ulrich Kainer

Abstract

Rodolfo González Martínez

The main objective of this research was to study the effects of aging treatments on the damping behaviour, hardness and microstructure of as-cast, solution treated, and extruded AZ alloys.

Magnesium alloy components for automotive industry may undergo changes in their mechanical properties as a result of natural aging. In general, during aging of magnesium-aluminium-zinc alloys, precipitation of the phase β takes place in two forms: discontinuous precipitation at grain boundaries and continuous precipitation in the matrix. The precipitation reactions are accompanied by changes in damping and hardness.

The age-hardening response of Mg-Al-Zn alloys is poor compared with many age-hardenable aluminium alloys. Therefore, new heat treatments are developed to improve the mechanical properties of the as-cast alloys in comparison to the traditional T6 heat treatment. In practice, direct aging treatments (T5) can be recommendable to replace the heat treatment (T6) in order to save the costs associated with a solution treatment step. In the other hand, one of the mechanical properties which is affected by aging treatments and that characterize magnesium alloys is damping. High damping capacity is very important for noise reduction, suppressing vibrations and enhancing the durability of components.

In order to study the effect of precipitation on the damping behaviour during isothermal aging, this investigation is divided into several sections. In the first section, damping of as-cast, solution treated and extruded magnesium-aluminium-zinc and magnesium-zinc alloys were measured. The second section relates to the obtaining of information about the influence of the direct aging on the damping of the as-cast alloy; the third section involving the effect of T6 heat treatment of AZ-series alloys on damping .Finally, the fourth section describes the effect of aging after extrusion on the damping behaviour. In this investigation, light optical and scanning electron microscopy were used to study the microstructure. Damping was measured in terms of the logarithmic decrement of freely decaying, bending beam vibrations.

The obtained results show that the aging in the temperature range of 150-300 °C leads to increase the strain-independent damping and hardness as a result of precipitation of $Mg_{17}Al_{12}$, i.e. removal of Al and Zn solute atoms from solid solution as a result of precipitation of the β-phase during aging produces an increase in the strain-independent damping.

The hardness increase is obtained by a fine dispersion of precipitates which are able to obstruct the movement of matrix dislocations. Aging treatments such as performed in the present work could thus be used to produce components with more stable microstructures and mechanical properties.

Abstract

Rodolfo González Martínez

Ziel dieser Arbeit war es, den Einfluss der Alterungswärmebehandlung auf das Dämpfungsverhalten, Härte und Mikrostruktur von AZ-Legierungen im Gusszustand, im lösungsgeglühten Zustand und im stranggepressten Zustand zu ermitteln.

Aufgrund natürlicher Alterung können sich die mechanischen Eigenschaften von Komponenten aus Magnesiumlegierungen während des Einsatzes im Automobil kontinuierlich verändern. Die Ausscheidung der β-Phase während der Alterung von Magnesium-Aluminium-Zink-Legierungen läuft dabei auf zwei Arten ab: diskontinuierliche Ausscheidung an den Korngrenzen und kontinuierliche Ausscheidung im Korn. Diese Ausscheidungsvorgänge werden von Änderungen der Dämpfungseigenschaften und der Härte begleitet.

Im Vergleich mit ausscheidungshärtbaren Aluminiumlegierungen ist die Härtbarkeit von Mg-Al-Zn-Legierungen durch eine Alterungswärmebehandlung gering. Deshalb werden neue Wärmebehandlungen entwickelt, um die mechanischen Eigenschaften von Legierungen im Gusszustand zu verbessern. In der Anwendung ist der T5 dem T6 Zustand vorzuziehen, um die hohen Kosten des für den T6 Zustand notwendigen Lösungsglühens zu vermeiden. Eine weitere Eigenschaft, die durch die Alterungsbehandlung beeinflusst wird und die Magnesiumlegierungen im Besonderen auszeichnet, ist die Dämpfung. Ein hohes Dämpfungsvermögen wirkt sich positiv auf Geräuschminimierung, Vibrationsunterdrückung und damit auf eine längere Lebensdauer von Bauteilen aus.

In dieser Arbeit wurde insbesondere der Einfluss des Auscheidungsvorgänge beim Altern auf die Dämfung untersucht. Die Untersuchungen sind in vier Abschnitte unterteilt. Im ersten Abschnitt werden die Dämpfungseigenschaften von Magnesium-Aluminium-Zink und Magnesium-Zink im Gusszustand, lösungsgeglühten Zustand und stranggepressten Zustand gemessen. Im zweiten Abschnitt wird der Einfluss der direkten Alterung nach dem Gießen (T5 Zustand) auf die Dämpfung behandelt. Der dritte Abschnitt beschäftigt sich mit der Dämpfung im lösungsgeglühten, abgeschreckten und artifiziell gealterten (T6) Zustand. Der vierte Abschnitt behandelt die Dämpfung nach der direkten Alterung (T5-Zustand) aus dem Strangpressen. In der vorliegenden Arbeit wurden Licht- und Rasterelektronenmikroskopie für die Gefügecharakterisierung eingesetzt. Die Dämpfung wurde als das logarithmische Dekrement der frei abklingenden Biegeschwingung ausgedrückt.

Die Ergebnisse zeigen, dass die Alterungsbehandlung im Temperaturbereich zwischen 150°C und 300°C zu einer Erhöhung der dehnungsunabhängigen Dämpfung und der Härte führt. Der Anstieg der Dämpfung kann durch die Ausscheidung von $Mg_{17}Al_{12}$ und die entsprechende Verringerung von gelösten Al und Zn Atomen aus dem Mischkristall erklärt werden.

Der Härteanstieg wird durch die vermehrt auftretenden, fein verteilten Ausscheidungen bewirkt, die die Bewegung von Versetzungen in der Matrix behindern. Dadurch können die in dieser Arbeit angewandten Wärmebehandlungen für die Herstellung von Bauteilen mit stabileren Mikrostrukturen und mechanischen Eigenschaften genutzt werden.

Acknowledgement

Firstly, I would like to thank to Prof. Dr. Ing. Karl Ulrich Kainer for giving me the opportunity to work under his group as well as guidance and supervision in my research.

I am truly grateful to my second supervisor, Prof. Dr. rer. nat. Dr.-Ing. habil. W. Riehemann for their constructive criticism and valuable advice.

I also would like to thank to my group chief Dr. rer. nat. Dietmar Letzig for his patient, support and gut mood. At the same time I would like to express my gratitude to all colleagues from my group WZW, especially to Mr Marcus René Nürnberg by his patience, help and friendship as well as his contribution in my work. I would like express my sincere respect and acknowledgment to Dr. Peter Beaven for his help during the writing and the corrections of this manuscript.

I am also grateful for financial support from the Mexican Council of Technology (CONACyT) and the German Academic Exchange Service (DAAD).

I would like to thanks to my Friends in Germany: Israel, Emma, Nico, Enrique Hoa and Rosario to make my stay in Germany very pleasant. My Friends in Mexico: Victor, Daniel, Joel, Felipe, Diego. I will not forget the help of my Professors: Dr. Victor M. López Hirata, Dr. Leticia M. Saucedo Munoz, Dr. Héctor J. Dorantes Rosales.

I would like to thanks to my family: My Fathers Javier and Graciela, my brothers Hilario and Guadalupe and my Aunt Rosario and my Uncle Eduardo for all you love and compression that they always gave me.

Especially, I would like to give my special thanks to my wife Gurutze whose patient love enabled me to complete this work. Finally, I would like to thanks to God for all the received blessings

Index

1 Introduction. 1
1.1 Aims of the work 3

2 Literature Review 4
2.1 Magnesium alloys and damping capacity. 4
2.2 Damping and internal friction. 5
2.2.1 Dislocation damping. 7
2.2.2 Thermoelastic damping. 10
2.3 Crystal structure and deformation of magnesium. 12
2.3.1 Crystal structure. 12
2.3.2 Deformation of single crystal and polycrystalline magnesium. 13
2.4 Magnesium-aluminium-zinc (AZ) alloys. 18
2.4.1 Alloying elements. 19
2.4.2 Precipitation phenomena in Mg-Al-Zn alloys. 20
2.5 Dislocation behaviour, precipitation and damping in magnesium alloys. 24

3 Experimental Procedures. 26
3.1 Materials 26
3.2 Chemical analysis. 26
3.3 Extrusion. 27
3.4 Heat treatment 28
3.5 Sample preparation for damping measurements. 29
3.6 Damping measurements. 29
3.7 Microstructure and phase characterisation 31
3.7.1 Optical microscopy (OM). 31
3.7.2 Scanning electron microscopy (SEM). 32
3.7.3 Grain size measurements. 32
3.8 Hardness testing 32

4 Results. 33
4.1 Damping in Mg-Al-Zn and binary Mg-Zn alloys 33
4.1.1 Damping and microstructure of the as-cast AZ alloys. 33

4.1.2 Damping and microstructure of the homogenised AZ alloys. 36
4.1.3 Damping and microstructure of the extruded AZ alloys. 38
4.1.4 Damping and microstructure of the homogenised Mg-Zn alloys. 40
4.1.5 Damping and microstructure of the extruded Mg-Zn alloys. 41
4.2 Direct aging of as-cast alloys. 43
4.2.1 Isochronal aging of the as-cast AZ61 Alloy. 43
4.2.2 Isothermal aging of as-cast AZ81. 47
4.3 The effect of aging after solution treatment. 52
4.3.1 Damping and hardness curves. 52
4.3.2 Microstructural development during aging. 56
4.3.3 The kinetics of precipitation in Mg-Zn-Al alloys. 60
4.4 The effect of aging after extrusion. 61
4.4.1 Damping and hardness curves. 62
4.4.2 Microstructural development during aging. 66

5 Discussion. 72
5.1 Effects of alloy composition and processing behaviour. 72
5.2 Assessment of the factors responsible for the damping behaviour. 76
5.3 Effects of aging on the damping and hardness of AZ alloys. 83
5.3.1 Aging of solution treated AZ alloys. 83
5.3.2 Aging of as-cast and extruded AZ alloys. 86
6 Conclusions. 89

7 Bibliography 92

1 Introduction

Magnesium alloys have great potential for applications in structural parts because of their low density of 1.74 g/cm^3, which is about two-thirds that of aluminium (2.7 g/cm^3) and almost about one-fifth that of steel (7.8 g/cm^3). A major objective of all car manufacturers is to reduce fuel consumption and harmful emissions; the use of magnesium alloy components in automobiles offers many weight-saving possibilities to help achieve this goal. The most commonly used magnesium alloys for structural applications in automotive engineering are based on the Mg-Al system. At the present time the most popular of these AZ commercial alloys is the casting alloy AZ91 (Mg-9 wt.% Al-1 wt.% Zn), while the AZ31 and AZ61 alloys represent a good compromise between strength, ductility, and cost [Nie01, Cel01, Pol95, Mar06].

Magnesium alloy components for automotive industry are produced by various processes, e.g. casting, extrusion, rolling and forging. These components may be exposed to moderate temperatures during service applications and thus undergo changes in their mechanical properties as a result of natural aging. Previous studies have been extensively carried out on kinetics and mechanisms of the precipitates for Mg-Al-Zn alloys during a conventional T6 (solution plus aging) heat treatment [Cel00, Nie01, Cra74, Zha03].

In general, during aging of magnesium-aluminium-zinc alloys, precipitation of the phase β takes place in two forms: discontinuous precipitation at grain boundaries and continuous precipitation in the matrix and thus causing a moderate increase in strength [Cra74, Dul94, Xiu06, Cla68], however, the age-hardening response of Mg-Al-Zn alloys is poor compared with many age-hardenable aluminium alloys. Therefore, new heat treatments are developed to improve the mechanical properties of the as-cast alloys in comparison to the traditional T6 heat treatment [Qud06].

In the other hand, in order to extend the application of Mg-Al-Zn alloys, a lot of studies are realized. It is well known that alloys produced by thermomechanical processing usually have refined microstructured and superior mechanical properties compared to conventional cast magnesium alloys. However, there are only a few studies on wrought magnesium alloys and few reports [Gjö70, Hil98] about the effect of aging treatment on wrought magnesium alloys. Recently, some studies [Qud06,

He07, Yan07, Zhe07] show that extruded alloys accelerate the age-hardening response and maximum hardness of the alloys.

One of the mechanical properties that are affected by aging treatments and that characterize magnesium alloys is damping. High damping capacity is very important for reducing noise, suppressing vibrations and enhancing the durability of components. Some examples of these components are the steering wheels, car-bodies, disc brakes, floors, roofs and doors or door-beams in automobiles or gyrocompasses, engine covers and turbine blades in rockets, missiles, jet planes and space vehicles [Bai00]. In all these components a high damping capacity is required for better performance and for the longest possible lifetimes of the vehicles.

In general, damping capacity of alloys is closely tied to the presence of defects including solute atoms, second phases and voids. The interaction between moving dislocations and point defects is one of the major internal friction mechanisms of magnesium alloys [Sug75], so the precipitates influence the damping capacity and contributes to damping properties. Pure magnesium has a very high damping capacity at room temperature due to the easy movement of dislocation [Rie98]. However, the increase of solute atoms, impurities and precipitates like Al, Ca and Zn restricting dislocation mobility generally lead to reductions in the damping capacity of magnesium alloys [Gök05, Wan08].

In the other hand, a good combination of the mechanical properties and of the damping capacity could be achieved if, after precipitation, the solid solution exhibits a low concentration of solute elements interacting weakly with the dislocations. It has been reported that precipitation exhibits various effects on the damping behaviour of magnesium alloys but the correlation between internal friction and precipitation is still not completely understood [Lam01, Gök02a, Lam04, Lam05, Zha05].

1.1 Aims of the work

In order to use magnesium alloys as structural material, it is necessary to establish the effect of alloying elements as well as of thermomechanical processing and heat treatments. All these variables affect the damping behaviour. Therefore, the objective of this work is to investigate the effect of precipitation on the damping capacity of AZ31, AZ61 and AZ81 alloys in as-cast, homogenised and extruded states exposed to different aging treatments. The changes on the microstructure and hardness after aging treatments of each state are also investigated.

According to the above mentioned objective, the work plan of this thesis is structured as follows:

a) examination of the effects of alloy composition and microstructure on the damping behaviour in the initial processes (as-cast, homogenised and extruded states).
b) investigation of the effects of various aging treatments on the mechanical properties of AZ-series alloys
c) determination of the influence of the as-cast microstructure on the subsequent isothermal aging behaviour
d) examination of the effects of heat treatment (T6) of AZ-series alloys on the damping behaviour
e) investigation of the effects of aging of the extruded Mg-Al-Zn alloys

The results of this work can be used to optimize the heat treatments and produce components with more stable microstructures. Moreover, a better understanding of the effect of aging on the damping behaviour is achieved.

2 Literature Review

2.1 Magnesium alloys and damping capacity

With suitable alloying the mechanical properties of magnesium can be improved without compromising its density advantage. Commercial alloys of magnesium exist for both casting and wrought applications, but currently most alloys are for casting. The casting alloys belong almost exclusively to the Mg-Al series; principally AZ91 (Mg-Al-Zn) and AM60 or AM50 (Mg-Al-Mn) [Mor01]. Other common cast alloys include the Mg-Al-Si (AS) and Mg-RE (rare-earths, AE) series. Mg-Al alloys find commercial applications as a result of their reasonable mechanical properties and excellent castability. Widely used wrought alloys include AZ31 and AZ61 and, for high temperature applications, the ZK alloys (Mg-Zn-Zr) [Kam00].

The damping of a material is defined as its capacity to dissipate energy during mechanical vibration under cyclic loading [Zha94]. From an engineering point of view there is a need for alloys with high damping capacity and good mechanical properties for use in vibration-resistant structures. Some of the fields of application where a high damping capacity is relevant are listed in Table 2.1 [Bai00].

Table 2.1 Uses of high damping capacity alloys [Bai00].

Field	Examples
Automobiles	Car-body, disc brakes, rotating parts of engines, transmission, air-cleaner, cylinder-head cover, timing-gear cover, floor, dash-panel, roof, door or door-beam, etc.
Electronic products	Air-conditioner, washing machines, audio speaker, springs, refrigerators, etc.
Engineering and construction	Rock drills for a bridge, expansion joints, steel reinforcing and steel frames for a skyscrapers, etc.
Flight and space vehicles	Gyrocompass, engine covers and turbine blades for rockets, missiles, jet planes, etc.
Machinery	Press, chain-guide or gear for chain-conveyer, generator, air-blower, compressor, etc.
Office automation	Typewriter, punch, etc.
Railroad	Rails, crossing rails, railroad bridge, soundproof wall, structural materials for subway, etc.
Ship	Rotating parts of engines, screw, etc.

Material damping can be caused by various mechanisms (magnetic, thermal or atomic [Nas85]). In magnesium and its alloys, damping is believed to be mainly due to the movement of dislocations and their interactions with impurity or solute atoms. [Lia05, Rie94], see section 2.2. Although pure magnesium and certain magnesium-based alloys show the highest damping capacities among the class of metallic materials, this is not generally true for all magnesium alloys as pointed out by Riehemann [Rie94]. The diagram shown in Fig. 2.1 provides an overview of the room temperature damping properties of various classes of materials as a function of their elastic moduli. Within the category denoted engineering alloys it is noteworthy that the loss coefficients of magnesium alloys extend from ~10^{-4} to ~10^{-1}, which in engineering terms covers the entire range from high to low damping capacity applications. The loos coefficient η is a common measurement of damping and can be interchangeable for the case of small damping capacities, see Eq. 2.2.

2.2 Damping and internal friction

Damping studies have become increasingly significant in three general areas: (a) materials science, (b) structural mechanics and (c) inspection methods. Damping measurements can also be used to detect fatigue damage [Gök04a, Gök04b, Mie06, Rie10].

The logarithmic decrement δ is a common measure of obtaining the damping of the free vibrations of a system. The method is based on the following equation

$$\delta = \frac{1}{n} \ln\left(\frac{A_i}{A_{i+n}}\right) \qquad 2.1$$

where A_i and A_{i+n} are the amplitudes of the i-th cycle and (i + n)-th cycle, respectively, separated by n periods of the free vibrations of the specimen (see Fig. 2.2) [Ota94, Jam68, Gra92].

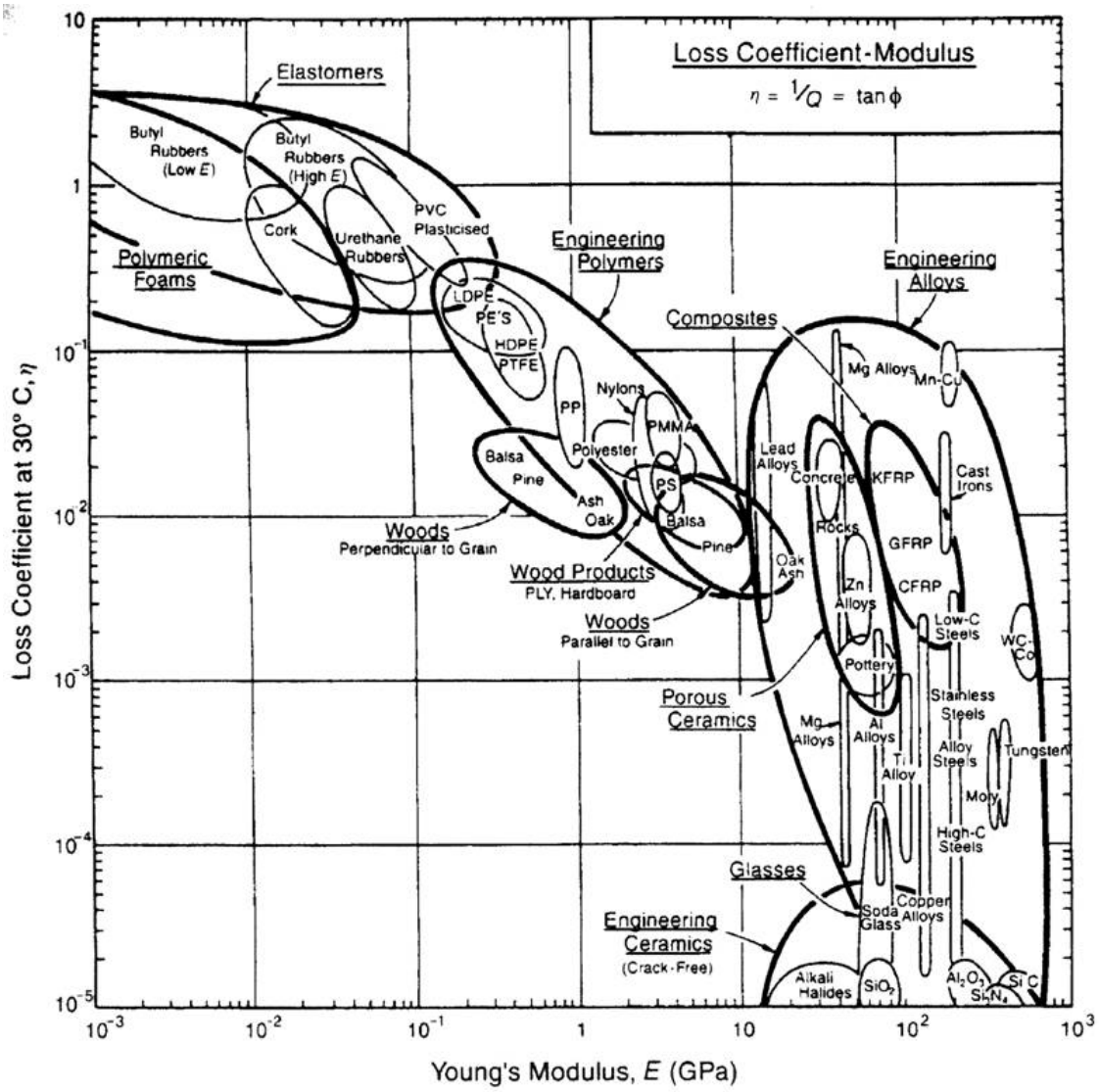

Fig. 2.1: Loss coefficients of various classes of materials as a function of Young's modulus [Ash99]

For the case of relatively small damping capacities ($\tan\phi$ << 1), the damping quantities η, Q^{-1}, δ and W measured by different methods are interchangeable and are related by the following equation [Gra92]:

$$\eta = \tan\varphi = Q^{-1} = \frac{\delta}{\pi} = \frac{\psi}{2\pi} \qquad 2.2$$

where Q^{-1} is the quality factor, η the loss coefficient, δ the logarithmic decrement, ϕ the loss angle and ψ the specific damping capacity.

In the area of materials science, internal friction measurements have been utilised to characterise the sub-micro, micro, and macrostructure of crystalline materials [Laz68]. In general, the behaviour is extremely sensitive to the presence of point defects, phase transformations, precipitation and changes in dislocation density.

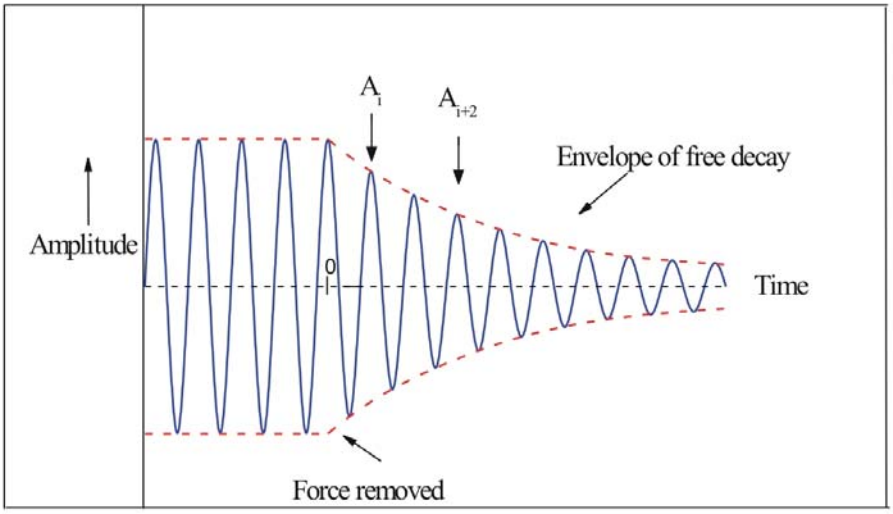

Fig. 2.2: Amplitude decay during free vibration.

2.2.1 Dislocation damping

A theory capable of describing that part of the internal friction and modulus changes in metals caused by the motion of dislocations was proposed by Koehler [Koe52]. It is assumed that the dislocation structure consists of strongly pinned segments of length L along which weak pinning points e.g. foreign atoms are randomly distributed with a mean separation of l (with l << L). Dislocation segments between such pinning points can vibrate under the influence of an applied external stress and the damping is characterised as the mechanical energy loss arising from dislocation motion. The value of the strain-independent logarithmic decrement δ_0 at low frequencies is given by[Gra56]:

$$\delta_0 = \frac{\pi\omega B_d}{36Gb^2}\rho l^4 \qquad 2.3$$

where ω is the angular frequency of the applied stress, B_d the damping force per unit length of dislocation per unit velocity, G the shear modulus, b the Burgers vector and ρ the mean dislocation density. For a given material and constant test conditions, δ_0 is therefore proportional to the product of the dislocation density ρ and the fourth power of the distance l between weak pinning points (e.g. impurity atoms, clusters of atoms) on dislocations:

$$\delta_0 \propto \rho l^4 \qquad 2.4$$

This theory was developed further by Granato and Lücke. According to their work, the logarithmic decrement δ can be expressed as [Gra56]:

$$\delta(\varepsilon) = \delta_0 + \delta_h(\varepsilon) \qquad 2.5$$

where δ_0 represents the amplitude-independent (or only weakly dependent on the maximum strain amplitude) component found at low strain amplitudes. As the strain amplitude increases beyond a critical value ε_{cr}, dislocations are able to break away from the weak pinning points and the damping behaviour is characterised by the amplitude-dependent component δ_h [Gra56]. The component δ_h depends on the strain amplitude ε and generally increases with increasing strain amplitude. In this regime the results of the measurements are generally referred to as damping capacities.

The physical basis of the Granato-Lücke analysis is the vibrating string model in which dislocation motion is restricted by the two kinds of pinning points depicted in Fig. 2.3. It is assumed that the dislocation is anchored at strong pinning points, A and B, where L is the distance between such anchoring points.

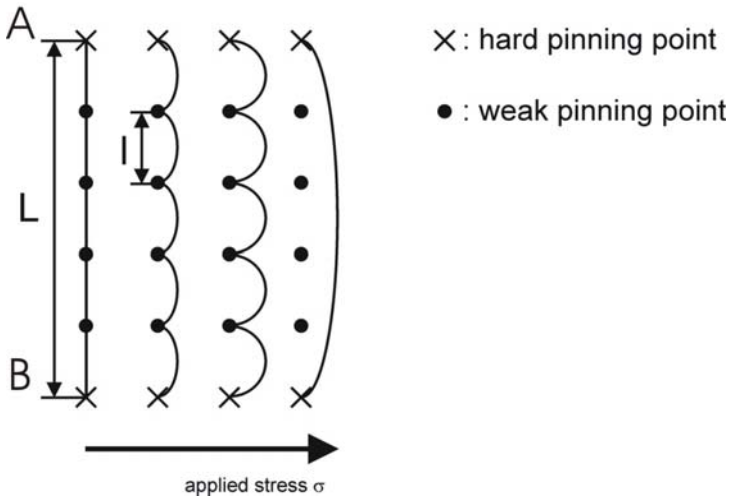

Fig. 2.3: Dislocation string model illustrating the bowing out and breakaway of dislocations with increasing applied stress σ from [Gra56].

For low stresses the dislocation can bow out between the weak pinning points, the distance between which is l. When the force acting on the dislocation becomes larger than the binding force F_B exerted by the weak pinning points, the dislocation will break free from these pinning points and bows out between the strong pinning points. This leads to an instantaneous increase in dislocation strain and the logarithmic decrement becomes dependent on strain amplitude. On reduction of the stress, the dislocation line will become re-pinned and on reversal of the stress, the same sequence will occur and as a result the stress-strain relation will exhibit a hysteresis loop, which is independent of the frequency of the applied stress.

Taking account of the distribution both in the distance between the weak pinning points, l, and that between the strong pinning points, L, Granato and Lücke showed that the amplitude-dependent dislocation damping can be written as [Gra56]:

$$\delta_h = (C_1/\varepsilon)\exp(-C_2/\varepsilon) \qquad 2.6$$

with

$$C_1 = (\rho F_B L^3)/(6bEl^2) \text{ and } C_2 = F_B/(bEl) \qquad 2.7$$

where ρ is the dislocation density, L and l the dislocation loop lengths, F_B the binding force between a dislocation and a weak pinner, b the magnitude of the Burgers vector, E the Young's modulus and ε the strain amplitude. If equation 2.6 is plotted as $\ln(\delta\varepsilon)$ vs $1/\varepsilon$ one may estimate the constants C_1 and C_2 from which information

on the concentrations of weak and strong pinning points can be obtained. The intercept and slope provide values of $Ln(C_1)$ and C_2 respectively as shown in Fig. 2.4.

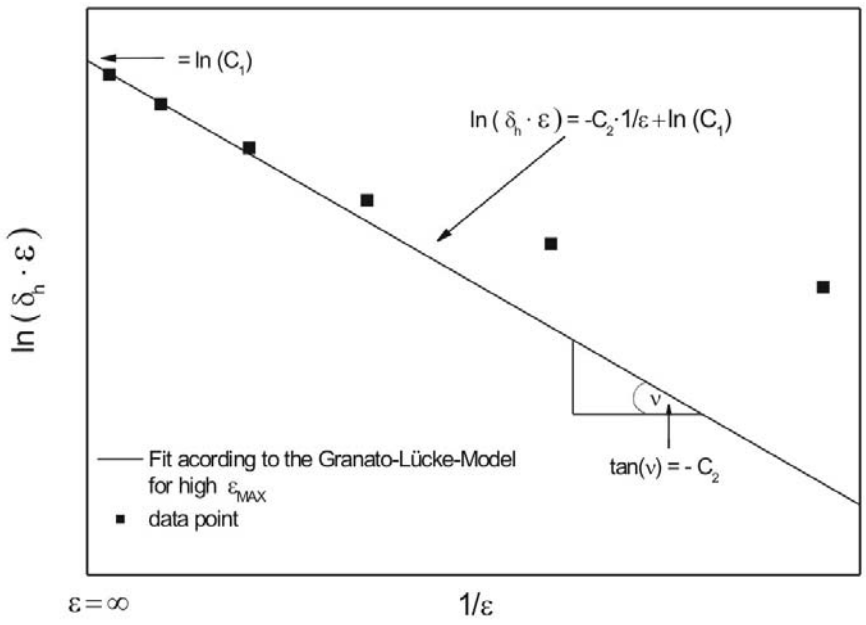

Fig. 2.4: Granato-Lücke plot for calculation of the constants C_1 and C_2 (Eqn. 2.6, 2.7).

2.2.2 Thermoelastic damping

Thermoelastic damping is a source of intrinsic material damping which results from the coupling between the elastic field in the structure caused by deformation and the temperature field. In any vibrating structure, the strain field causes a change in the internal energy such that compressed regions become warmer and extended regions become cooler. As shown by Zener's classical work on thermoelastic damping [Zen38], flexural vibrations in beams cause alternating tensile and compressive strains to build up on opposite sides of the neutral axis of the beam leading to a thermal imbalance. Irreversible heat flow which is driven by the temperature gradient causes vibrational energy to be dissipated giving rise to internal friction.

Damping due to the thermo-elastic effect has a maximum when the time of stress reversal is equal to the time necessary for heat flow from the compressed to the extended regions of the sample. It is therefore dependent on the frequency and sample thickness, i.e. is dependent on the chosen experimental parameters for the measurements.

The magnitude of the thermoelastic damping δ_{th} depends on the physical properties of the material: Young's Modulus (E), the coefficient of linear thermal expansion (α), the specific heat/unit volume (C_σ), the absolute temperature T and the thermal conductivity (κ). The maximum thermoelastic damping is given by:

$$\delta_{max}^{th} = \frac{\pi \alpha^2 T E}{2 C_\sigma} \tag{2.8}$$

Since the light metals have relatively high coefficients of thermal expansion, thermoelastic effects are strong and have to be taken into account in investigations of internal friction in these materials. Although the values of E, α and C_σ of magnesium are not dramatically altered by the alloying elements Al and Zn, the maximum thermo-elastic damping is slightly higher in the AZ alloys compared to unalloyed magnesium, mainly as a consequence of the slightly higher thermal expansion coefficients.

The frequency dependence of the damping due to transversal heat flow in a bending beam of thickness 'a' can be described by a Debye peak[Now72, Rie94]:

$$\delta_{th}(f) = \delta_{max}^{th} \frac{2 f / f_0}{(f / f_0)^2 + 1} \tag{2.9}$$

in which the frequency f_0 at which the thermoelastic damping has its maximum is given by:

$$f_0 = \frac{\pi D_t}{2a^2} \tag{2.10}$$

and the thermal diffusivity D_t is determined by the quotient of the thermal conductivity, κ, and the specific heat per unit volume, C_v:

$$D_t = \frac{\kappa}{C_v} \tag{2.11}$$

The thermal conductivity of magnesium is a physical property which is influenced by the presence of alloying elements in solid solution. For example, κ is strongly reduced by Al in solid solution but less so by Zn. It should be noted that the literature data for the effects of alloying elements on the thermal conductivity of magnesium alloys are generally ancient, sparse and often inconsistent. Some of the inconsistencies in the data appear to be related to the processing history and

microstructure of the alloys investigated and this suggests that decreases in the matrix concentration of Al during aging lead to an increased thermal conductivity.

2.3 Crystal structure and deformation of magnesium

2.3.1 Crystal structure

Magnesium has a close packed hexagonal crystal structure with lattice parameters of a = 0.3203 nm and c = 0.52 nm. The axial ratio (c/a) of magnesium is 1.623, which is close to the ideal value of 1.633. The important crystallographic planes and directions are illustrated in Fig. 2.5 using the four index Miller-Bravais system.

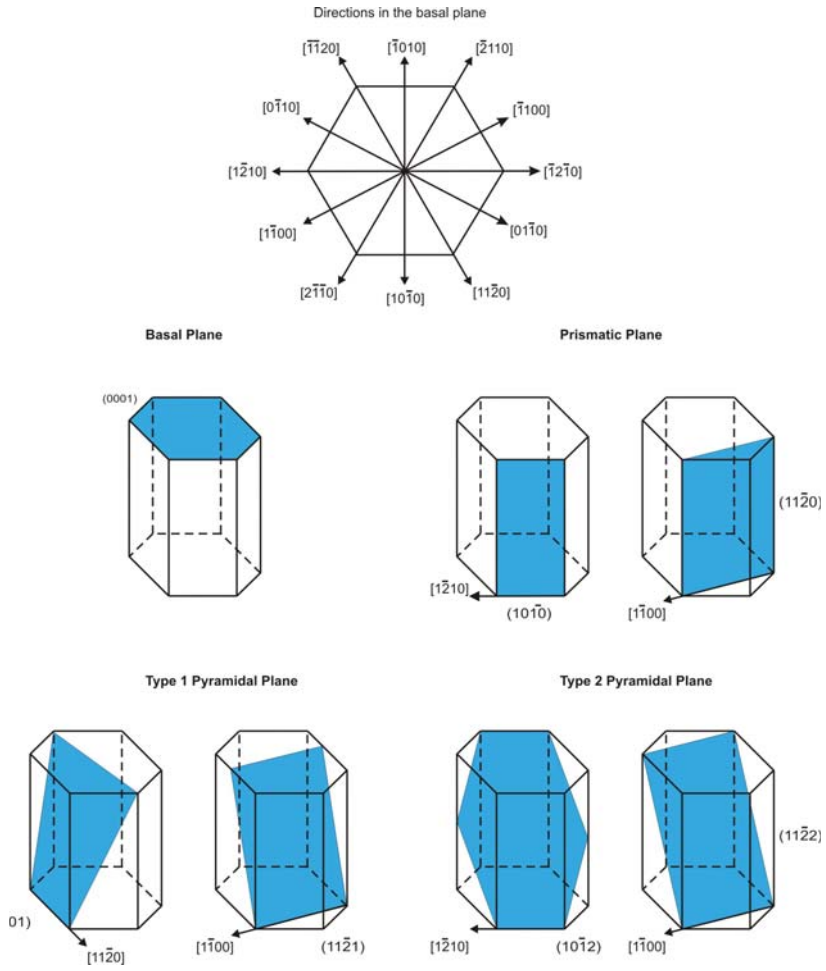

Fig. 2.5: The important slip planes and directions in magnesium, taken from [Eml66].

Most investigations on the deformation behaviour of magnesium were carried out over three decades ago; consequently, considerable gaps in the knowledge exist. For example, more recent studies on polycrystalline magnesium and its alloys have almost exclusively been performed on extruded or rolled materials resulting in possible preferred orientation effects, making the interpretation of some data difficult.

2.3.2 Deformation of single crystal and polycrystalline magnesium

The slip systems of the hexagonal metals are shown in Table 2.2. Plastic deformation in magnesium and its alloys involves the basal $\{0001\}\ <11\bar{2}0>$, prismatic $\{10\bar{1}0\}\ <11\bar{2}0>$ and pyramidal $\{10\bar{1}1\}\ <11\bar{2}0>$ slip systems and pyramidal twinning $\{10\bar{1}2\}\ <10\bar{1}1>$.

Table 2.2: The slip systems in close packed hexagonal metals [Bow02].

Slip system	Burgers vector type	Slip direction	Slip plane	No. of slip systems total	No. of slip systems independent
1	a	$<11\bar{2}0>$	Basal $\{0001\}$	3	2
2	a	$<11\bar{2}0>$	Prismatic $\{10\bar{1}0\}$	3	2
3	a	$<11\bar{2}0>$	Pyramidal $\{10\bar{1}1\}$	6	4
4	c+a	$<11\bar{2}3>$	Pyramidal $\{11\bar{2}2\}$	6	5
5	c	$<0001>$	Prismatic $\{10\bar{1}0\}$	3	2
6	c	$<0001>$	Prismatic $\{11\bar{2}0\}$	3	2

At room temperature, plastic deformation occurs predominantly by basal slip and pyramidal twinning [Eml66, Agn05]. The prevalence of pyramidal slip $\{10\bar{1}1\}\ <11\bar{2}0>$, increases as the temperature increases. In highly stressed regions, pyramidal and prismatic slip have been reported to occur at room temperature in both single crystals and polycrystals (for example, at grain boundaries in polycrystals).

In a polycrystal, it is generally accepted that five independent slip systems are required for homogenous strain with no volume change (von Mises criterion). It is often argued that if fewer than five systems are active, slip in one grain cannot be accommodated at the boundary by slip in the adjacent grain. In magnesium at room temperature, basal slip is dominant, with two of the three combinations being

independent. When both the {0001} and $\{10\bar{1}0\}$ slip systems are activated, there are four independent slip systems, fewer than the number required by the von Mises criterion. Pyramidal slip on $\{10\bar{1}1\}$ is equivalent to the basal and prismatic systems together and so does not increase the number of independent slip systems. Despite lacking the required number of slip systems, magnesium exhibits moderate room temperature ductility, with fracture strains in the range 5-10 %. It has been suggested that five independent slip systems may not be required [Yoo81, Koc67], and that localised high levels of stress (for example, at grain boundaries) may be relieved by grain boundary shearing [Hau56a] and localised prismatic and pyramidal slip [Bur52, Hil57, Hau56b]. These mechanisms, together with twinning account for the observed ductility [Par67, Koc67].

For the basal, prismatic and pyramidal slip (systems 1, 2 and 3 in Table 2.2) there is no slip direction parallel to the c-axis. Deformation in the c-direction in Mg-Al alloys can occur by $\{10\bar{1}2\}$ $<10\bar{1}1>$ twinning or <c+a> slip. While twinning can allow c-axis deformation, the strain is relatively small, but the twinned region may be re-oriented to allow basal slip [Won67, Kel68]. There are only a few instances where <c+a> slip has been observed in magnesium [Sto72, Ton02]. If <c+a> slip occurs, this alone would provide five independent slip systems (see Table 2.2), thus satisfying the von Mises criterion. Obara et al. [Oba73] observed <c+a> slip in magnesium crystals oriented for c-axis compression tested at temperatures between 20 ºC and 500 ºC. Similarly, Stohr and Poirier [Sto72] observed $\{11\bar{2}2\}$ $<11\bar{2}3>$ slip between -196 ºC and 177 ºC, and Tonda and Ando [Ton02] also observed $\{11\bar{2}2\}$ $<11\bar{2}3>$ slip between -196ºC and 20ºC. Morozumi et al. [Mor76] observed <c+a> slip in tensile deformation of magnesium, but only in, and around $\{10\bar{1}2\}$ twins. In contrast to these observations, Wonsiewicz and Backofen [Won67] and Kelley and Hosford [Kel68] performed c-axis compression tests but only observed $\{10\bar{1}1\}$ twins. The $\{10\bar{1}1\}$ twins subsequently re-twinned on $\{10\bar{1}2\}$ and the re-twinned regions then underwent basal slip accommodating the c-axis deformation; <c+a> slip was not observed. The prevalence of <c+a> slip and the effect of solute additions on the critical resolved shear stress for the Mg-Al system is unclear at this time.

In magnesium alloys, $\{10\bar{1}2\}$ twinning is readily observed, and occurs with a shear strain of 0.065 [Koc67]. In compression, twinning occurs when the stress is parallel to the basal plane and, in tension, when it is parallel to the c-axis. Re-twinning of $\{10\bar{1}1\}$ followed by $\{10\bar{1}2\}$ and of $\{10\bar{1}3\}$ followed by $\{10\bar{1}2\}$ has been reported in magnesium [Won67, Kell68]. De-twinning may also take place if the stress is applied in the reverse sense or, as a result of residual stress [Hau55, Woo55]. As the grain size is decreased, the applied stress required to nucleate a twin increases and as such, twinning occurs more readily in larger grain size materials [Mey99].

The critical resolved shear stress for either prismatic or pyramidal slip is approximately 100 times larger than that for basal slip, indicating that even in grains unfavourably oriented for basal slip, basal slip may still occur, and indeed this is observed [Kell68]. The dramatic effect of crystal orientation on the stress-strain curves can be seen in Figure 2.6. Crystals oriented with the basal plane nearly parallel to the tensile axis exhibit much higher work hardening rates than crystals oriented for easy basal slip. The large difference between single crystal and polycrystalline behaviour can also be seen. The polycrystal exhibits a substantially higher yield stress and limited ductility. The high work hardening rate is a result of the limited number of slip systems.

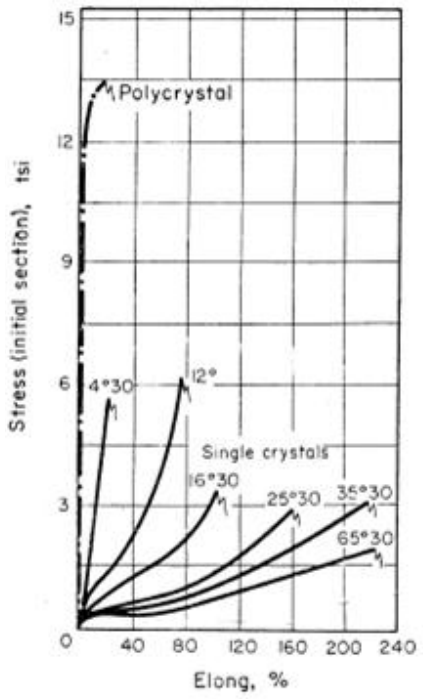

Fig. 2.6: Work hardening curves for differently oriented single crystals compared to a polycrystalline sample. The direction of the basal plane relative to the tensile axis is indicated, [Bec40].To convert; 1 tsi = 15.4 MPa.

The influence of solute atoms on the critical resolved shear stress is an important consideration in magnesium alloys. Both aluminium and zinc act as solid solution strengtheners, with zinc as a more potent strengthener than aluminium [Các01, Các02]. Most analysis of solid solution strengthening in magnesium alloys has, to date, been confined to low solute contents, less than 2 wt. % [Lev59, Akh72, Akh69, Akh68, Luk92].

Models of solid solution strengthening predict an increase in stress with a c^n relationship, where c is the solute content in atom fraction and n is either 1/2 [Fle64] or 2/3 [Lab70]. Akhtar and Teghtsoonian [Akh72] proposed that a $c^{2/3}$ relationship is more appropriate in Mg-Al alloys.

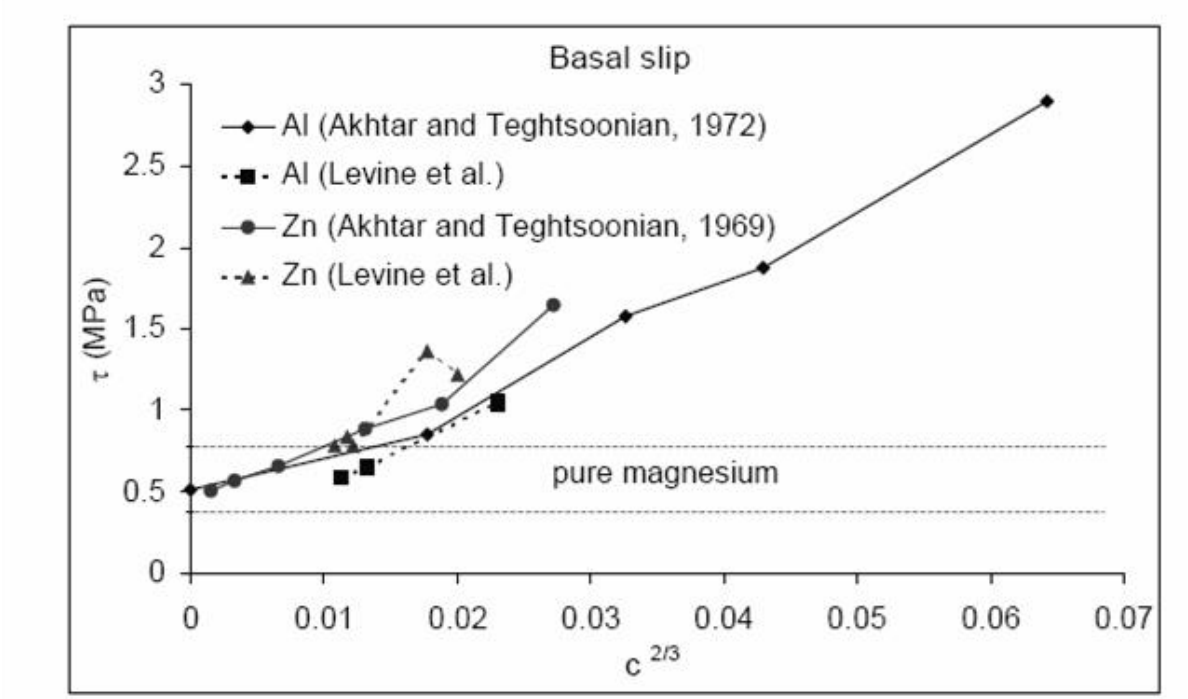

Fig. 2.7: The critical resolved shear stress (τ) for basal slip $\{0001\}\langle 11\bar{2}0\rangle$ as a function of $c^{2/3}$ (c is the solute atom fraction), with solute additions of aluminium (Al) and zinc (Zn) [Bow02] The dashed lines indicate the range of critical resolved shear stress values for basal slip in pure magnesium.

Solute additions of either aluminium or zinc result in an increase in the critical resolved shear stress for basal slip (Fig. 2.7), but both solutes appear to decrease the critical resolved shear stress for prismatic slip at concentrations greater than 0.09 at. %Al and 0.006 at. %Zn (Fig. 2.8).

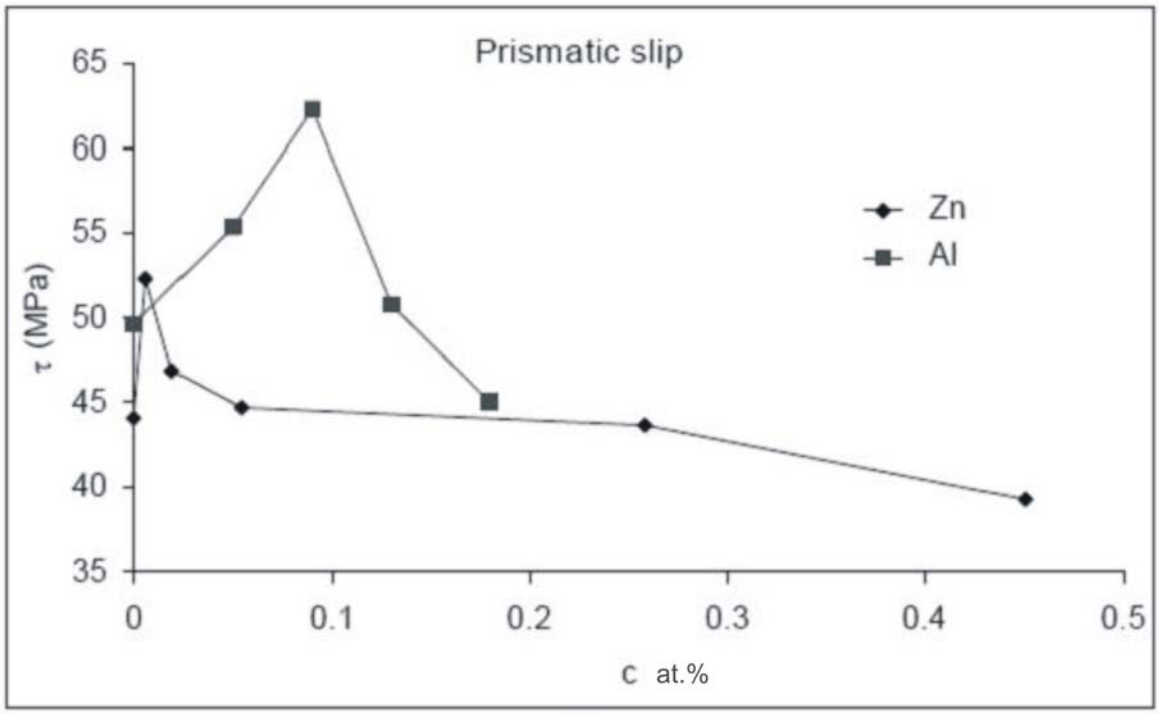

Fig. 2.8: The critical resolved shear stress for prismatic slip $\{10\bar{1}0\}<1\bar{2}10>$ as a function of c with solute additions of aluminium (Al) and zinc (Zn) at 300 K. [Bow02]

The effects of aluminium and zinc on the critical resolved shear stress for prismatic slip have only been confirmed up to concentrations of 1.2 wt. %Zn [Các02] and 0.2 wt. %Al [Các02]. Extrapolating the data in Fig. 2.8 for aluminium would indicate that the critical resolved shear stress for prismatic slip at a solute content of 9 wt. % Al is zero, which is unlikely.

As noted by Akhtar and Teghtsoonian [Akh69] zinc has no effect on the axial ratio of magnesium and aluminium increases the axial ratio [Bus50] so that the influence of these elements on the critical resolved shear stress for prismatic slip has been attributed to a decrease in the Peierls-Nabarro force, which is a general solid solution softening effect not necessarily related to the axial ratio [Akh69]. The limited data on the effect of higher aluminium solute levels on the critical resolved shear stress for prismatic slip makes it impossible to estimate the effect of commercial solute levels (6-9 wt. % Al).

More recently, Cáceres and Rovera [Các01] examined the effect of aluminium solute up to 8 wt. %, on the yield stress of polycrystalline magnesium. They reported an increase of approximately 4 MPa/at. % Al in the yield stress; this is in reasonable

agreement with Akhtar and Teghtsoonian [Akh68] who found an increase of approximately 6.2 MPa/at. % Al in the yield stress of polycrystalline specimens.

Cáceres and Blake [Các02] also examined the solid solution strengthening effect of zinc up to 6.5 wt. % Zn in polycrystalline samples. Mg-Zn alloys containing up to 1.9 wt. % Zn follow a $c^{2/3}$ relationship. Mg-Zn alloys containing greater than 1.9 wt. % Zn exhibit a much higher hardening rate and it was suggested that it is likely that short range ordering occurs in Mg-Zn alloys and the yield stress follows a $[c(1-c)]^2$ relationship.

2.4 Magnesium-aluminium-zinc (AZ) alloys

The AZ-series is an important group of magnesium alloys which can be strengthened by precipitation hardening [Nie03, Cel00]. The principal alloying elements Al, Zn and Mn are added in different amounts to obtain optimum mechanical properties. Natural aging occurs at room temperature. Artificial aging takes place through controlled heating in a furnace, referred to as precipitation heat treatment. The precipitation process in these alloys appears to involve solely the formation of the equilibrium phase β ($Mg_{17}Al_{12}$) as indicated in Fig. 2.9.

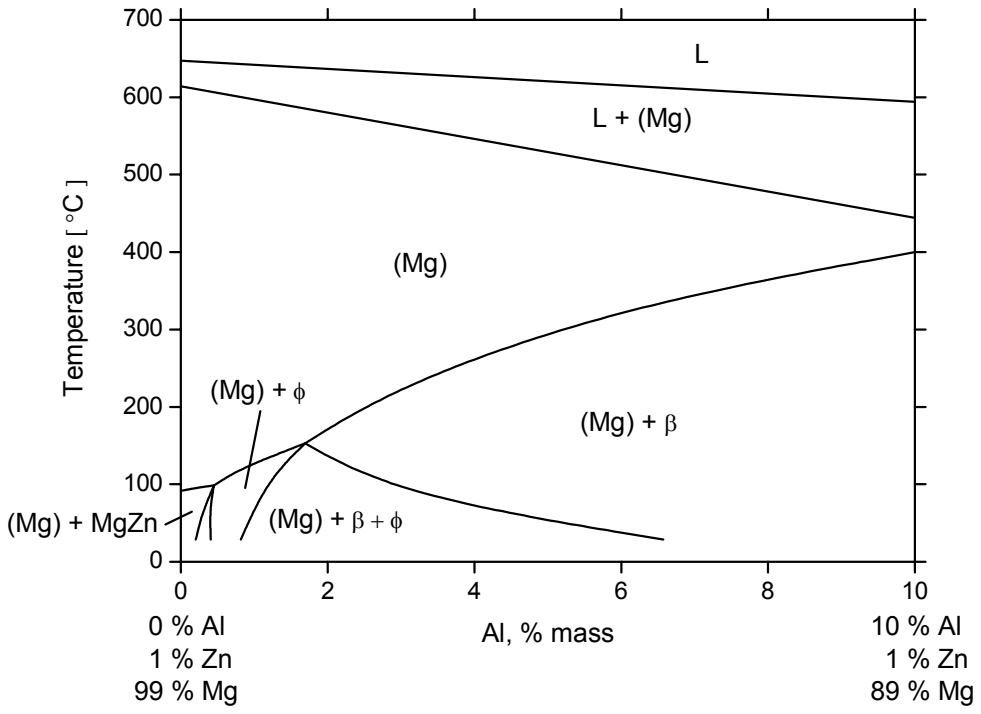

Fig. 2.9: Vertical section of the Mg-Al-Zn system at 1% mass Zn after [Kam00].

The β phase exists in the region 42 wt. % to 57 wt. % Al. At room temperature, $Mg_{17}Al_{12}$ has a bcc crystal structure, with an α-manganese type unit cell containing 58 atoms (34 Mg atoms and 24 Al atoms). Below 120 ºC the β phase is essentially a line compound containing 42.5 wt. % Al. The stoichiometric composition of $Mg_{17}Al_{12}$ is approximately 44 wt. % Al so the phase is always deficient in magnesium. Table 2.3 lists a number of properties of $Mg_{17}Al_{12}$.

Table 2.3: Selected properties of $Mg_{17}Al_{12}$

Yield Stress	1 GPa
Youngs Modulus	58.7 GPa
C_{11}	86.9 GPa
C_{12}	32.6 GPa
C_{44}	19.5 GPa
Shear Modulus	24 GPa
Hardness	188.2 ± 22.8 HV
Lattice parameter, a	1.0469 -1.0591 nm

2.4.1 Alloying elements

The maximum solid solubility of aluminium in magnesium is 12.7 wt. % at 437 ºC. A eutectic is formed between α (Mg) and β ($Mg_{17}Al_{12}$) at 437 ºC. Aluminium provides solid solution strengthening and at contents greater than ~2 wt. %, precipitation of the β phase occurs and further enhances hardening. While the potential for precipitation hardening is evident from the phase diagram (Figure 2.9) this potential is not realised, principally because no intermediate precipitates form prior to the equilibrium precipitate, $Mg_{17}Al_{12}$ (β). The β precipitates are also aligned on the basal planes and are therefore relatively ineffective in blocking dislocation movement as the primary slip system is basal [Cla68, Ave99]. Increasing the aluminium content leads to increases in both the yield strength (YS) and the ultimate tensile strength (UTS), while the elongation to fracture (PE) undergoes a decrease [El08].

Zinc (Zn) is the second most important alloying element in AZ alloys. The maximum solid solubility of zinc in magnesium is 6.2 wt. % at 340 ºC. In binary Mg-Zn alloys, zinc acts as both a solid solution strengthener and at contents greater than ~2 wt. % produces precipitation hardening. Zinc is a more potent solid solution strengthener

than aluminium [Các01]. Zinc is often said to be added to Mg-Al alloys to impart solid solution strengthening [Các02]. However, it is well accepted that zinc segregates heavily to the β phase; in AZ91, 3-5 wt. % Zn is found in the β phase and 0.2-1 wt. % in the matrix. Addition of zinc to AZ alloys reduces the solubility of aluminium which serves to increase the volume fraction of the β phase precipitated during aging and thus produces a moderate increase in strength [Kam00, Cel00, Ven00].

Manganese (Mn) is added to AZ alloys in small quantities (<1 wt. %) to improve the corrosion resistance. The manganese combines with iron, removing it from solution. The intermetallics that form settle to the bottom of the melt due to their higher density, almost eliminating them from castings. Nevertheless, small Mn-containing intermetallics are often observed in the microstructure of the AZ alloys, for example Al_8 (Mn, Fe) $_5$ and α-AlMnFe[Lun07]. These intermetallics have not been reported to affect the mechanical properties or the aging response of Mg-Al alloys [Kie07], presumably because they are present in the microstructure as isolated particles, and are not associated with any solute segregation. Commercial AZ alloys do not contain more that 1.5 wt. % manganese [Ave99].

2.4.2 Precipitation phenomena in Mg-Al-Zn alloys

The most important methods to improve the resistance to plastic deformation of alloys are: refinement of grain size, solid solution strengthening, precipitation hardening and cold working. Many modern high strength alloys depend on a combination of one or more of these processes [Mar68].

Precipitation processes can be expressed in reaction terms as follows:

$$\alpha' \rightarrow \alpha + \beta \tag{2.12}$$

where α´ is a metastable, supersaturated solid solution, β is a stable or metastable precipitate phase, and α is a more stable solid solution with the same crystal structure as α´, but with a composition closer to equilibrium [Por92].

A prerequisite for precipitation hardening is that the solute element in the alloy shows a significant decrease in solid solubility with decreasing temperature. This is illustrated schematically in Fig. 2.10 for a theoretical binary system of solute element B in matrix element A. Considering an alloy of composition X_1, at room temperature,

the equilibrium structure consists of the two phases, α and β. When heated to the temperature T_1, the alloy becomes single phase α' during the so called solution treatment. After sufficient time at T_1 for the alloy to become fully homogenised, the

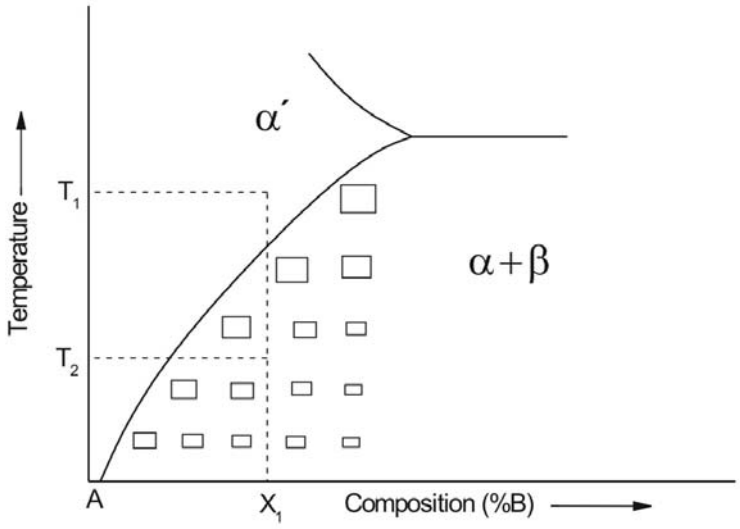

Fig. 2.10: Binary phase diagram illustrating decreasing solid solubility of solute B in solvent A with decreasing temperature and variation of precipitate size with solute content and aging temperature [Mar68].

alloy is rapidly cooled to room temperature by quenching into water or some other cooling medium. The rapid cooling suppresses the separation of the β-phase and a metastable, supersaturated solid solution is produced. This is a high-energy state and a potential driving force exists for the precipitation of the β equilibrium phase. An aging heat treatment at a temperature T_2 provides the required activation energy to enable the precipitation of the β phase. This process can occur directly, or more usually, via one or more transition phases. Each transition phase offers a reduction in the free energy of the system. The nature of the transition phases formed during the precipitation sequence is dependent on many factors such as the alloy composition, solution treatment temperature, quenching rate, aging time, aging temperature and the presence of dislocations and other defects in the alloys. The diagram (Fig. 2.10) indicates the effects of one of the main parameters on precipitation hardening, i.e. the solute supersaturation at the aging temperature. The degree of solute supersaturation controls the precipitate nucleation rate so that the fineness of the precipitate increases if the aging temperature is lowered and the precipitate size decreases with increasing solute content for a given aging temperature.

Precipitation in Mg-Al-Zn alloys is accompanied by substantial changes in the mechanical properties. These changes are due to the formation of the β-phase ($Mg_{17}Al_{12}$) as plate-shaped precipitates on the prismatic or basal planes of the matrix [Nie01, Lai08]. Precipitation occurs over a wide aging temperature range in two distinct morphologies, discontinuous precipitates at grain boundaries and continuous precipitates within the grains [Cra74, Dul94a, Xiu06, Cla68], where the continuous precipitates are responsible for age-hardening and the discontinuous precipitates are detrimental to the age hardening response of the alloys [Skl01, Svo02]. Another important advantage associated with the formation of $Mg_{17}Al_{12}$ precipitates is that the corrosion resistance increases with increasing volume fraction of the β-phase [Koi03, Son04b].

A diagram or "morphology map" showing the variation in precipitate morphology with aging temperature in binary Mg-Al alloys was proposed by Duly et al. [Dul95] (Fig. 2.11). In this diagram it can be observed that under certain conditions of solute content and temperature two regions can exist, a region where only one precipitation type is present and the other region where both types coexist.

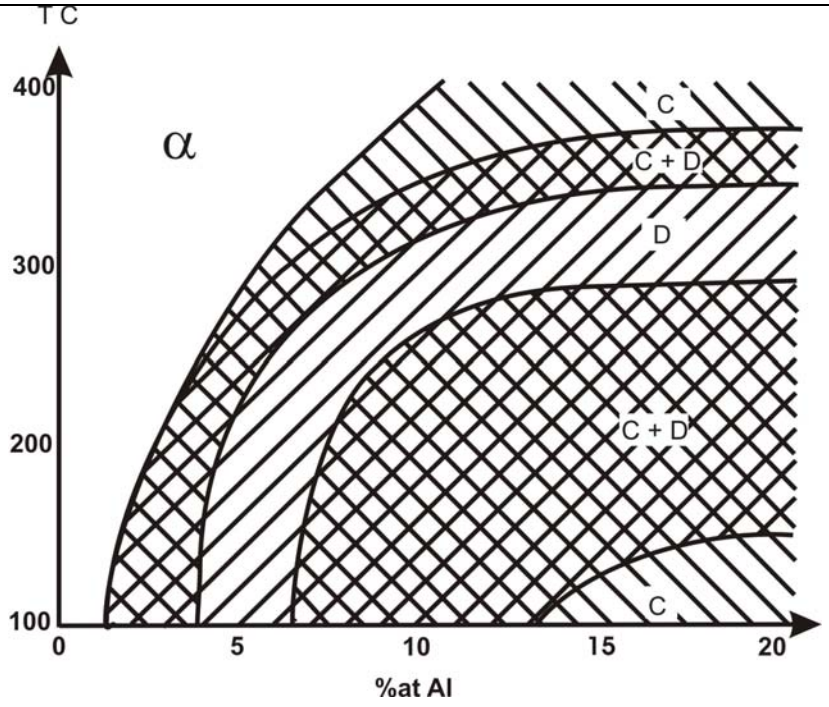

Fig. 2.11: Precipitate morphology diagram for solution treated and aged Mg-Al alloys indicating regions where continuous (C) and discontinuous (D) precipitates will form [Dul95].

Continuous precipitates of $Mg_{17}Al_{12}$ appear in three different crystallographically aligned morphologies: rods, laths or lozenges. Most of the precipitates that form in Mg-Al-Zn alloys are plates parallel to the basal plane [Cel01, Cra74, Zhe09]. These precipitates grow in size with aging time at all temperatures reaching several microns in length up to peak hardness. It is generally accepted that they provide a greater degree of strengthening than the discontinuous precipitates because they are smaller and more closely spaced. The predominant orientation relationship between the β-phase plates and the magnesium matrix is the so-called Burgers orientation relationship with $(110)_p$ // $(0001)_m$, and $[\bar{1}\bar{1}1]_p$ // $[11\bar{2}0]_m$ [Cla68, Cra74]. The major axis of the precipitates is parallel (or near) to the $[11\bar{2}0]$ direction in the matrix. There are six variants of the Burgers orientation relationship. Consequently, the microstructure consists of long laths parallel to the basal plane with a Widmanstätten morphology. Some precipitates have also been observed to lie perpendicular to the basal plane of the matrix. Two different orientation relationships have been reported for these precipitates: $[111]_p$ // $(0001)_m$ with $[11\bar{2}]_p$ // $[11\bar{2}0]_m$ by Crawley and Lagowski and Crawley and Milliken and $(110)_p$ // $(1\bar{2}11)_m$ with $[110]_p$ // $[10\bar{1}0]_m$ by Duly et al. [Dul95] and Celotto [Cel01].

Although the volume fraction of β-phase precipitates in Mg-Al-Zn alloys can be relatively high, the age-hardening response is relatively poor in comparison with many age-hardenable aluminium alloys for a number of reasons. Celotto [Cel01] has maintained that the orientation and coarseness of the continuous precipitates makes them inefficient obstacles to dislocation movement on the basal slip planes. However, the fact that the elements aluminium and zinc are known to have strong effects as solid solution hardeners, especially with regard to basal slip, is another important factor [Các01, Các02]. The increase in strength due to precipitation hardening will be offset by the concomitant loss in solid solution hardening. In AZ magnesium alloys overaging is not clearly observed [Cel00a, Nie02, Bet03, Zhe03].

The discontinuous precipitation reaction is initiated at high-angle grain boundaries and generates β-phase lamellae which are completely incoherent with the matrix, but have the same type of orientation relationship with the matrix as the continuous precipitates. The coarsening of discontinuous precipitates results in an increase in the lamellar spacing, but no spheroidisation. However the formation of globular

precipitates has also been reported in association with discontinuous precipitation [Cra74, Dul94b]. It has been observed that the discontinuous precipitation reaction can be slightly inhibited by pre-strain [Duy93] and also by the addition of trace elements such as Pb, Sb, Bi, Si or Au [Bet03, Lia05, Lih07 Bal07, Sri07].

2.5 Dislocation behaviour, precipitation and damping in magnesium alloys

In this section, some examples of previous work on the damping behaviour of magnesium and its alloys will be referred to and related to the deformation and precipitation behaviour as described in sections 2.3 and 2.4. Earlier work has been fully reviewed by Riehemann [Rieh94].

Until the classical work by Sugimoto et al [Sug77] on the amplitude-dependent damping of single crystals of magnesium, it was generally believed that the high damping capacity of pure magnesium was connected with its propensity to deform by twinning. However, Sugimoto et al. were able to show that the orientation dependence of the damping was entirely in keeping with the easy motion of dislocations on basal planes, i.e. as a consequence of the low critical resolved shear stress for basal slip (see Fig. 2.7). The stress dependence of the damping could be interpreted within the framework of the Granato-Lücke model. This behaviour was also confirmed for polycrystalline magnesium by comparing samples with random and preferred orientations (texture). Interestingly, the textured polycrystalline sample showed no amplitude-dependent damping up to strain amplitudes of 2×10^{-4}. Further work by Riehemann and Abed El-Al [Abe99, Rie00] on polycrystalline magnesium samples with different purities established that the Granato-Lücke model could be used to explain the damping behaviour in terms of the interactions between impurity atoms and bowing dislocation segments. Aging effects could be induced either by the application of alternating strains of the order of 10^{-3} or by annealing at high temperatures.

Since the high damping capacity of pure magnesium is associated with the easy motion of dislocations it is not surprising that the yield strength levels are also too low for commercial applications. Maintaining the high damping capacity and simultaneously improving strength levels can only be achieved, for example, by refining the grain size with the help of zirconium additions, or, incorporating inert

ceramic particles to produce composites [Tro02, Tro04]. Strengthening methods such as solid solution hardening or precipitation hardening which are based on the principle of restricting dislocation mobility generally lead to reductions in the damping capacity. A good combination of mechanical strength and damping capacity could be achieved if on the one hand dislocations are firmly pinned by precipitates of spacing L, but on the other hand are allowed to vibrate between these pinning points. This would require a low concentration of solute in the matrix after precipitation such that the spacing l between weak pinning points is large. Such effects have been observed in commercial aluminium alloys [Xie98].

However, it has been reported that precipitation exhibits various effects on the damping behaviour of magnesium alloys but the correlation between internal friction and precipitation is still not completely understood [Lam01, Gök02, Lam04, Lam05, Zha05].

3 Experimental Procedures

3.1 Materials

The AZ-series alloys were melted in steel crucibles using a resistance furnace (Fig. 3.1). The melts were held at 760 ºC for 1 h to ensure that the alloying elements were completely dissolved. Casting was performed into cylindrical steel containers 10 cm in diameter and 41 cm in length under a protective atmosphere of argon and SF_6. The mass of the cast billets was about 8 kg.

Fig. 3.1: Resistance furnace.

3.2 Chemical analysis

Chemical analysis of the as-cast alloys was carried out by spectroscopic analysis using SPECTROLAB (Model II 2003) equipment. The results presented in Table 3.1 are in good agreement with reference data [Ave99], which indicate the standard chemical compositions of the alloys.

Table 3.1: Chemical compositions of the alloys in wt %

Alloy	Zn	Al	Si	Cu	Mn	Fe	Ni	Others
AZ81	1.05	8.1	0.003	0.0035	.022	0.015	0.0005	<0.30
AZ61	0.99	6.5	0.002	<0.001	0.20	0.003	<0.001	<0.30
AZ31	1.16	3.3	0.008	0.002	0.22	0.008	0.002	<0.30
AZ21	0.93	2.0	0.02	0.0036	0.23	0.007	0.001	<0.30

For comparison purposes, some additional damping measurements were performed on pure magnesium of commercial purity (99.94 wt. %, see impurity content in Table 3.2) and four binary Mg-Zn alloys containing 1 - 3.6 wt. % Zn (called Z1, Z2, Z3, Z4) are summarised in Table 3.3.

Table 3.2: Impurities in the commercially pure Mg used in this work (all in wt. %)

Mg	Fe	Si	Ni	Cu	Al	Fe	Mn
99.94	0.0231	0.0087	<0.0002	0.00025	0.0096	<0.1	<0.15

Table 3.3: Chemical composition of the Mg-Zn alloys (all in wt %, Mg balance).

Alloy	Zn
Z1	1
Z2	2
Z3	3
Z4	3.6

3.3 Extrusion

Billets for indirect extrusion (Fig. 3.2) were machined to a diameter of 93 mm and length of 300 mm. All billets were then homogenised at 400 ºC for 20 h and air-cooled. An initial billet temperature of 300 ºC was chosen and rod profiles were extruded with an extrusion ratio of 1:30. The extrusion speed selected was 1 m/min. With these extrusion parameters, rod profiles with diameters of approximately 17mm were obtained from which damping specimens were prepared.

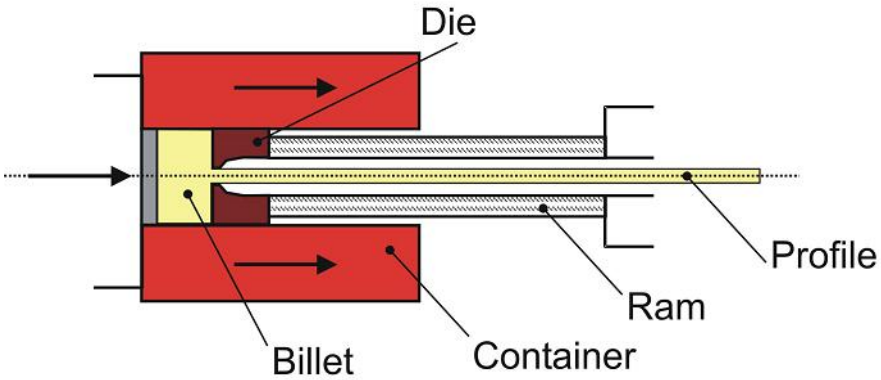

Fig 3.2: Schematic diagram of the indirect extrusion process.

3.4 Heat treatments

A preliminary survey of the effects of aging temperature on the damping behaviour of cast material was made by performing isochronal heat treatments on the alloy AZ61. These involved increasing the aging temperature in steps of 50 ºC from room temperature up to 400 ºC with aging times of 1 h (Fig. 3.3 a). The effects of aging time were investigated by employing isothermal heat treatments on the alloy AZ81. These T5 treatments involved direct aging at temperatures of 150 ºC, 200 ºC, 250 ºC and 300 ºC for times up to 1000 h (Fig. 3.3 b).

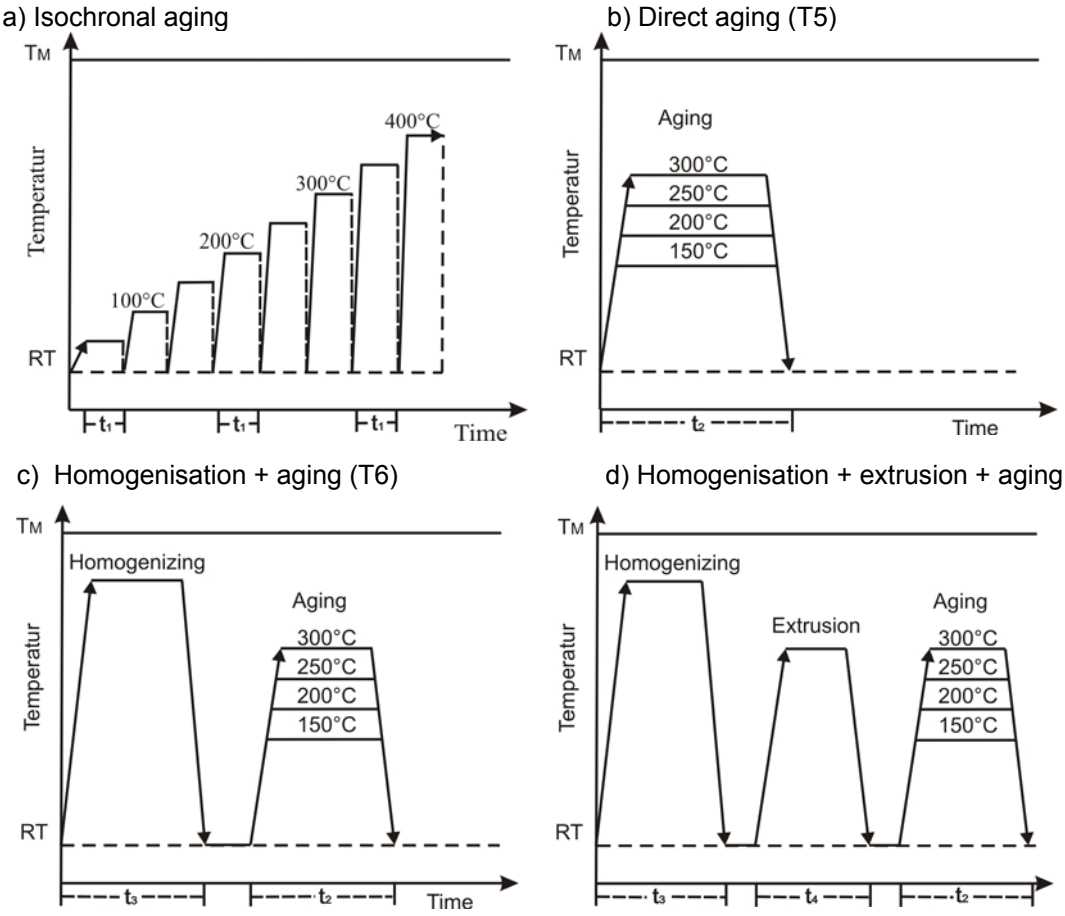

Fig. 3.3: Schematic representations of the heat treatment procedures used.
T_M: Melting temperature, RT: Room temperature, t_1: 1h, t_2: (0.5,1, 5, 12, 25, 50, 100, 200, 500 and 1000)h, t_3: 20h, t_4: 0.5h.

In order to study the kinetics of precipitation during isothermal aging via damping and hardness measurements a typical T6 heat treatment procedure (Fig. 3.3 c) was used. The alloys AZ31, AZ61 and AZ81 were solution-treated at 400 ºC for 20 h followed by water quenching to ambient temperature. All samples were encapsulated in glass tubes under vacuum in order to prevent oxidation. The thermal shock on quenching

was sufficient to crack the glass capsules and rapid quenching was achieved. Aging was then carried out at temperatures of 150 ºC, 200 ºC, 250 ºC and 300 ºC for times of up to 1000 h. To finally extruded material was directly aged at the same temperatures as for T6 same times up to 1000h to observe the effect of aging in material previously deformed.

3.5 Sample preparation for damping measurements

Specimens for damping measurements (Fig. 3.4) were produced with identical dimensions of 120 mm length, 10 mm width and 2 mm thickness in order to rule out geometrical effects when making comparisons between differently treated samples (as-cast, solution treated, extruded and aged).

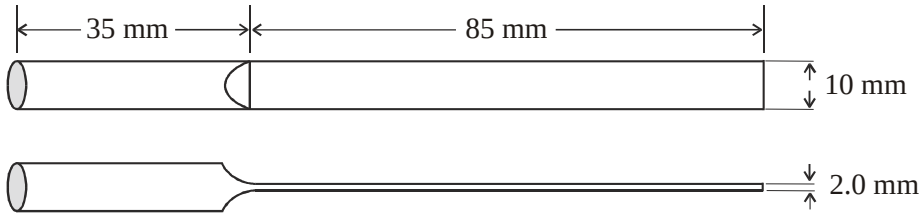

Fig. 3.4: Specimen geometry for damping measurements[Abe99].

In order to investigate frequency effects some additional measurements were carried out on samples with thicknesses of 2.5 or 3 mm. All bending beams were prepared by electro-erosion in order to avoid any plastic deformation of the samples which could influence the damping properties of the samples.

3.6 Damping measurements

Damping was measured in air in terms of the logarithmic decrement of freely decaying, bending beam vibrations. A schematic representation of the apparatus is shown in Fig. 3.5. In order to avoid external vibrations produced by machines near to the damping apparatus, the setup was mounted on a wooden structure with a high damping capacity. Additionally plates of marble and aluminium were placed over the wooden structure. Finally, a brass block was placed to hold down the bending beam and all this with an overall weight of about 250 Kg. All components were connected firmly by screws to minimise external friction.

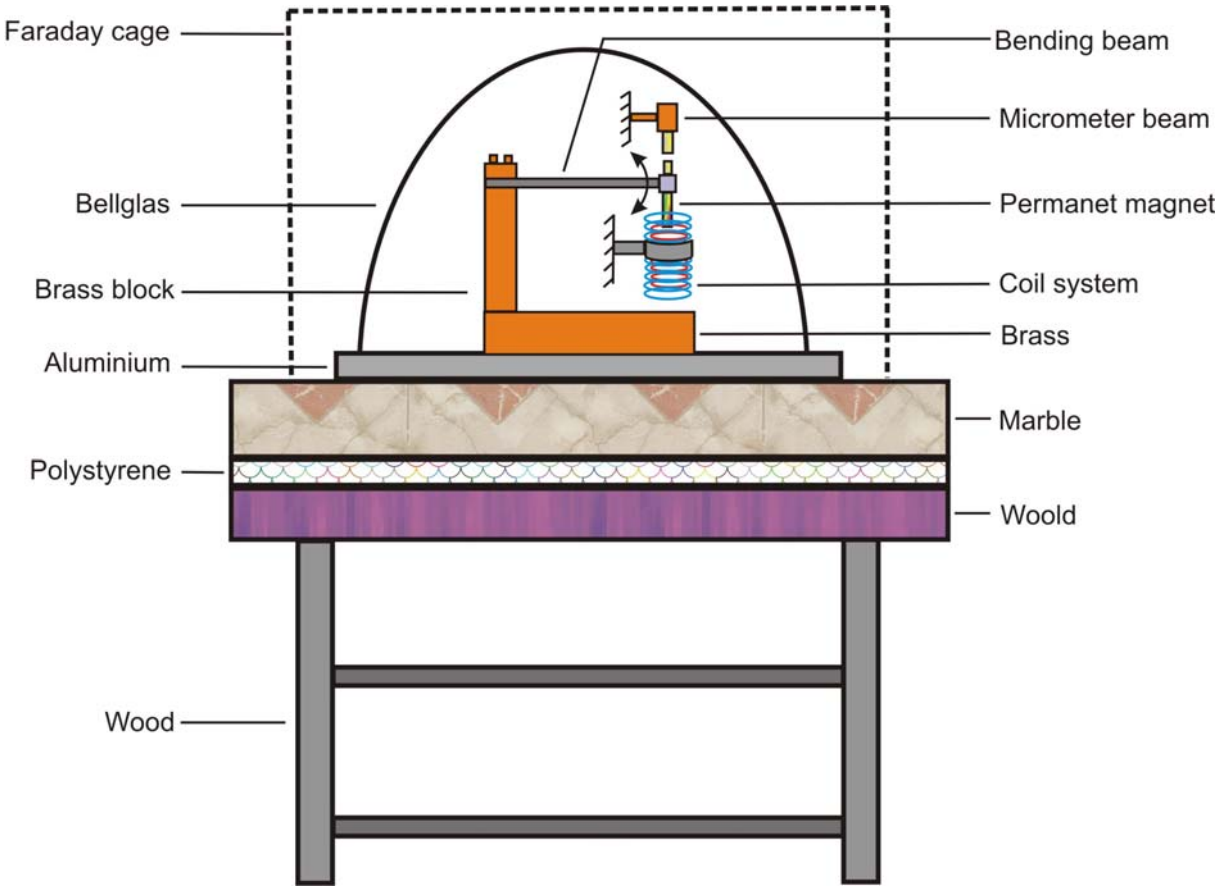

Fig. 3.5: Schematic representation of the damping apparatus[Gök02b].

Fig. 3.6 is a diagram showing the electromagnetic feedback used to measure the logarithmic decrement, where a permanent magnet fixed at the free end of a bending beam is immersed into a system of coils consisting of an excitation and an induction coil. At the other end, the bending beam is fastened to the brass block.

The bending beam was excited to mechanical resonance via electromagnetic feedback. A digital multi-meter with a resolution of 6 mV and sampling rate of 10 Hz was employed to measure the effective induced voltage at the induction coil, which is proportional to the amplitude of vibration. By measuring simultaneously the effective, induced voltages and the amplitudes of various beam vibrations with a micrometer screw, the induced voltage was calibrated in terms of strain.

When the amplifier was cut from the coil system by relays, the decreasing induced voltage measured by the multi-meter was transmitted to a computer. From these data, the logarithmic decrement δ was calculated as a function of strain ε.

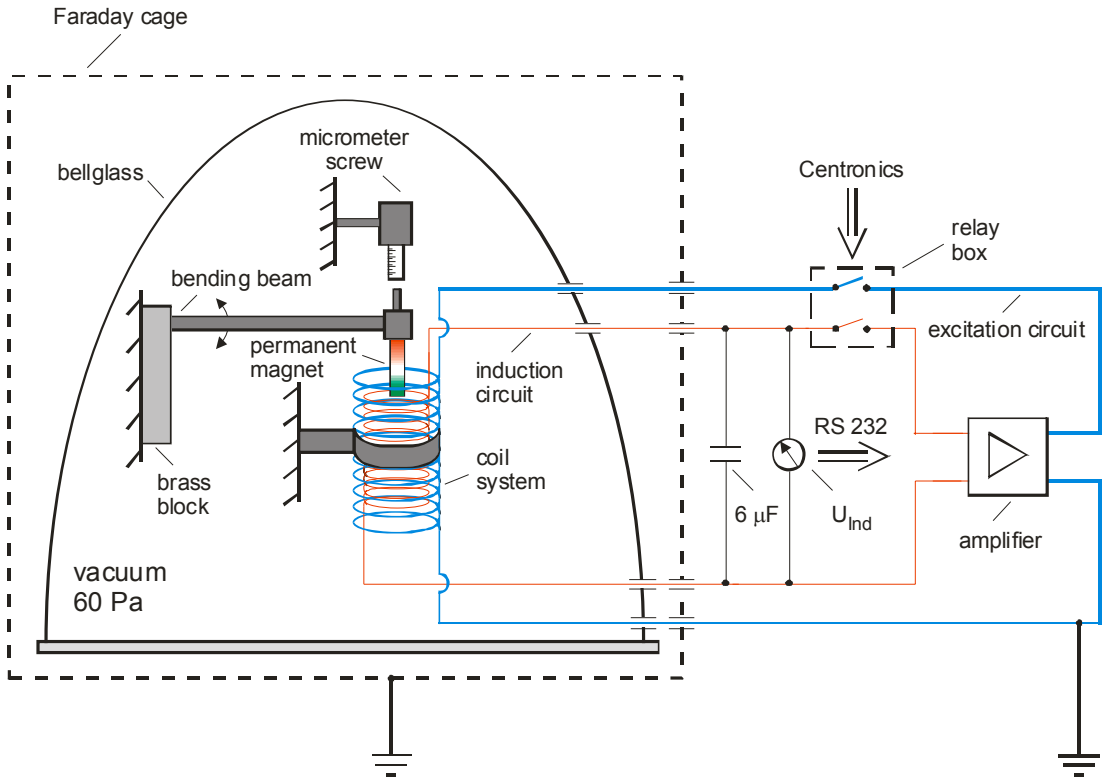

Fig. 3.6: Setup for damping measurements using electromagnetic feedback[Gök03]

3.7 Microstructure and phase characterisation

Specimens for optical microscopy (OM) and scanning electron microscopy (SEM), were prepared by mounting samples in epoxy resin (Demotec 70), which solidified after approximately 30 min and mechanical polishing at variable speed (Saphir360E) using a sequence of SiC abrasives from 400 to 2000 grit. After grinding, the specimens were polished with a 3 µm diamond suspension using soap and water as lubricant. Finally, the specimens were cleaned with ethanol. Specimens were then etched by submerging them into a solution of picric acid for approximately 5 to 10 s; immediately after etching, the samples were cleaned with ethanol and dried with a drier.

3.7.1 Optical microscopy (OM)

Optical microscopy was performed using a Leica DMI 5000M microscope equipped with a digital camera and a computer. Micrographs were evaluated using software (a4i Docu) installed on the computer. Micrographs were taken at various magnifications depending on the different states of the materials (as-cast, homogenised or extruded).

3.7.2 Scanning electronic microscopy (SEM)

Microstructural observations were made using either a ZEISS DSM 962 or a ZEISS Ultra 55 at accelerating voltages from 8-20 keV. Both microscopes are equipped with energy-dispersive X-ray analysis systems (EDX) for chemical microanalysis. Images were recorded using secondary electrons (SE) and back scattered electrons (BSE).

3.7.3 Grain size measurements

Grain sizes were determined from optical micrographs using the a4i software by the linear intercept method in accordance with ASTM E 112-96. The determination of average grain sizes was difficult, because the β phase does not form a complete network around the grain boundaries especially in aged specimens.

3.8 Hardness testing

Macro-hardness measurements were carried out using an EMCOTEST-M1CO10 testing machine (Fig. 3.7). A 10 kg load was applied for a period of 15 s and the size of the indent was measured. Tests were performed on the samples isochronally and isothermally aged directly after the casting process, on the samples aged after homogenisation and on the specimens aged directly after the extrusion process. All hardness values are the average of a minimum of 10 readings.

Fig. 3.7: Macro-hardness tester (EMCOTEST-M1CO10).

4 Results

4.1 Damping in Mg-Al-Zn and binary Mg-Zn alloys

4.1.1 Damping and microstructure of the as-cast AZ alloys

Fig. 4.1 shows the measured damping capacities of the as-cast Mg-Al-Zn alloys at room temperature as a function of the maximum strain amplitude. The form of the curves corresponds in all cases with that to be expected from the Granato-Lücke model, i.e. at a critical strain amplitude ε_{cr} there is a clear transition from a strain amplitude-independent regime at low strain amplitudes to a strain amplitude-dependent regime characterised by δ_h.

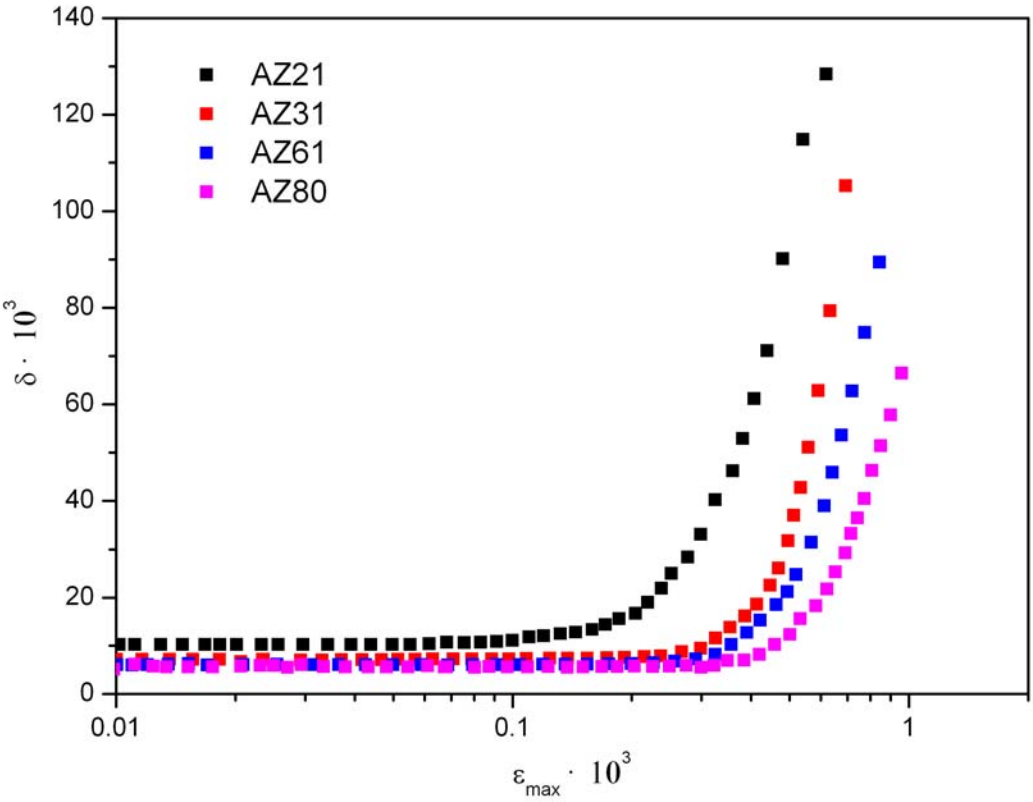

Fig. 4.1: Damping capacity of as-cast AZ21, AZ31, AZ61 and AZ81 as a function of strain amplitude

The results in Fig. 4.1 and Table 4.2 clearly demonstrate that the damping capacities in both regimes decrease with increasing Al content. Fig. 4.1 also shows that the critical strain ε_{cr} increases with increasing Al content. It is noteworthy that the ε_{cr} value for the AZ21 alloy is significantly lower than for the remaining alloys.

In Fig. 4.2 optical micrographs of the microstructures of the conventionally cast Mg-Al-Zn alloys are shown. The microstructures of AZ21 and AZ31 alloys consist of primary α-Mg grains with occasional particles of the β-$Mg_{17}Al_{12}$ phase at the grain boundaries, whereas the AZ61 and AZ81 alloys contain divorced eutectic colonies of α-Mg and the β-$Mg_{17}Al_{12}$ phase distributed in the interdendritic regions [Cai06]. The proportion of eutectic present increases with increasing Al content.

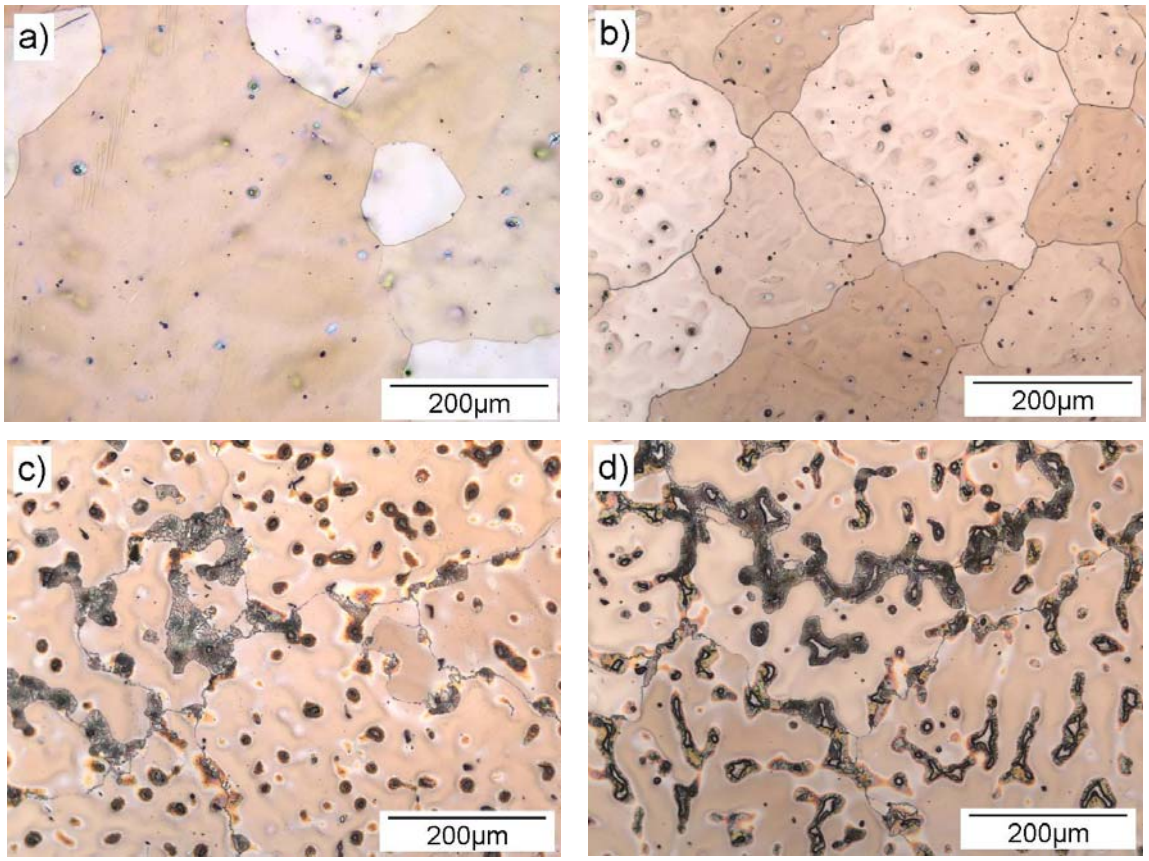

Fig. 4.2: Optical micrographs of the as-cast alloys; a) AZ21, b) AZ31, c) AZ61 and d)AZ81

The as-cast microstructures were also investigated using SEM and EDX-analysis techniques. The SEM micrographs in Fig. 4.3 show the distribution of the β-$Mg_{17}Al_{12}$ phase in the alloys AZ21 and AZ61 as examples. The corresponding X-ray maps reveal the aluminium distributions in the alloys. Solute segregation to the interdendritic regions during solidification is clearly indicated. The aluminium contents in the primary α-Mg grains were measured using. The green areas show the distribution of Al content.

EDX spot analyses and the results are summarised in Table 4.1.

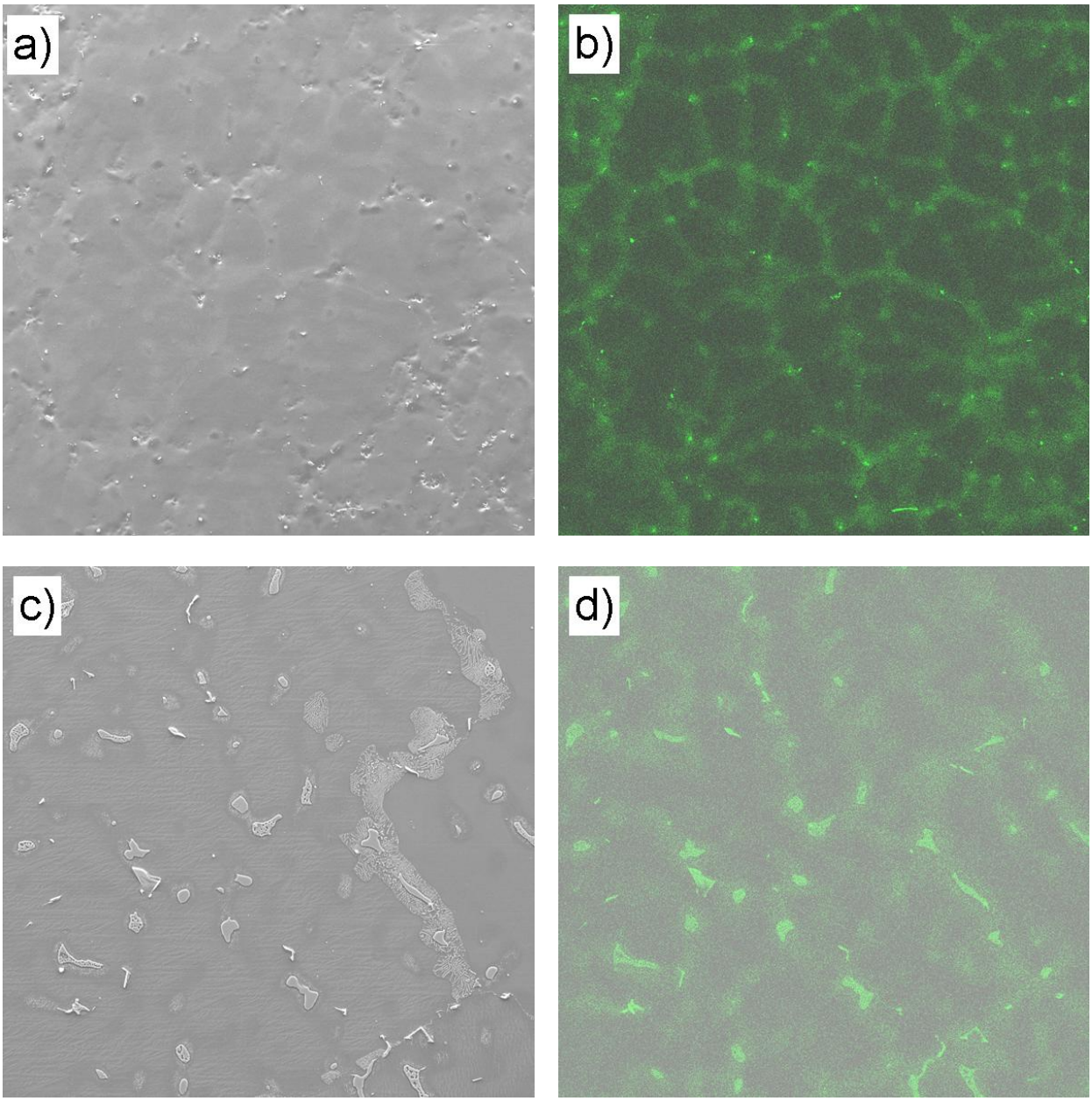

Fig. 4.3: SEM micrographs and corresponding Al-X-ray maps of the as-cast alloys AZ21 (a, b) and AZ61 (c,d)

Table 4.1: Al concentrations in the primary grains of AZ21, AZ31, AZ61 and AZ81

Alloy	AZ21	AZ31	AZ61	AZ81
wt. % Al (bulk)	2.0	3.3	6.5	8.1
As-cast	0.54	1.23	3.12	4.37

4.1.2 Damping and microstructure of the homogenised AZ alloys

The effects of the homogenisation treatment on the damping behaviour of the AZ31, AZ61 and AZ80 alloys are shown in Fig. 4.4. In this figure it is observed that the strain-dependent damping decreases significantly after homogenisation of the as-cast materials. Moreover, the critical strain ε_{cr} for the transition is increased considerably, especially for the alloys AZ61 and AZ80.

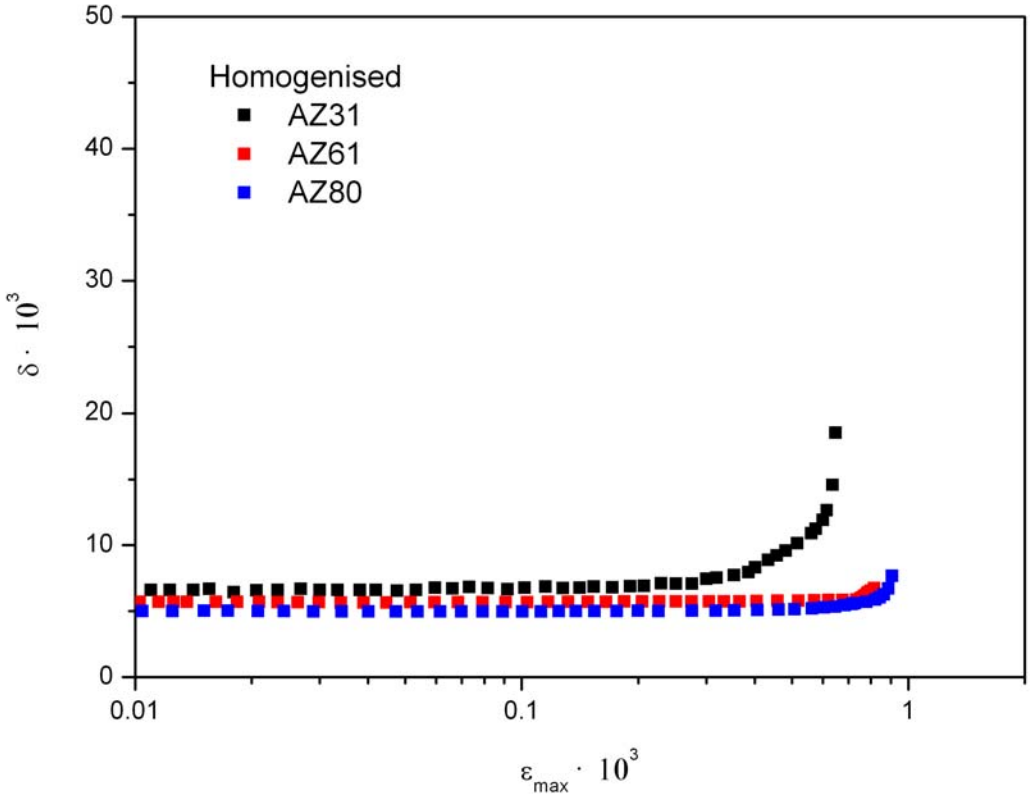

Fig 4.4: Damping curves of the homogenised AZ31, AZ61 and AZ80 alloys

The microstructures of the homogenised AZ-series alloys are shown in Fig. 4.5. After solution treatment at 400 ºC for 20 h, the eutectic disappears and all alloys are transformed to single phase, supersaturated solid solutions.

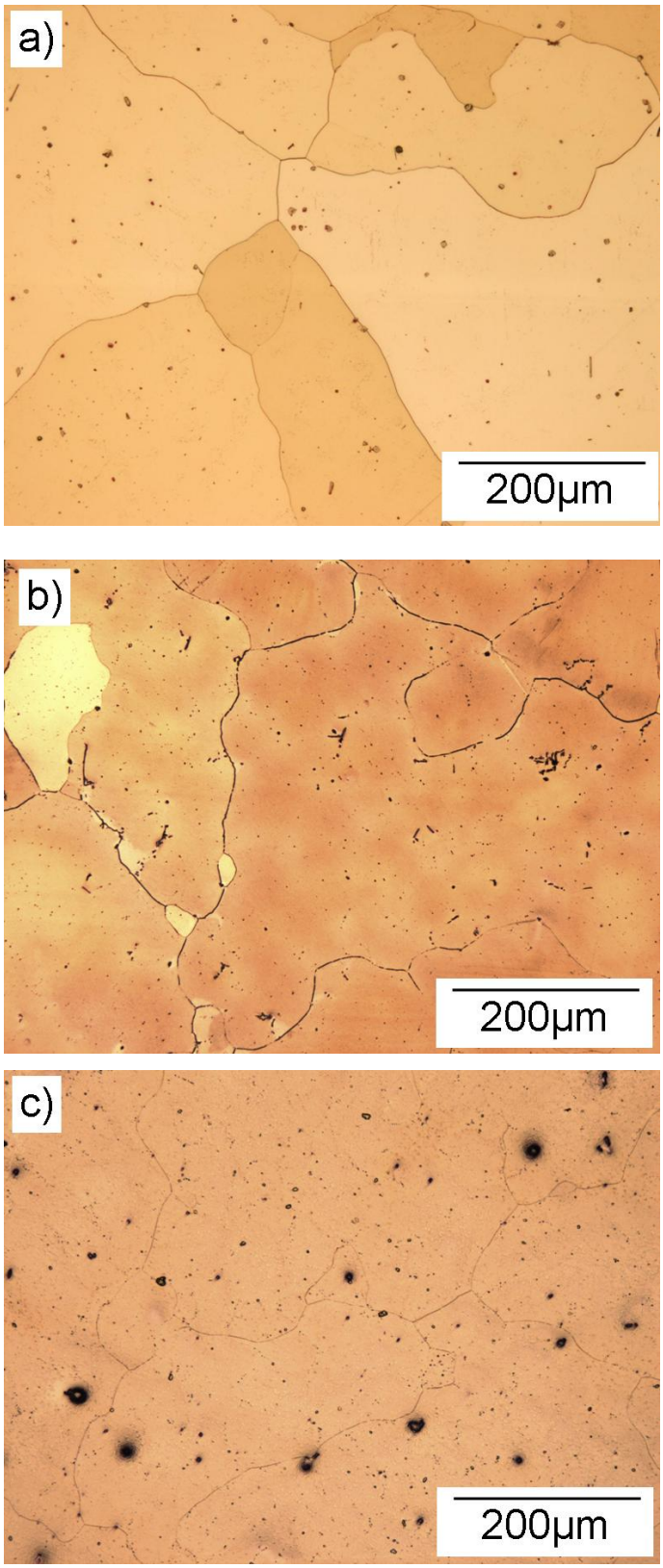

Fig. 4.5: Optical micrographs of the AZ31, AZ61 and AZ80 alloys after solution treatment (400 ºC/ 20 h)

4.1.3 Damping and microstructure of the extruded AZ alloys

The effects of extrusion on the damping behaviour of the AZ-series alloys as a function of maximum strain amplitude are shown in Fig. 4.6. The strain-dependent damping regime is shifted to greater maximum strain amplitudes compared to the homogenised alloys and the magnitude of δ_h is reduced dramatically.

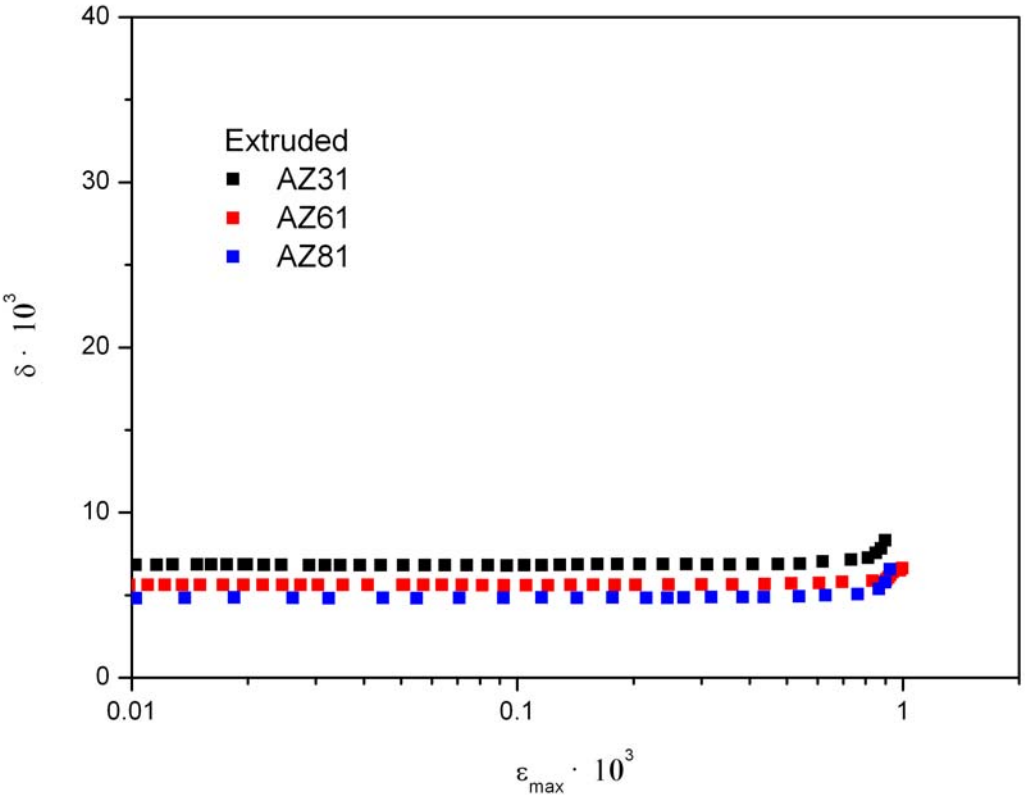

Fig 4.6: Damping curves of the extruded AZ31, AZ61 and AZ81 alloys

Table 4.2 summarises the measured values of the strain-independent damping and Vickers hardness the as-cast, homogenised and extrude alloys

Table 4.2: δ_0 and HV values for the as-cast, homogenised and extruded cp-Mg, AZ21, AZ31, AZ61 and AZ81 alloys

Alloy	cp-Mg	AZ21	AZ31	AZ61	AZ81
$\delta_0 \cdot 10^3_{\text{As-cast}}$	—	9.26	7.14	5.97	5.56
$\delta_0 \cdot 10^3_{\text{Homogenised}}$	—	—	6.6	5.7	5.25
$\delta_0 \cdot 10^3_{\text{Extruded}}$	—	—	6.97	5.64	5.08
$HV_{\text{As-cast}}$	—	—	47	52	57.5
$HV_{\text{Homogenised}}$	—	—	46	54	56
HV_{Extruded}	—	—	53	58	67

Fig. 4.7 shows the microstructures of the extruded AZ31, AZ61 and AZ81 alloys. The AZ31 alloy is characterised by a relatively broad grain size distribution which suggests that the material has not completely recrystallised during extrusion. The isolated particles seen in Fig. 4.7(a) correspond to the manganese-containing inclusions referred to in section 2.4.1.

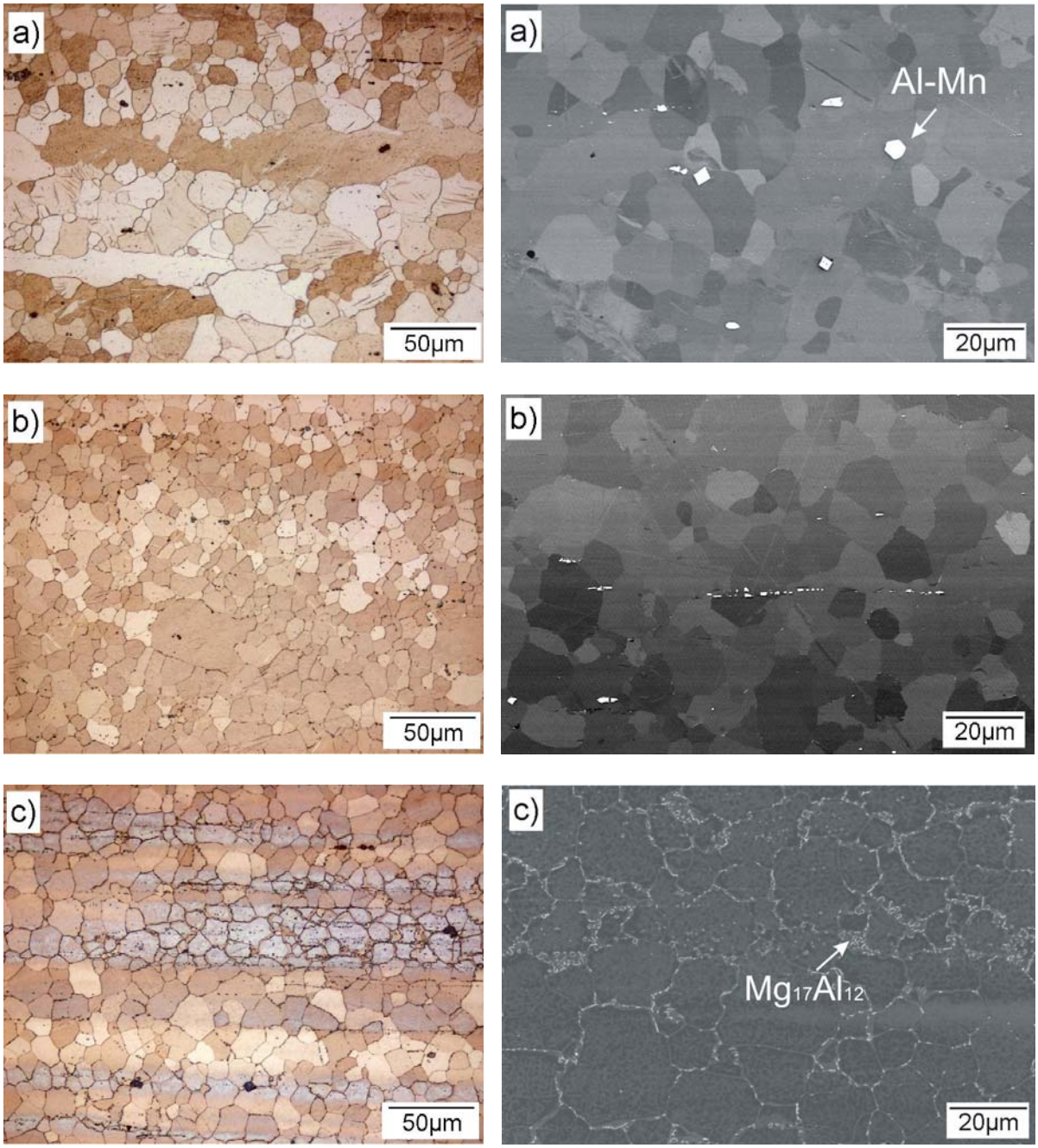

Fig. 4.7: Optical and SEM micrographs of the extruded alloys
(a) AZ31, (b) AZ61 and (c) AZ81

SEM studies reveal that all alloys exhibit some $Mg_{17}Al_{12}$ precipitates at the grain boundaries and as the Al content increases the volume fraction of these precipitates increases (Fig. 4.7). In the alloys AZ61 and AZ81 they become interconnected to form a network. The more homogeneous average grain sizes observed in the alloys AZ61 and AZ81 are probably a result of these precipitates acting as obstacles to inhibit grain growth [Mue06, Boh04, Din07].

4.1.4 Damping and microstructure of the homogenised Mg-Zn alloys

Fig. 4.8 shows the measured damping capacities of the homogenised (375 ºC for 2 h) Mg-Zn alloys at room temperature as a function of the maximum strain amplitude.

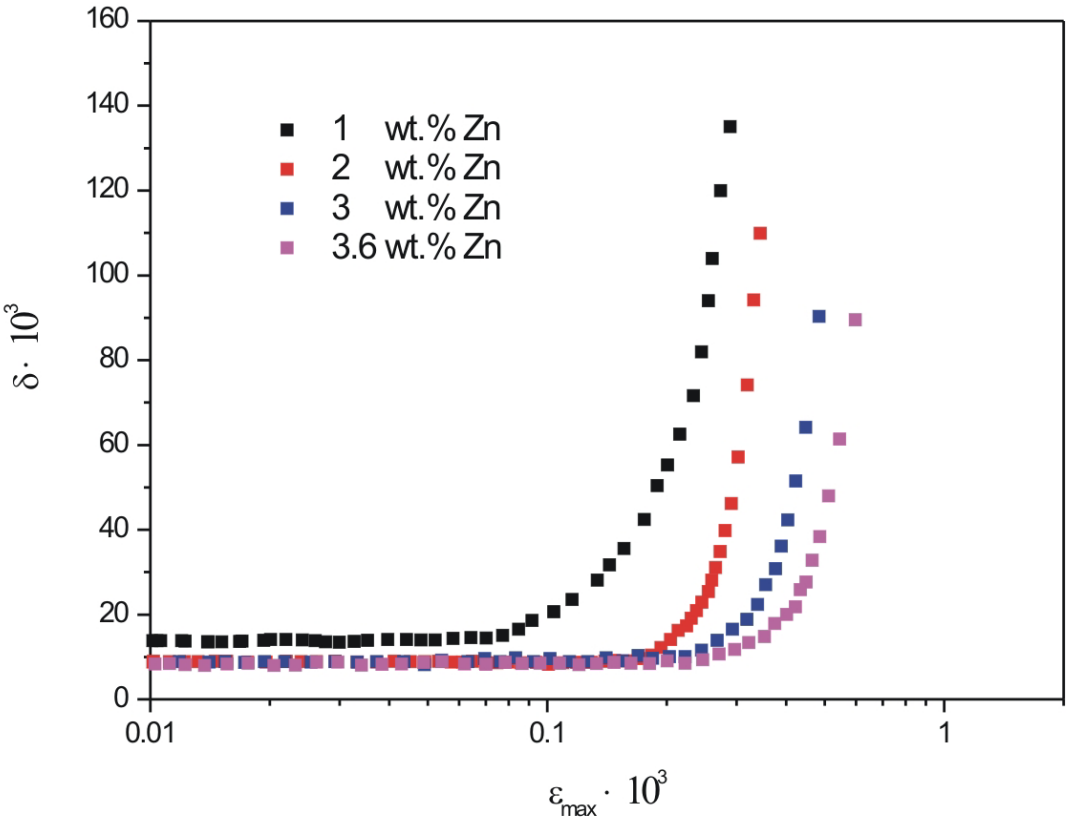

Fig. 4.8: Damping capacity of homogenised binary Mg-Zn alloys as a function of strain amplitude

The form of the curves again corresponds with that to be expected from the Granato-Lücke model, i.e. at a critical strain amplitude ε_{cr} there is a clear transition from a strain amplitude-independent regime at low strain amplitudes to a strain amplitude-dependent regime characterised by δ_h. Fig. 4.8 also shows that the critical strain ε_{cr} for this transition clearly increases with increasing Zn content.

Fig. 4.9 (a)-(d) shows the effect of Zn additions in solid solution on the microstructure of the homogenised alloys. The microstructures consist of homogeneously distributed, equiaxed grains. The addition of Zn leads to significant refinement of the grain size. Scanning electron micrographs alloys revealed only some occasional, randomly distributed impurity particles and pores.

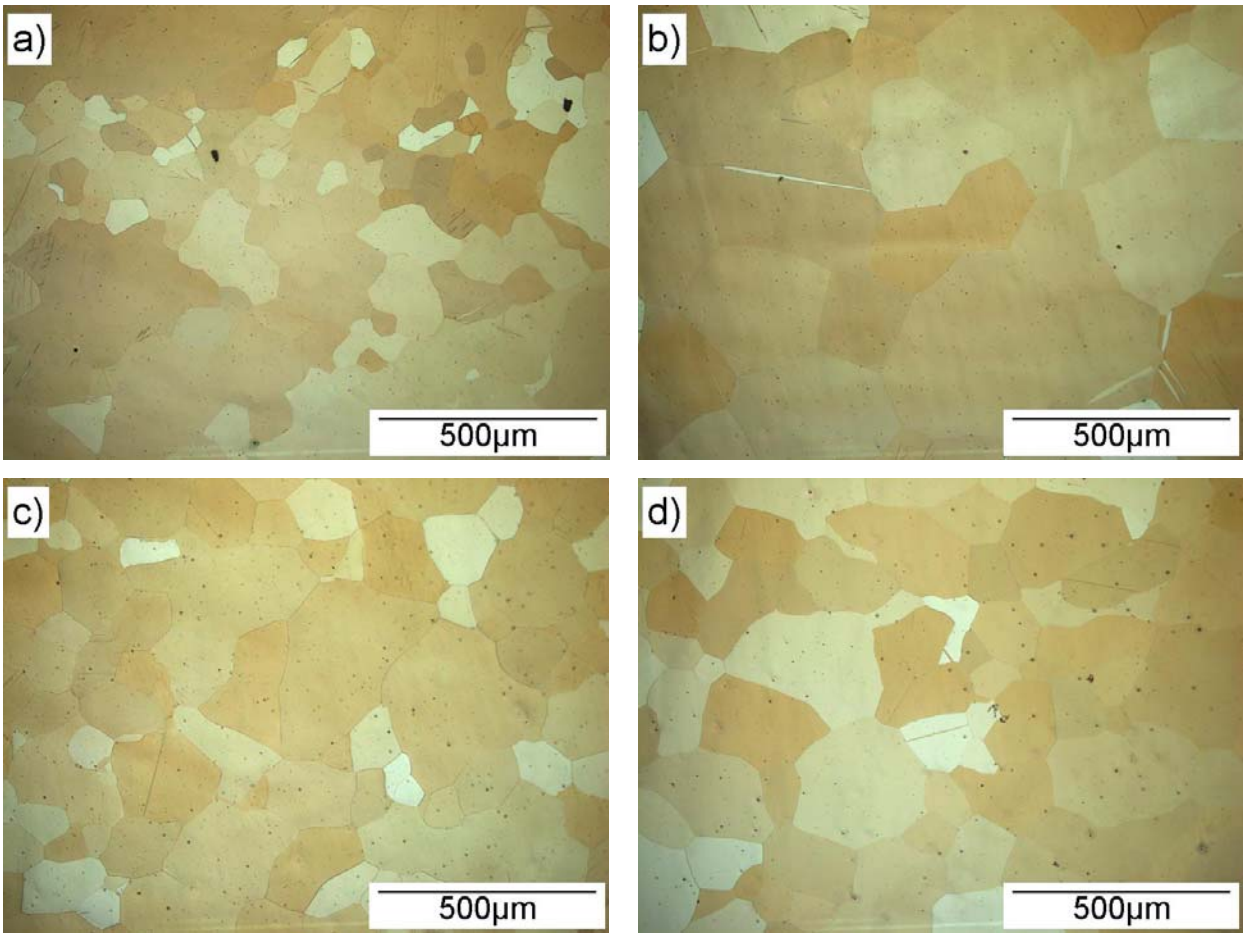

Fig. 4.9 (a-d): Microstructures of the cast Z-series alloys after homogenisation at 350 ºC for 15 hours

4.1.5 Damping and microstructure of the extruded Mg-Zn alloys

The effects of extrusion on the damping behaviour of the binary Mg-Zn alloys are shown in Fig. 4.10. Compared to the homogenised samples the strain amplitudes ε_{cr} at which the transition to the strain amplitude-dependent damping regime begins are shifted to higher strain amplitudes. The magnitude of δ_h is also reduced significantly for all the alloys.

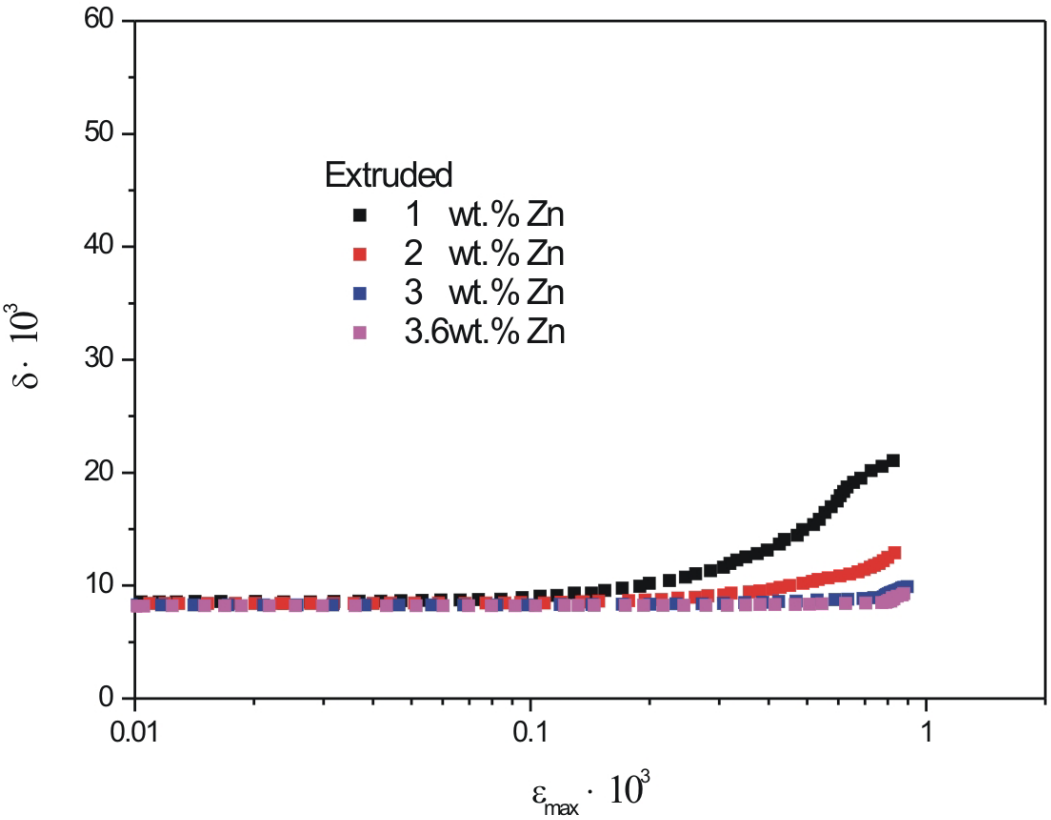

Fig. 4.10: Damping curves of the extruded binary Mg-Zn alloys

Table 4.3: summarises the measured values of the strain-independent damping and Vickers hardness for the homogenised and extruded Mg-Zn alloys.

Table 4.3: δ_0 and HV values for the homogenised and extruded Mg-Zn alloys

Alloy	Z1	Z2	Z3	Z4
$\delta_0 \cdot 10^3$ homogenised	14.1	9.18	8.79	8.2
$\delta_0 \cdot 10^3$ extruded	8.67	8.43	8.29	8.24
HV homogenised	32.54	36.64	41	41.1
HV extruded	44.62	46.67	51.3	53.6

The hydrostatically extruded pure magnesium and Z-series alloys show very homogenous and very fine microstructures, see Fig. 4.11 (a)-(e). All the Z-series alloys showed an average grain size of around 10 μm, regardless of the Zn content. In Fig. 4.11, only some occasional, randomly distributed impurity particles can be observed.

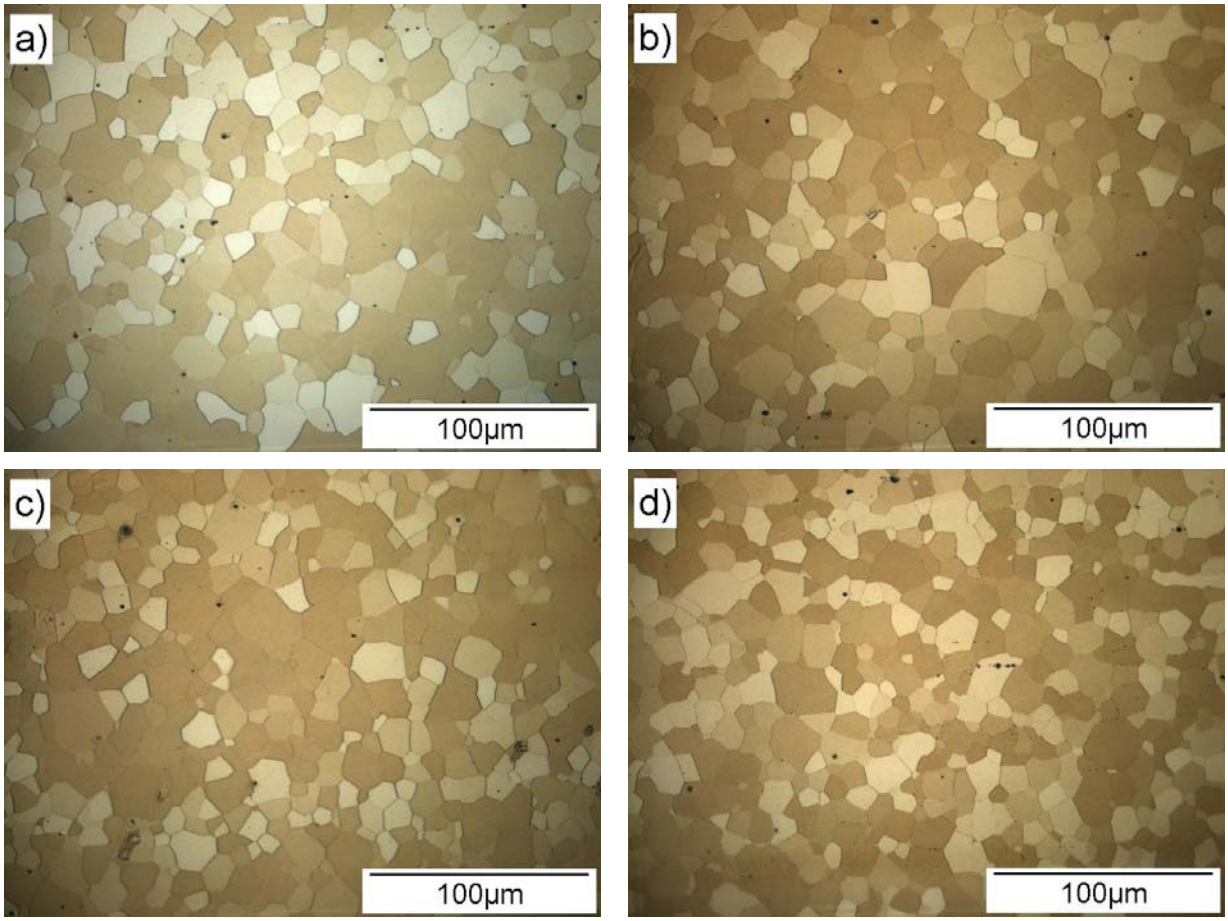

Fig. 4.11: Microstructures (extrusion direction ←) of (a) Z1, (b) Z2, (c) Z3 and (d) Z4 after hydrostatic extrusion at 300 ºC.

4.2 Direct aging of as-cast AZ alloys

Precipitation in AZ alloys after direct aging involves both discontinuous and continuous precipitation. However, as described in section 4.1, the aluminium supersaturation in as-cast material is much lower than in the solution heat treated condition (T6).

4.2.1 Isochronal Aging of the as-cast AZ61 Alloy

In Fig. 4.12 the logarithmic decrement δ of the as-cast alloy AZ61 is plotted versus the maximum strain amplitude after isochronal heat treatments of 1 h duration at temperatures ranging from room temperature up to 400 ºC. For comparison, the data for the as-cast material is included. The curves can generally be divided into two regimes, a strain-independent part δ_0 at low strain amplitudes and a strain-dependent part δ_h at higher strain amplitudes.

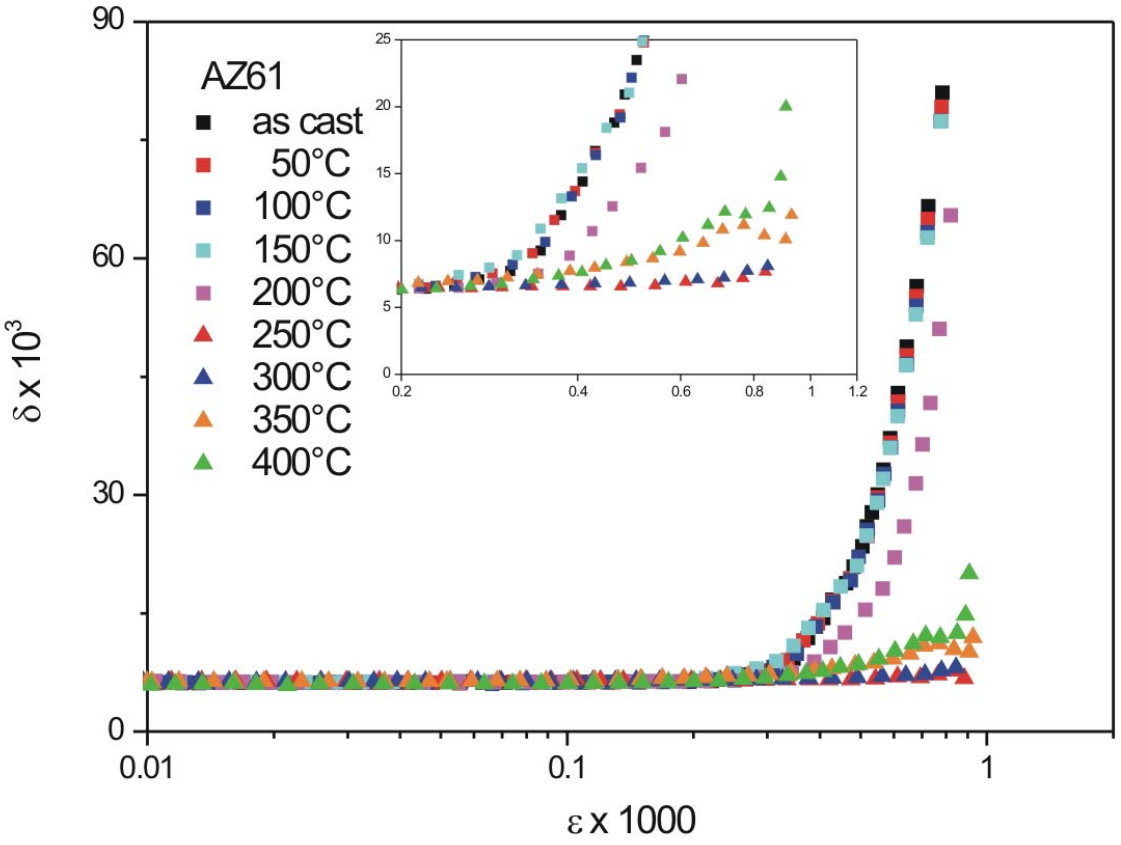

Fig. 4.12: The damping behaviour of AZ61 after stepwise increases in aging temperature

It is clear that after heat treatments between room temperature and 150 ºC the damping behaviour remains very similar to that observed in the as-cast sample. After heat treatment at 200 ºC, the transition to the strain amplitude-dependent damping regime is shifted to higher maximum strain amplitudes ε, i.e. the value of ε_{cr} is increased and a significant decrease in the strain amplitude-dependent damping is observable. After aging at 250 ºC and 300 ºC significant reductions in the strain-dependent damping δ_h are observed.. This trend ceases after heat treatments at 350 ºC and 400 ºC. In these cases, the strain-dependent damping parts are increased. At the highest strain amplitudes, the measurements show an increase in damping as obtained for the measurements after heat treatments from room temperature to 200 ºC.

The hardness and the strain-independent damping δ_0 versus the heat treatment temperature are illustrated in Fig. 4.13. The strain-independent damping δ_0 is plotted using two different starting maximum strain amplitudes of 0.2 x 10^{-3} and 1.0 x 10^{-3}. In both cases, δ_0 increases with increasing aging temperature and shows a slight maximum after the heat treatment at about 260 ºC. After aging at higher

temperatures, δ_0 decreases. However, the results also exhibit an influence of ε on δ_0. The strain-independent damping is overlapped by another mechanism to be taken into account when using higher starting strain amplitudes.

In both cases, the changes in δ_0 and hardness are more pronounced after aging at temperatures higher than 150 ºC. A hardness peak with a maximum at around 250 ºC develops and a steep decrease in the hardness after passing the maximum occurs. Therefore, it can be assumed that the strain-independent damping δ_0 and the hardness are correlated and are dependent on the same microstructural changes.

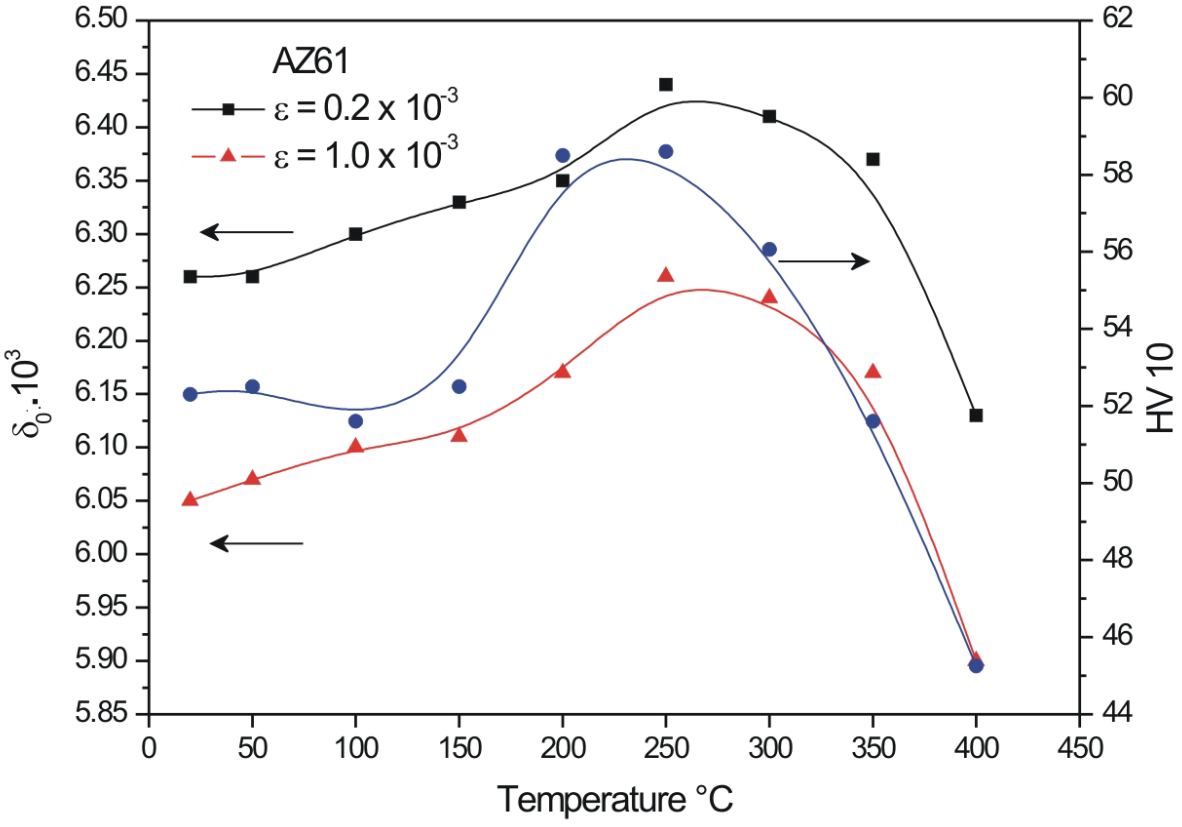

Fig. 4.13: Vickers hardness and the strain-independent damping of AZ61 at ε =0.2 x 10^{-3} and ε =1.0 x 10^{-3} versus the aging temperature

Fig. 4.14 shows SEM micrographs of the alloy AZ61 after different heat treatments. .In the as-cast condition (Fig. 4.14a) the microstructure contains residual eutectic which is stable up to a heat treatment temperature of about 400 ºC. After aging at 200 ºC (Fig. 4.14 c), the presence of a new phase near the eutectic zone is visible.

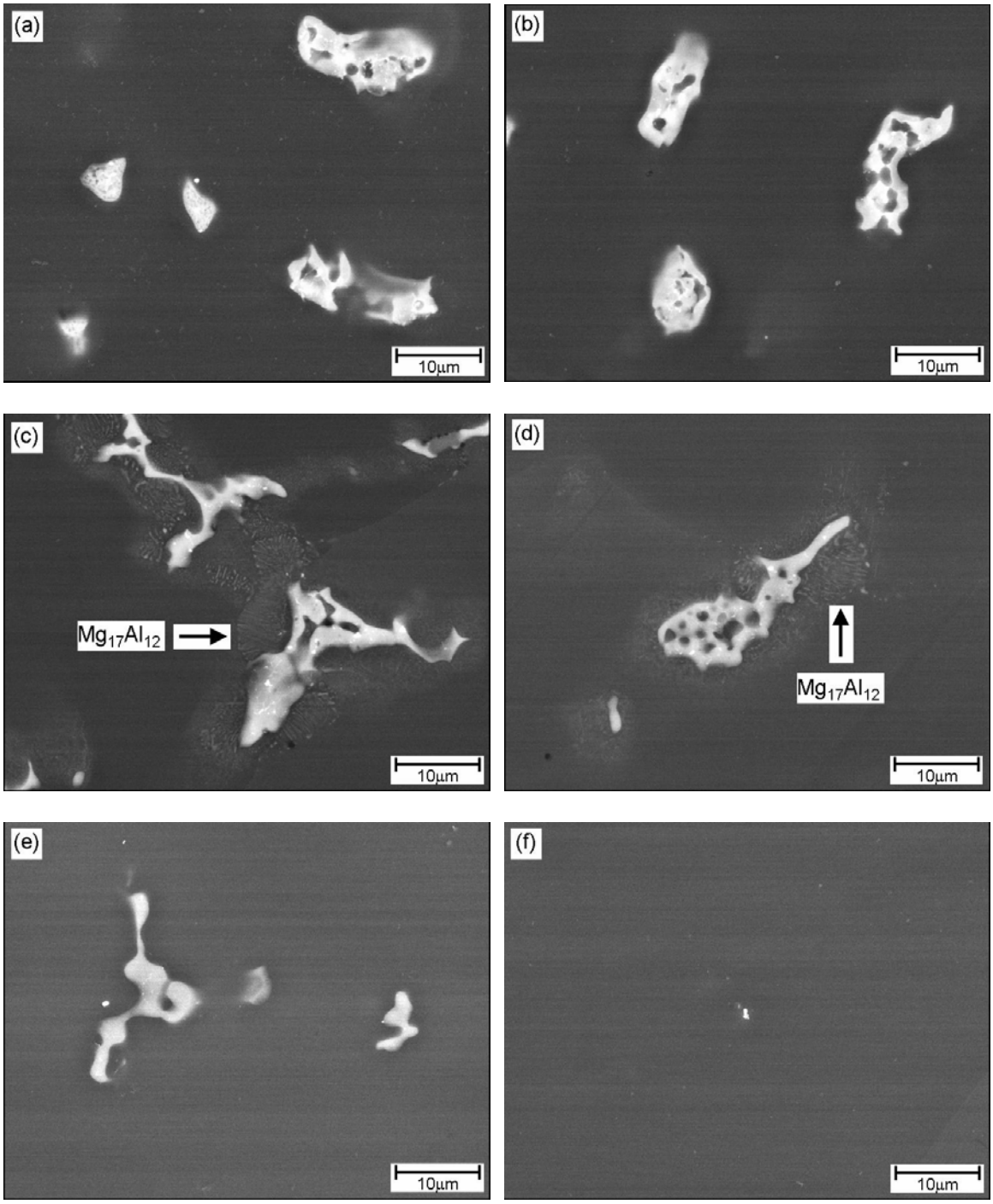

Fig. 4.14: Microstructures of AZ61 in (a) the as-cast condition and after heat treatments at (b) 100 ºC, (c) 200 ºC, (d) 250 ºC, (e) 350 ºC and (f) 400 ºC

This was analysed as the precipitate phase $Mg_{17}Al_{12}$ in accordance with the corresponding phase diagram [Ave99] and previous work demonstrating that the precipitation process in the Mg-Al-Zn system appears to involve solely the formation of the equilibrium phase $Mg_{17}Al_{12}$ [Nie03].

The $Mg_{17}Al_{12}$ phase is still present after aging at 250 ºC (Fig. 4.14 d) but is no longer present after heat treatment at 350 ºC (Fig. 4.14 e) and 400 °C. This behaviour is in agreement with electrical resistivity measurements on the alloy AZ91 indicating strong activation of precipitation around 230 ºC followed by a decreased influence of the temperature and regression of the precipitates [Kie97, Cer02]. Moreover, at the final annealing temperature of 400 ºC the matrix becomes almost free of eutectic (Fig. 4.14 f).

4.2.2 Isothermal aging of as-cast AZ81

In Fig. 4.15, the δ_0 values of the alloy AZ81 are plotted versus the aging time t on a logarithmic scale. Three different aging temperatures T were chosen to obtain information on the influence of the aging temperature on the time dependency of the strain-independent damping δ_0. It is clear that for all aging temperatures T the damping increases with increasing aging time. For some temperatures and longer aging times a saturation effect can be observed. This effect seems to be achieved earlier when the aging temperature is higher. The level of δ_0 in this saturated condition is also dependent on the aging temperature. It is reduced as T increases. At the lowest aging temperature of 150 ºC saturation is not yet reached.

Fig. 4.16 show the isothermal hardening versus aging time curves for the AZ81 alloy at different temperatures. The hardness increases with aging time and decrease in aging temperature. For these results it is not possible to observe an incubation period between the initial state of the material and the peak hardness. The hardness slowly increases up to the maximum hardness and does not show a drop after long aging times. After aging for 2500 h at a temperature of 150 ºC, the maximum hardness has still not been reached.

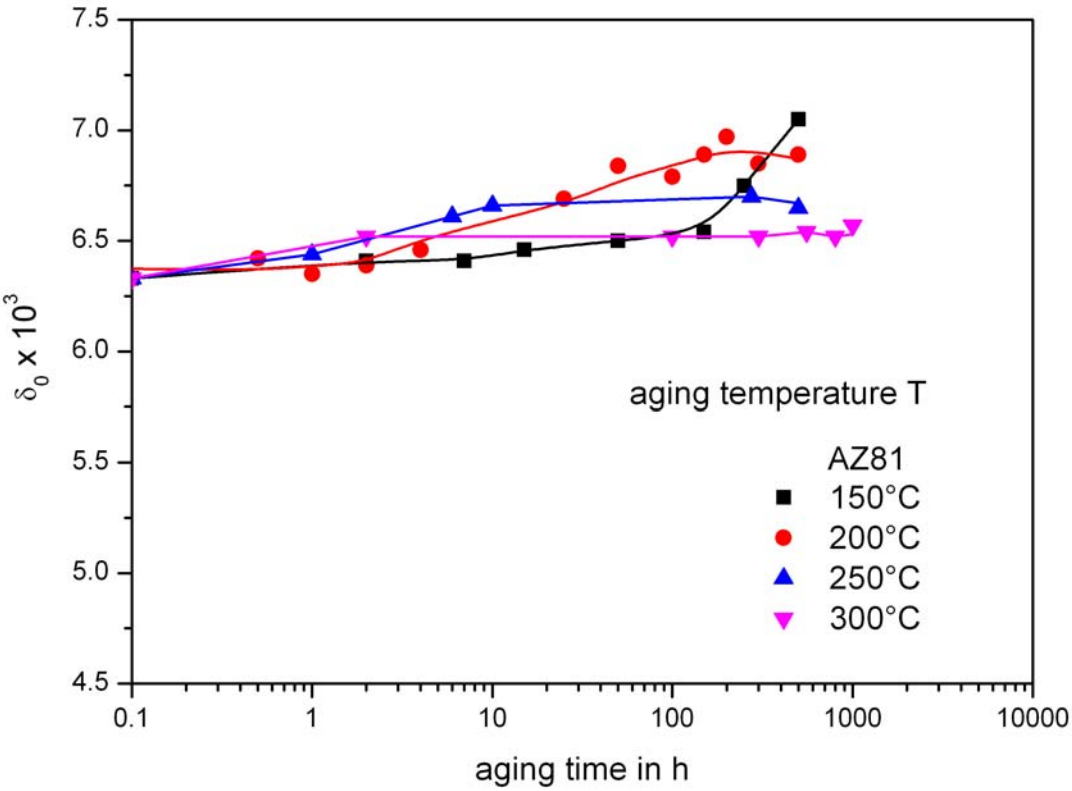

Fig. 4.15: Strain-independent damping δ_0 of AZ81 as a function of aging time after direct aging at different aging temperatures T

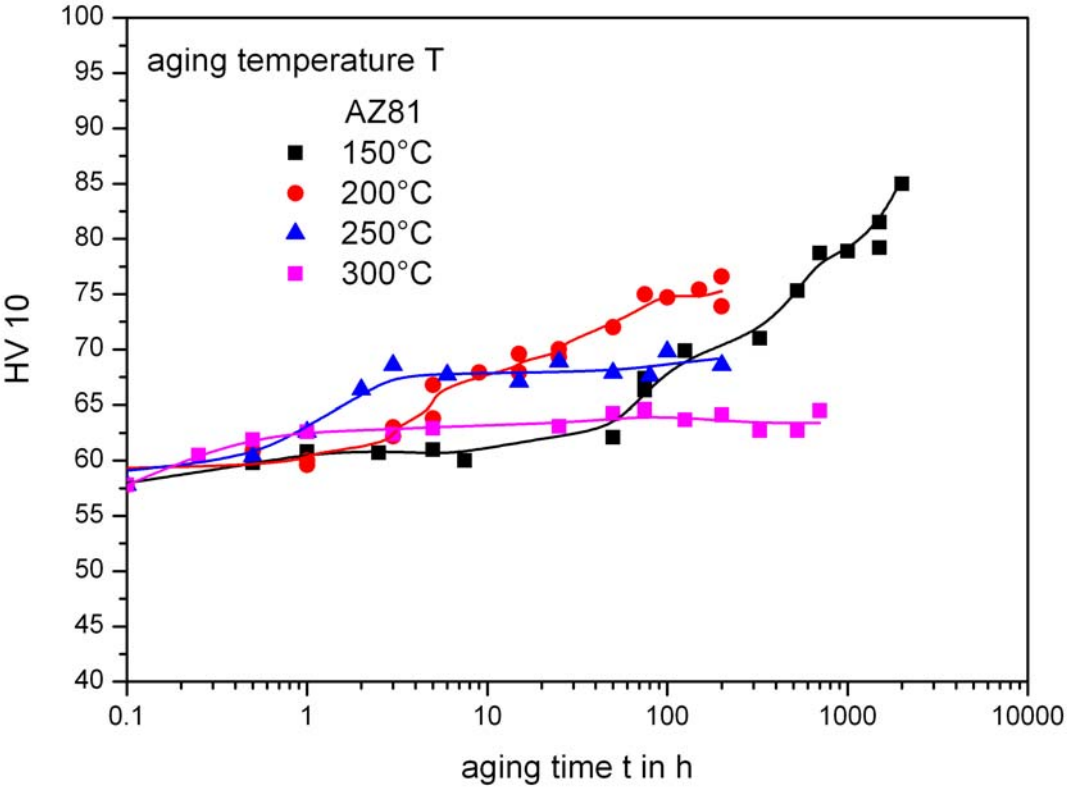

Fig. 4.16: Vickers hardness of AZ81 as a function of aging time t after direct aging at different temperatures T

Figs. 4.17 and 4.18 show the development of the microstructure after aging at temperatures of 150 ºC and 300 ºC. The starting microstructure consists of primary α grains with a divorced eutectic β ($Mg_{17}Al_{12}$). Initially, discontinuous and continuous precipitates appear in the regions supersaturated in aluminium, i.e. in the regions next to the β phase and along the grain boundaries. It can be seen that the volume fraction of precipitates increases with aging time at both aging temperatures.

At longer aging times these zones of precipitation appear to advance into the neighbouring grains [Cai00, Sak93]. The largest increase in hardness is obtained after long time aging at the lowest aging temperature (150 ºC) for which the precipitate distribution is expected to be fine and the volume fraction high. Although Fig. 4.17 only shows the formation of discontinuous precipitates at 150 ºC, the hardness results would suggest that finely dispersed, continuous precipitates of the β-phase are present that are beyond detection by the SEM technique. These observations are in a good agreement with the findings of Duly et al. [Dul95] and Malik [Mal09].

The morphology of the continuous precipitates after aging at 300 ºC is significantly different compared with 150 ºC. Coarsening of the continuous precipitates at 300 ºC was observed, whereas for aging at 150 ºC, precipitate coarsening is not observed. This is not surprising since the damping and hardness measurements suggest that the precipitation process at the lower temperature is by no means complete after aging times of the order of 1000 h.

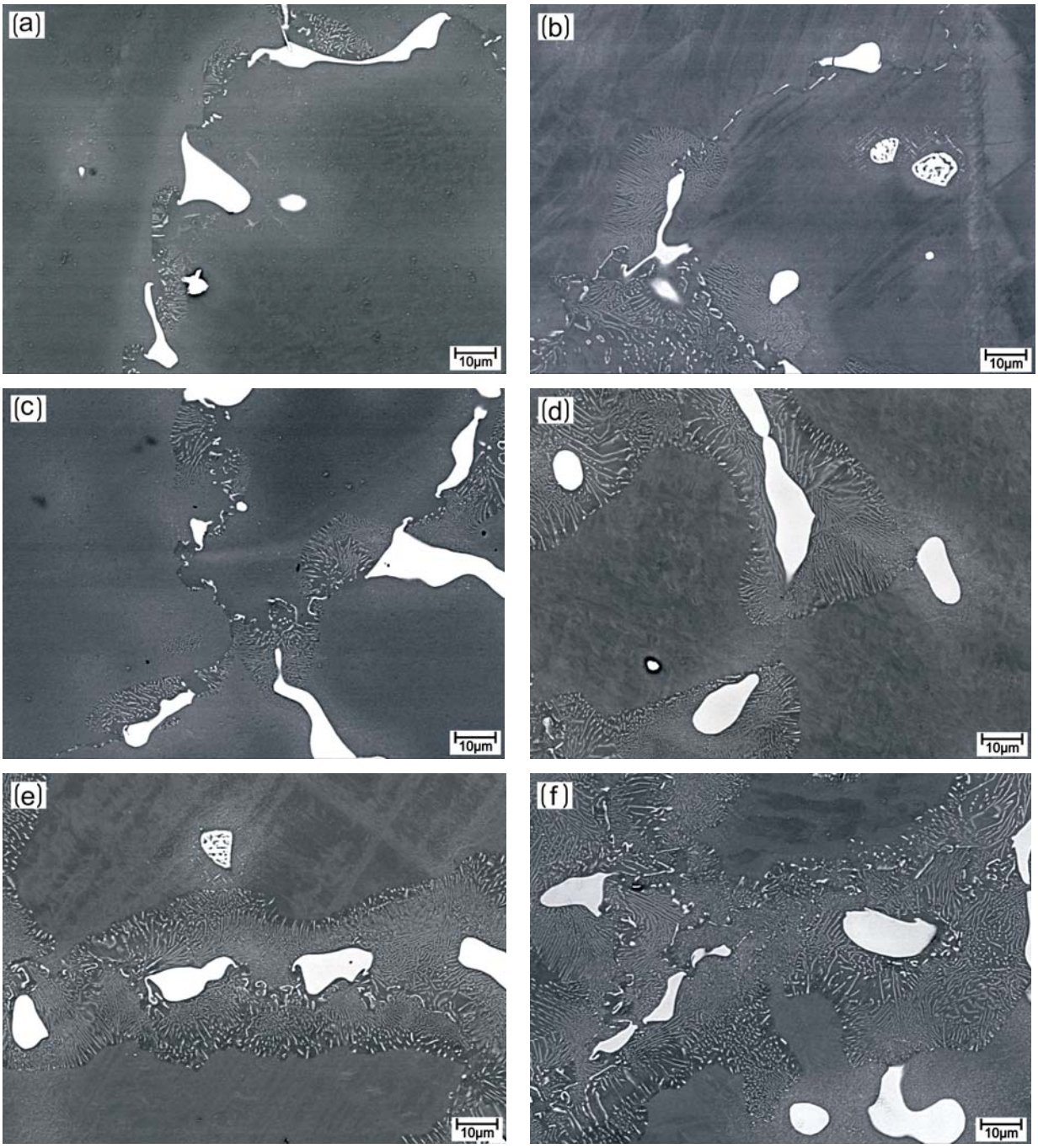

Fig. 4.17: SEM micrographs of a) as-cast AZ81 and after direct aging for b) 1 h, c) 25 h, d) 200 h, e) 525 h and f) 1000 h at 150 ºC

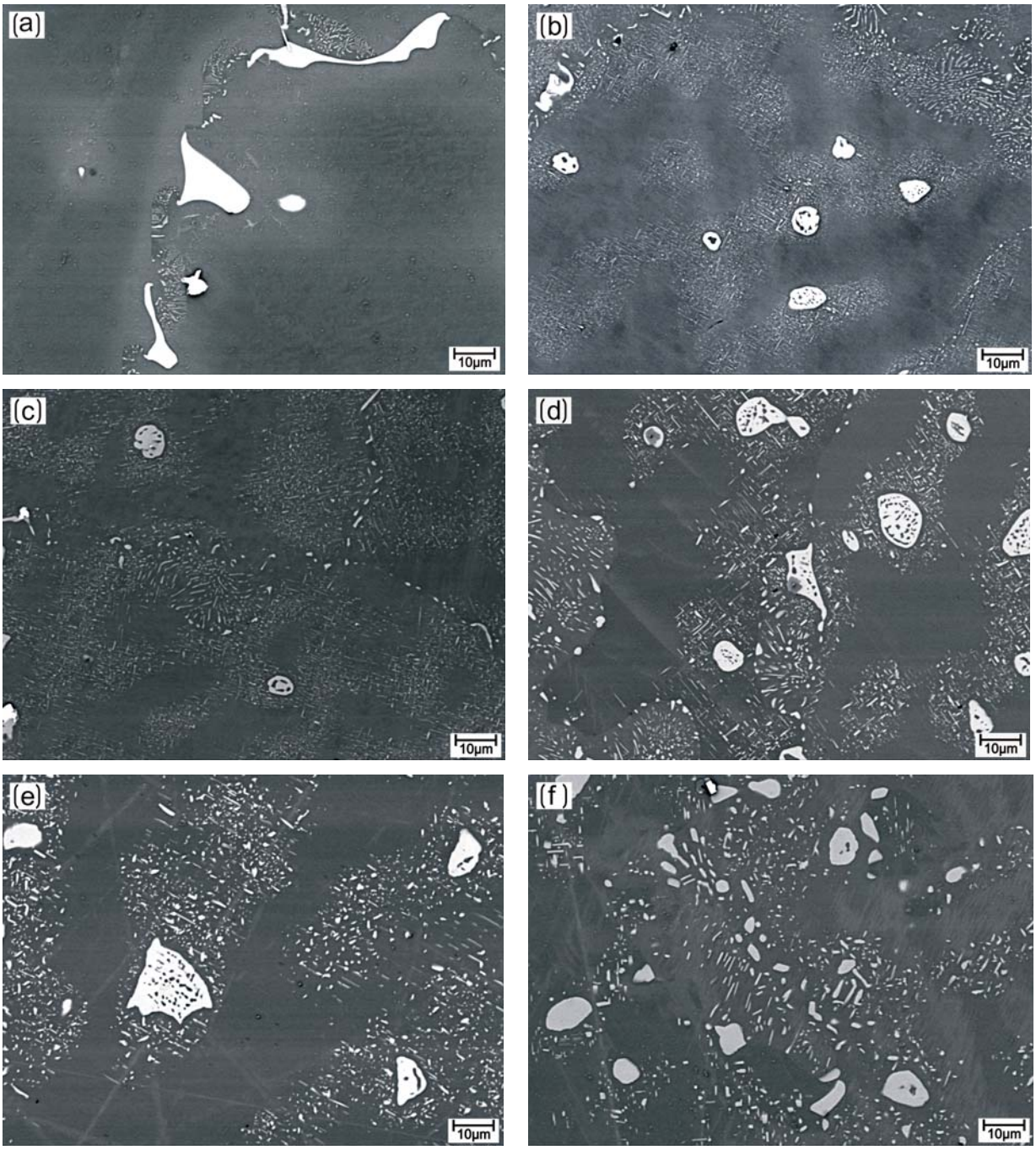

Fig. 4.18: SEM micrographs of a) as-cast AZ81 and after direct aging for b) 1 h, c) 5 h, d) 50 h e) 200 h and f) 1000 h at 300 ºC

4.3 The Effect of Aging after Solution Treatment

Precipitation hardening is one of the classical methods to generate higher strength alloys. The distribution, size, form, structure and chemical composition of the precipitates is controlled by means of diffusion. The process (T6) as applied to AZ alloys involves first a solution treatment followed by various aging treatments.

4.3.1 Damping and Hardness Curves

In Fig. 4.19, measured values of δ_0 for the alloy AZ81 are plotted versus the aging time t for three different aging temperatures T. It is seen that the damping increases with increasing aging time at all aging temperatures. At longer aging times a saturation effect can be observed. This effect appears to be achieved earlier when the aging temperature is higher. The level of δ_0 in the saturated condition is also dependent on the aging temperature. It is reduced as T increases. The time to reach a fixed amount of transformation is express by the time constant τ and increase with decreasing aging temperature. A narrow description of τ is given later on, see section 4.3.3.

The corresponding hardness measurements for the alloy AZ81 as a function of aging time t at the same three aging temperatures are illustrated in Fig 4.20. As well as seen for δ_0 a saturation of the Vickers hardness is obtained which is higher at lower T. The time t to reach saturation is likewise dependent on the aging temperature and shifts to longer times with decreasing aging temperature.

If precipitation effects were responsible for the results obtained so far on the alloy AZ81, the lower aluminium supersaturation in AZ61 should lead to a reduction in the driving force for precipitation (section 2.4) and in the volume fraction of $Mg_{17}Al_{12}$. In Fig. 4.21, the strain-independent damping δ_0 of AZ61 is plotted versus the aging time for the same aging temperatures as used for AZ81. The form of the curves is similar, i.e. the saturation effect is reached earlier when the aging temperature is higher and the magnitude of the change is greater at lower temperatures. However, the curves are shifted to significantly longer aging times as a result of the lower Al supersaturation.

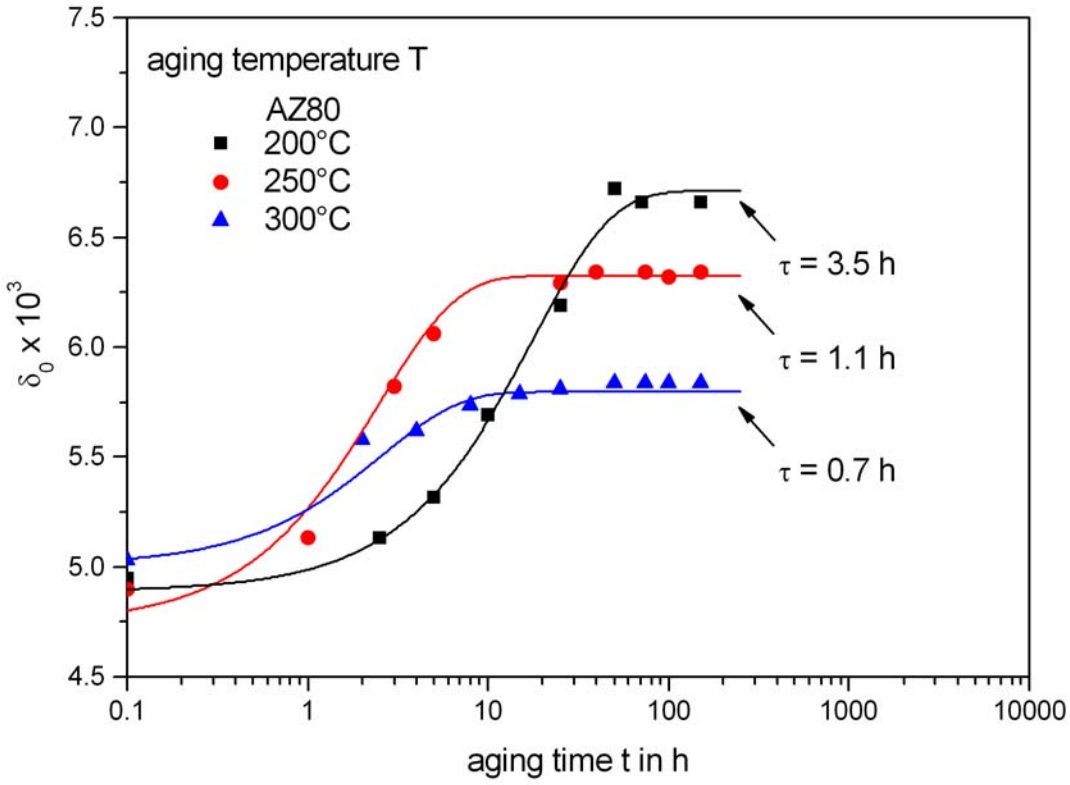

Fig. 4.19: Strain-independent damping δ_0 of AZ81 as a function of aging time t at different temperatures T

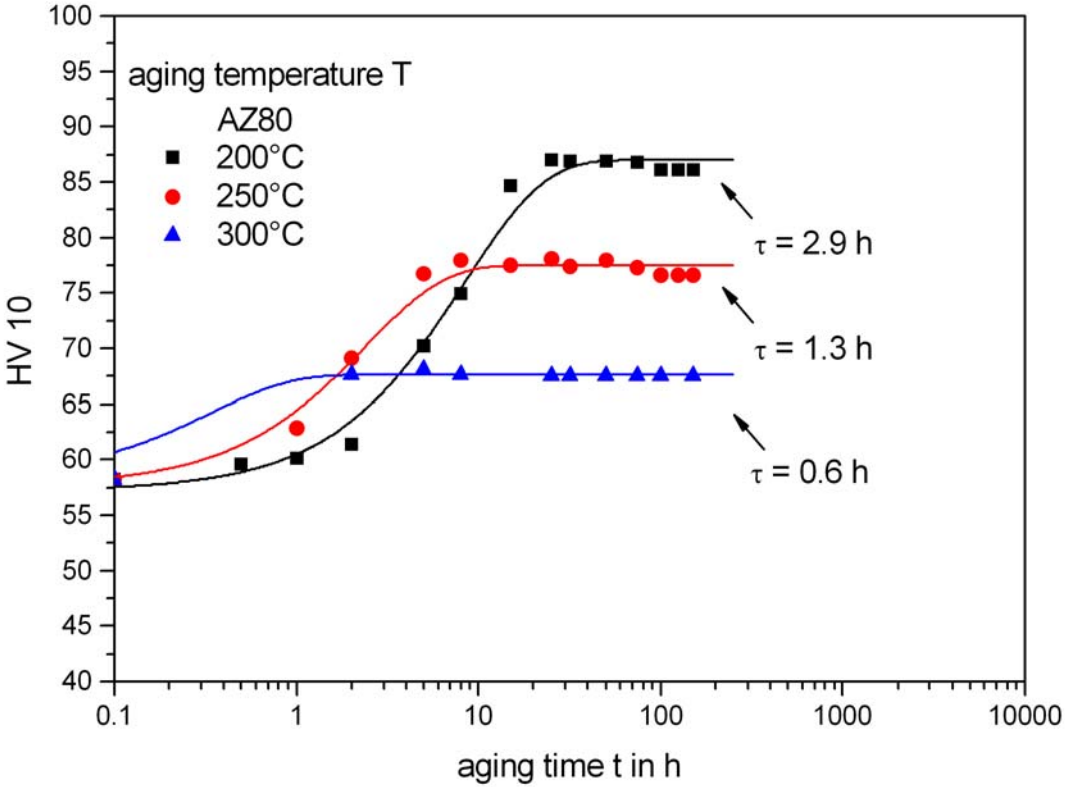

Fig. 4.20: Vickers hardness of AZ81 as a function of aging time t at different temperatures T

Table 4.4 summarises the constants from strain-independent damping (Fig. 4.19) and Vickers hardness (Fig 4.20) of Eq. 4.3 describing the kinetics of precipitation, where a_i is the value of the supersaturated solution solid and $a\infty$ is the value when the reactions is complete, m is a constant mainly dependent on the precipitates shape (see Eq. 4.3).

Table 4.4: Constants of Eq. 4.3 describing the kinetics of precipitation.

δ_0	a_i	$a\infty$	m
200ºC	4.888	6.7	0.195
250ºC	4.738	6.39	0.43
300ºC	5.0	5.79	0.27
HV			
200ºC	57.1796	86.98	0.345
250ºC	57.6	77.49	0.549
300ºC	58.29	67.64	1.63

Comparing the hardness data for AZ81 (Fig. 4.20) with those of AZ61 illustrated in Fig. 4.22, reveals that a reduction in aluminium content generally leads to a decrease in the hardness increment during aging. This is a result of the lower volume fraction of precipitates with an increased interparticle spacing as reported by Lagowski and Clark [Lag74, Cla68].

The results of measurements of the strain-independent damping δ_0 of the alloy AZ31 are shown in Fig. 4.23. At aging temperatures of 250 ºC and 300 ºC practically no dependence on either the aging time or the temperature can be observed. After aging at 150 ºC or 200 ºC, a small increase in the strain-independent damping was detected.

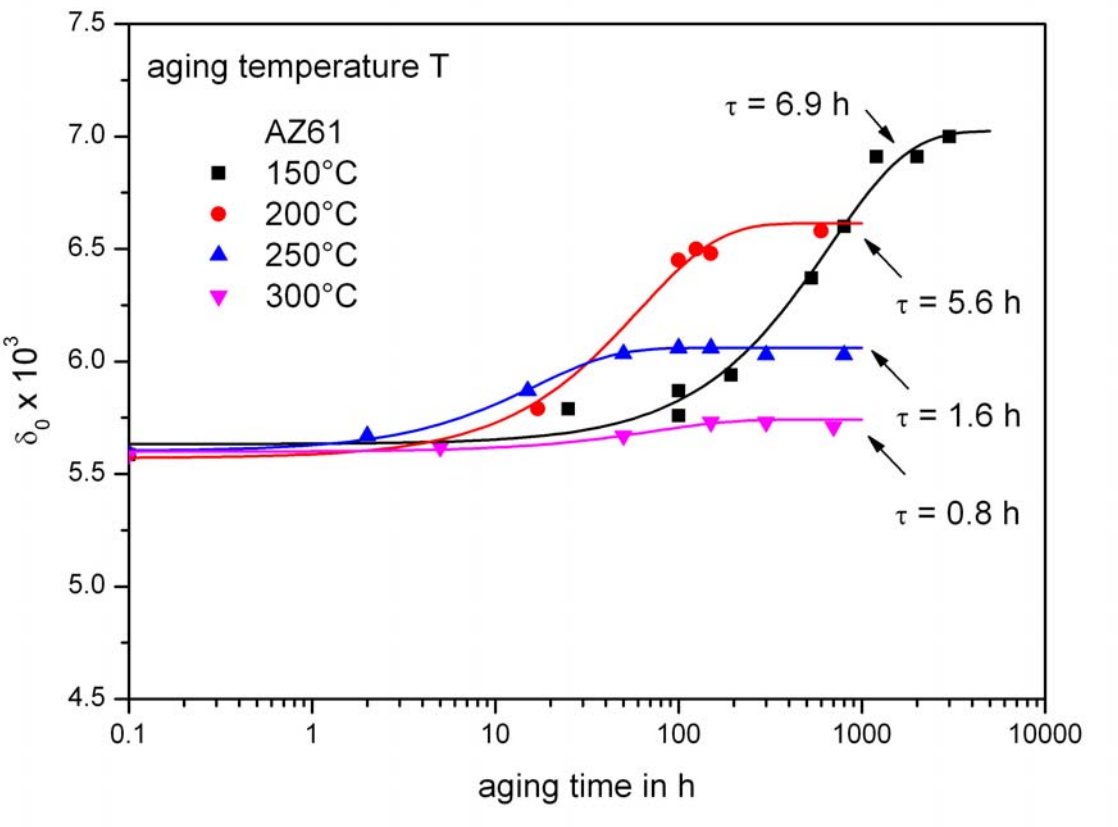

Fig. 4.21: Strain-independent damping δ_0 of AZ61 as a function of aging time t at different temperatures T

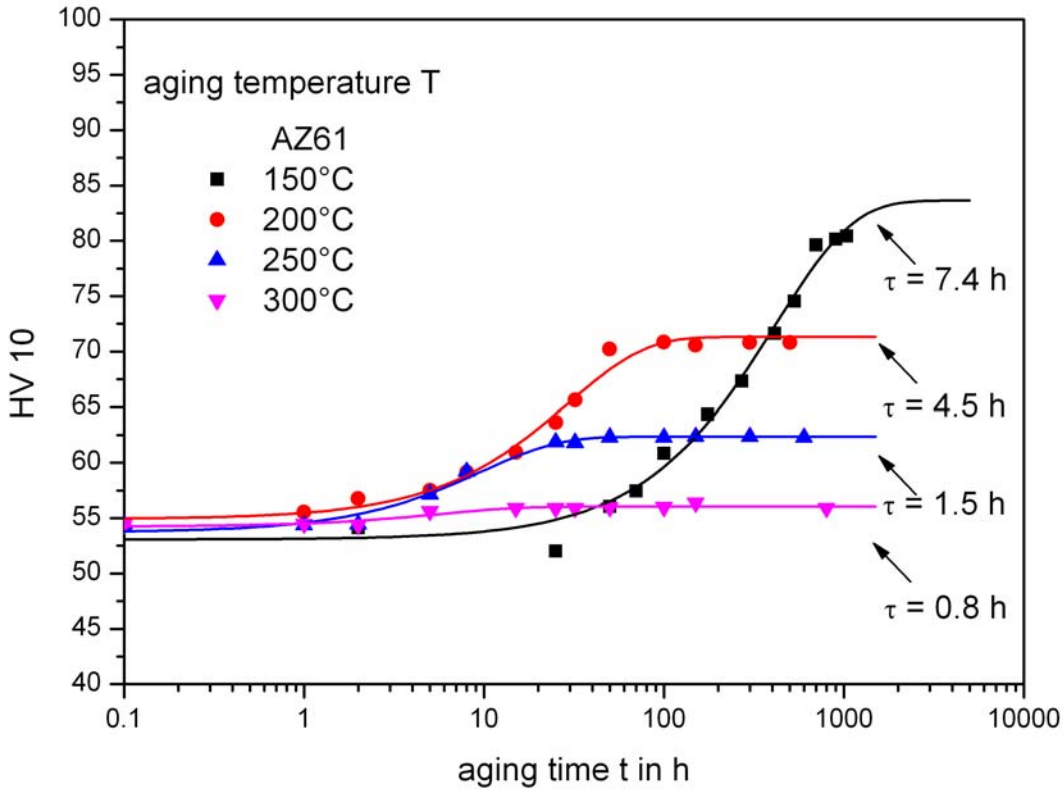

Fig. 4.22: Vickers hardness of AZ61 as a function of aging time t at different temperatures T

Table 4.5 summarises the constants from strain-independent damping (Fig. 4.21) and Vickers hardness (Fig 4.22) of Eq. 4.3 describing the kinetics of precipitation, where a_i is the value of the supersaturated solution solid and $a\infty$ is the value when the reactions is complete, m is a constant mainly dependent on the precipitates shape (see Eq. 4.3).

Table 4.5: Constants of Eq. 4.3 describing the kinetics of precipitation.

δ_0	a_i	$a\infty$	m
150ºC	5.6	7	0.01
200ºC	5.57	6.61	0.09
250ºC	5.6	6.0	0.09
300ºC	5.5	5.7	0.01
HV			
150ºC	53.07	83.63	0.017
200ºC	54.92	71.32	0.15
250ºC	53.72	62.34	0.1584
300ºC	54.24	55.3	0.14

After aging at 250 ºC and 300 ºC the hardness in AZ31 (Fig. 4.24) remains unchanged. The Mg-Al-Zn phase diagram (Fig. 2.9), which can be taken as a reference to determine the precipitation limits in the different alloys used in this work, indicates that the alloy AZ31 should consist of α-Mg without any $Mg_{17}Al_{12}$ phase at the given aging temperatures of 250 ºC and 300 ºC [Ave99]. From this point of view a drastic change in δ_0 or hardness would not be expected. However, at temperatures of 150 ºC and 200 ºC some age hardening due to precipitation is observed.

4.3.2 Microstructural Development during Aging

SEM micrographs of AZ81, AZ61 and AZ31 after aging at 250 ºC for 25 h are shown in Fig. 4.29. Fig. 4.25 a) and b) show the formation of colonies of discontinuous precipitation at grain boundaries. Very little continuous precipitation within the grains is observed. As expected, no significant precipitation of the β-phase occurs in the AZ31 alloy at this temperature. (Fig. 4.25 c) shows a small amount of precipitates on the grain boundary and this is possibly attributable to the slightly higher Al content of 3.3 wt. % as given in Table 1.

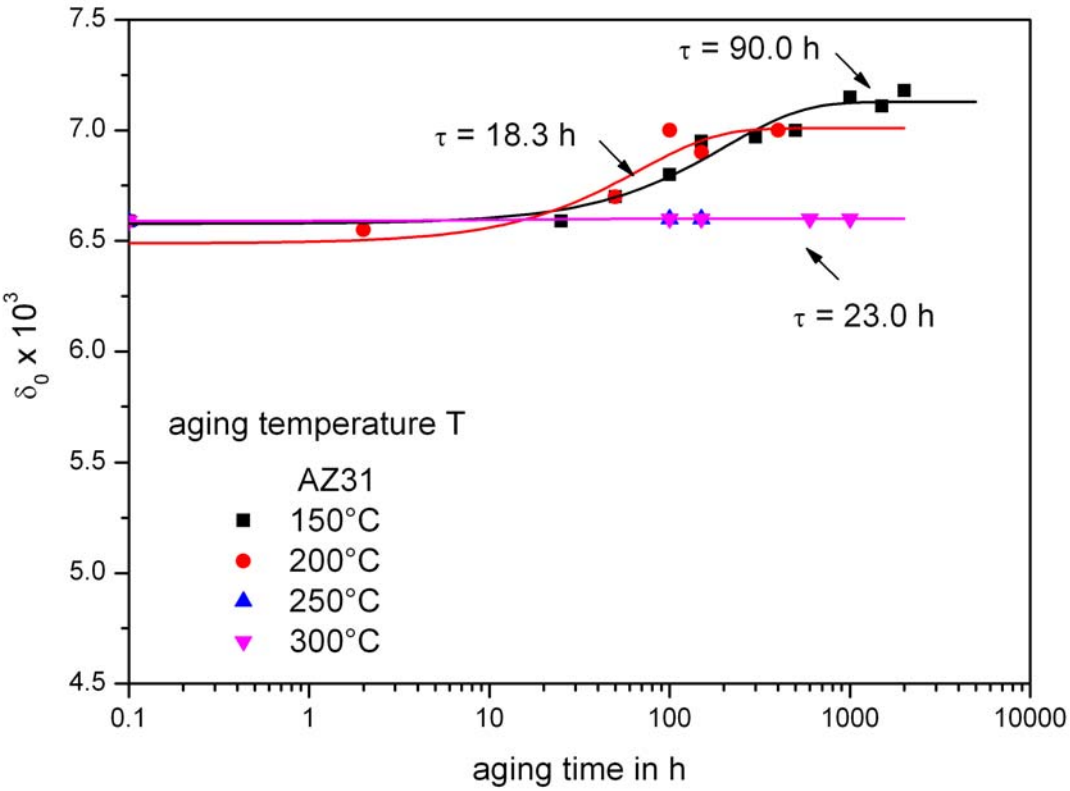

Fig. 4.23: Strain-independent damping δ_0 of AZ31 as a function of aging time t at different temperatures T

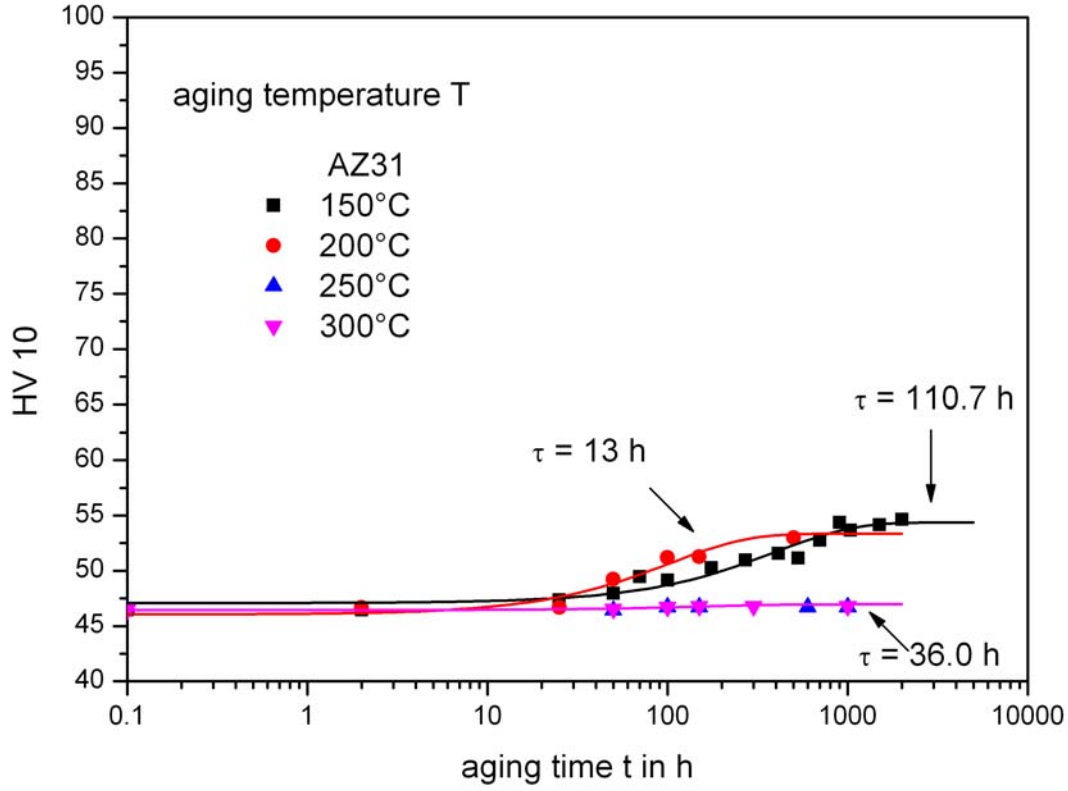

Fig. 4.24: Vickers hardness of AZ31 as a function of aging time t at different temperatures T

Table 4.6 summarises the constants from strain-independent damping (Fig. 4.23) and Vickers hardness (Fig 4.24) of Eq. 4.3 describing the kinetics of precipitation, where a_i is the value of the supersaturated solution solid and $a\infty$ is the value when the reactions is complete, m is a constant mainly dependent on the precipitates shape (see Eq. 4.3).

Table 4.6: Constants of Eq. 4.3 describing the kinetics of precipitation.

δ_0	a_i	$a\infty$	m
150ºC	6.57	6.488	0.44
200ºC	6.488	7.00	0.27
300ºC	65.8	65.801	1.4
HV			
150ºC	47.08	54.36	0.28
200ºC	46.04	46.44	0.12
300ºC	46.64	46.95	0.22

The dependence of the hardness on aging time and temperature can be attributed to the balance between precipitation hardening, loss of solid solution hardening and the lower volume fraction of precipitates at higher temperature, especially as the grain sizes of all samples were nearly equal. Based on these results it can be stated that both hardening and damping depend on the precipitate development as a function of time and aging temperature [Gon07]. The hardening effect increases with increasing aluminium content and decreases with increasing aging temperature. Moreover, saturation is reached at shorter aging times when the alloy is more highly alloyed. The lower the aging temperature, the later this saturation effect occurs.

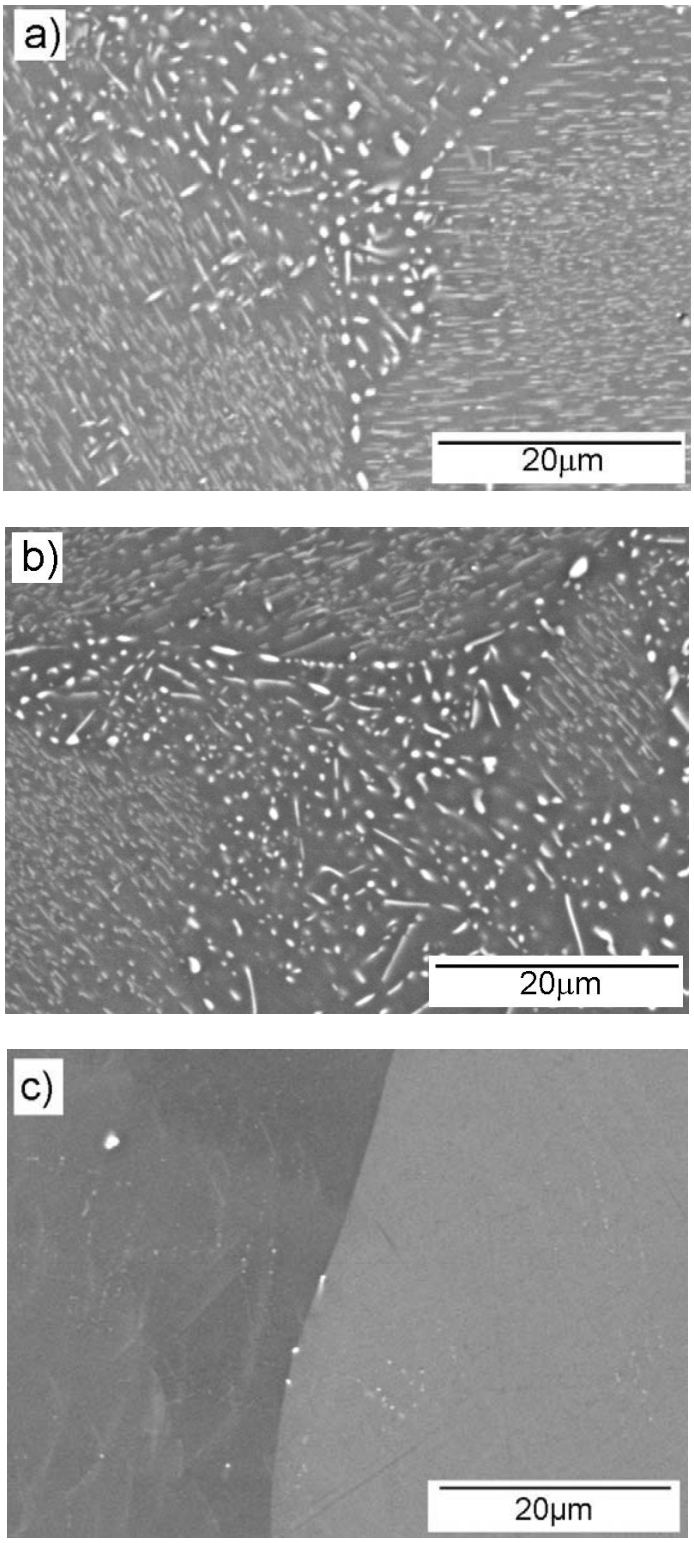

Fig. 4.25: SEM micrographs of a) AZ81, b) AZ61 and c) AZ31 aged for 25 h at 250 °C;

4.3.3 The Kinetics of Precipitation in Mg-Zn-Al Alloys

The changes in the strain-independent damping and hardness as a function of the aging time and temperature may be used to establish the kinetics of the diffusion-controlled precipitation process. The kinetics of the precipitation process are characterised by a more or less strong incubation period at the beginning, a period of high segregation rate followed by a continuous precipitation velocity at the end. The relationship between the degree of precipitation x and the aging time t can be quantitatively expressed by the Johnson-Mehl-Avrami (JMA) equation [Fer02, Avr39, Avr40, Böh68]:

$$x = 1 - \exp(-t/\tau)^m \qquad 4.1$$

in which τ is the time constant and m is a constant mainly dependent on the precipitate shape. x is defined by the relation:

$$x = \frac{a(t) - a_i}{a_\infty - a_i} \qquad 4.2$$

At a given temperature T, a_∞ is the residual aluminium concentration in the matrix when the reaction is complete, a_i is the initial aluminium concentration of the supersaturated solid solution and $a(t)$ the aluminium concentration (all values as atomic fraction) at a given time t. The Johnson-Mehl-Avrami equation was adopted to describe the measured time-dependent damping and hardness curves and can be written in the form:

$$a(t) = a_\infty - (a_\infty - a_i)\exp(-t/\tau)^m \qquad 4.3$$

The curves were fitted by Eq. 4.3, as shown in Figs. 4.19, 4.21, 4.23 (damping measurements) and Figs. 4.20, 4.22, 4.24 (hardness measurements). All measured points could be well described within the framework of this model. The time constant τ is smaller when the aging temperature increases. This is valid for AZ81 and AZ61 but not reasonable for AZ31 where a diffusion process to precipitates is negligible.

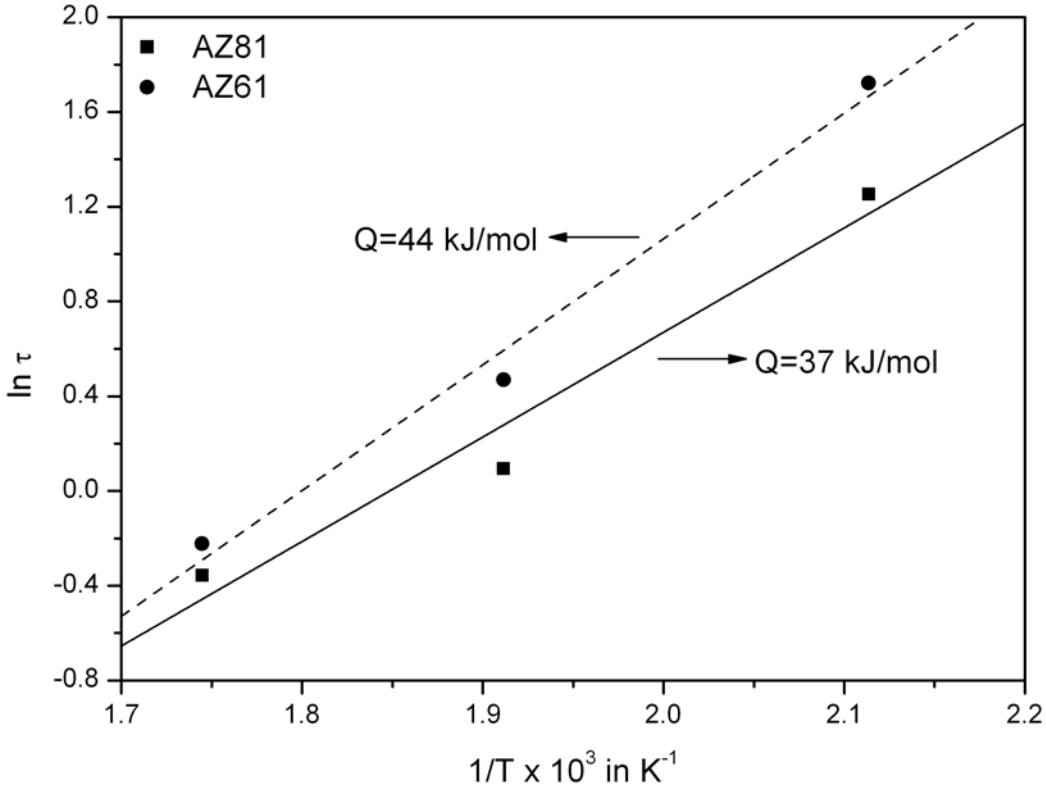

Fig. 4.26: Determination of the activation energy Q for the precipitation process using an Arrhenius plot

The time constant τ was taken to estimate the activation energy for the diffusion-controlled process according to the Arrhenius equation:

$$\tau = \tau_0 \exp\left(\frac{-Q}{RT}\right) \qquad 4.4$$

where τ is the time constant of the individually fitted damping measurements, Q describes the activation energy of the process, R is the gas constant and T the absolute temperature. In Fig. 4.26, the logarithmic time constant τ is plotted versus the reciprocal temperature $1/T$. The activation energy calculated from the slope of the fitted data points is about 40 kJ / mol.

4.4 The Effect of Aging after Extrusion

Magnesium alloys have great potential as structural materials for applications in the automobile industry; in particular Mg-Al-Zn alloys are of great interest due to their combination of light weight, adequate strength and relatively good formability and

weldability [Smi93]. However, the presence of defects such as porosity, inclusions and chemical inhomogeneities in Mg-Al-Zn castings can restrict their use. It has been reported that wrought alloys produced by extrusion generally have better mechanical properties than cast alloys [Zhe07].

Extrusion is a very competitive process for producing a wide variety of magnesium alloy profiles, such as bars, rods and tubes. Many of these profiles are used as parts in cars. During service, these parts are exposed to moderate temperatures and so may undergo aging and changes in their mechanical properties. Changes in the mechanical properties will have a direct effect on the useful lifetime of the material. Song et al. [Son06] have reported that as-extruded AZ31 has a longer vibration lifetime than AZ61, because less intergranular $Mg_{17}Al_{12}$ precipitates are present.

In order to minimise the effects of vibration as well as natural aging due to the high temperatures that can be reached in the interior of the automobile, high damping capacity in these profiles is very important to extend the component lifetime. Therefore the objective of this part is to study the effect of aging on the damping capacity of extruded Mg-Al-Zn alloys. After extrusion, samples were aged at four different temperatures in order to investigate the influence of the aging temperature on the time dependency of the strain-independent damping.

4.4.1 Damping and hardness curves

Fig. 4.27 shows the values of the strain-independent logarithmic decrement δ_0 as a function of aging time for the extruded AZ81 alloy. The results show that for all temperatures T the damping increases with increasing aging time and the time to saturation increases with decreasing aging temperature. However, saturation was reached in less time than that with the process (T6) shown in Fig. 4.19. The maximum value of the amplitude independent component δ_0 is also dependent on the aging temperature. It is reduced when T increases in all cases.

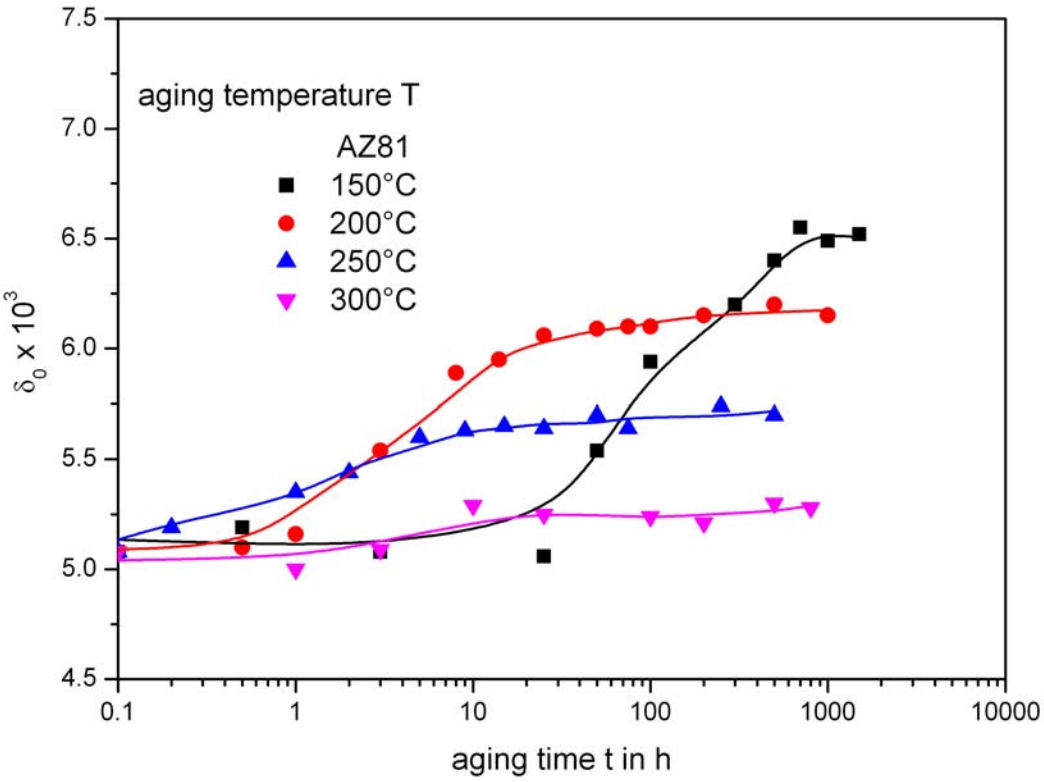

Fig. 4.27: Strain independent damping δ_0 of extruded AZ81 as a function of time t at different aging temperatures T

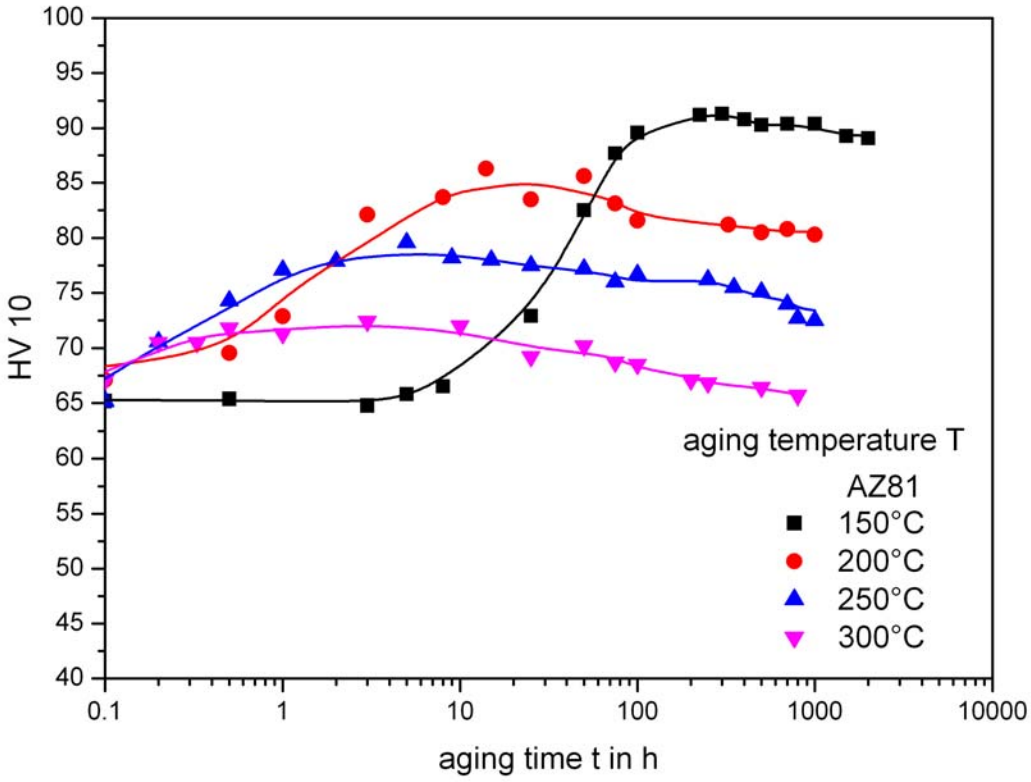

Fig. 4.28: Vickers hardness of extruded AZ81 as a function of time t at different aging temperatures T

Fig. 4.28 illustrates the corresponding hardness measurements on the alloy AZ81 as a function of the aging time at different aging temperatures T. The results show an increase in hardness and a dependence on aging temperature. i.e. the hardness increases when the aging temperatures decreases. The results show an acceleration of the precipitation process in comparison with the T6 treatment, see Fig. 4.20. This acceleration is mainly due to the finer grain size of the extruded alloys which is known to enhance the nucleation rate of colonies of discontinuous precipitates [Duly95]. The higher dislocation density of the extruded alloys will also affect the kinetics of precipitation with the dislocations acting as heterogeneous nucleation sites for the $Mg_{17}Al_{12}$ phase [Cla68 Dut02, Cer05, Gao03e, Hil98, Zha03, Zhe07].

After extended aging times the AZ81 specimens show a slight decrease in hardness and this drop was more clearly observed at higher aging temperatures. Both δ_0 (Fig. 4.27) and the hardness (Fig. 4.28) are dependent on the aging temperature and increase when the aging temperature decreases. A decrease in hardness with extended aging time was not observed in AZ81 after T6 heat treatments (Fig 4.20) or after direct aging of as-cast material (Fig 4.16).

In Fig. 4.29, the strain independent damping δ_0 is plotted versus the aging time for the AZ61 alloy. In contrast to the results for AZ81, the plots in Fig. 4.29 show a slight decrease in the strain-independent damping δ_0 in the initial stages of aging, which may be associated with a decrease in the dislocation density due to recovery processes. The decrease in the value of δ_0 becomes greater as the aging temperature is increased. In the later stages of aging as precipitation takes place the strain-independent damping δ_0 increases again. If we compare the results of AZ81 (Fig. 4.28) with those of AZ61 illustrated in (Fig. 4.30) a reduction in aluminium content generally leads to a decrease in the hardness increment on aging.

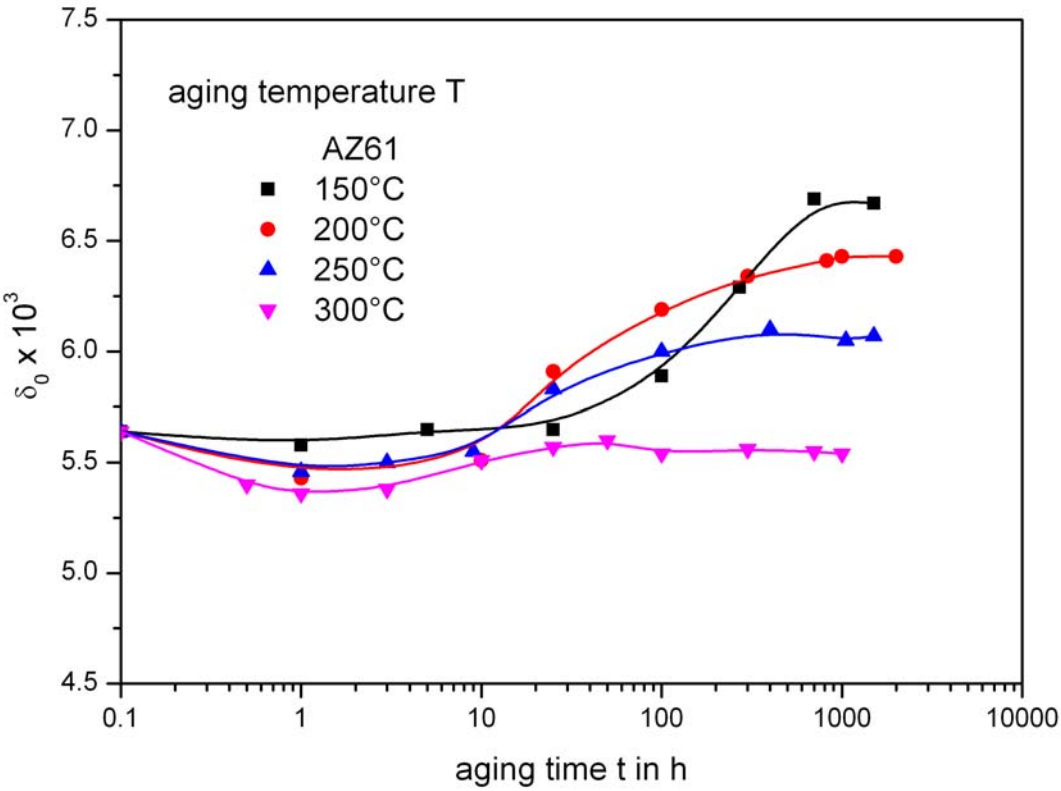

Fig. 4.29: Strain-independent damping δ_0 of extruded AZ61 as a function of time t at different aging temperatures T

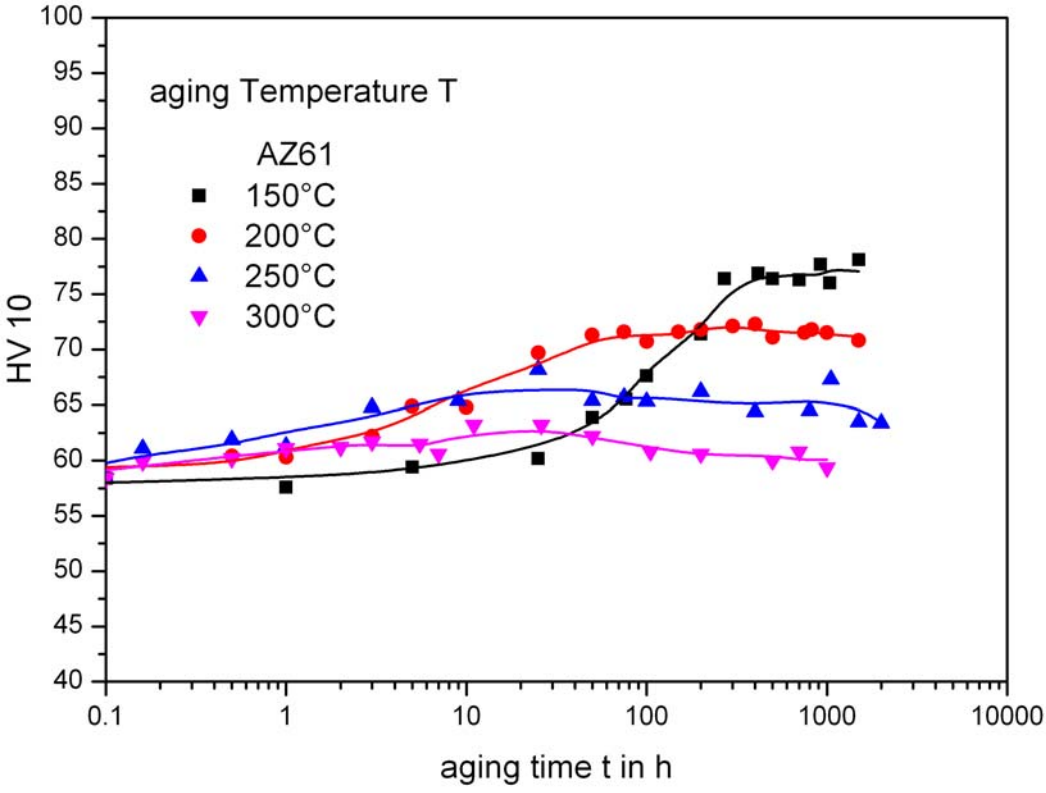

Fig. 4.30: Vickers hardness of extruded AZ61 as a function of time t at different aging temperatures T

The strain-independent damping δ_0 of the alloy AZ31 was also measured (Fig. 4.31) after similar aging treatments. δ_0 is observed to decrease at all aging temperatures with the exception of 150 ºC. At this temperature δ_0 remains virtually unchanged. This behaviour is probably a result of recovery and recrystallisation processes during heat treatment which lead to a reduction in dislocation density or possible changes in texture. In Fig. 4.32, the hardness plots for AZ31 do not show any changes with aging time. This is due to the lower aluminium content in comparison with the AZ61 and AZ81 alloys [Soh07]. However, it should be noted that after T6 aging treatments (Fig. 4.24) at 150 and 200 ºC slight hardness increases in AZ31 were recorded.

4.4.2 Microstructural Development during Aging

The microstructures developed after aging the extruded AZ81, AZ61 and AZ31 alloys are shown in Fig. 4.33. Colonies of discontinuous $Mg_{17}Al_{12}$ precipitates are observed in AZ81 and AZ61 after aging at 300 ºC for 25 hours. For AZ31, Fig. 4.33 c), no precipitation of $Mg_{17}Al_{12}$ occurs during aging at 300 ºC, in accordance with the Mg-Al phase diagram [Ave99].

The micrographs in Figs. 4.34 a)-b) show colonies of discontinuous precipitation with globular precipitation of the β-phase located mainly at the triple grain boundary junctions. This type of precipitation was reported by Crawley and Milliken [Cra74] and such precipitates are completely non-coherent with the matrix. In the AZ31 alloy, Fig. 4.34 c), precipitation of the β-phase was not observed, again in accordance with the binary phase diagram of the Mg-Al system. The occasional particles seen in Fig. 4.34 c) correspond to the inert, Mn-containing intermetallic phases formed during casting.

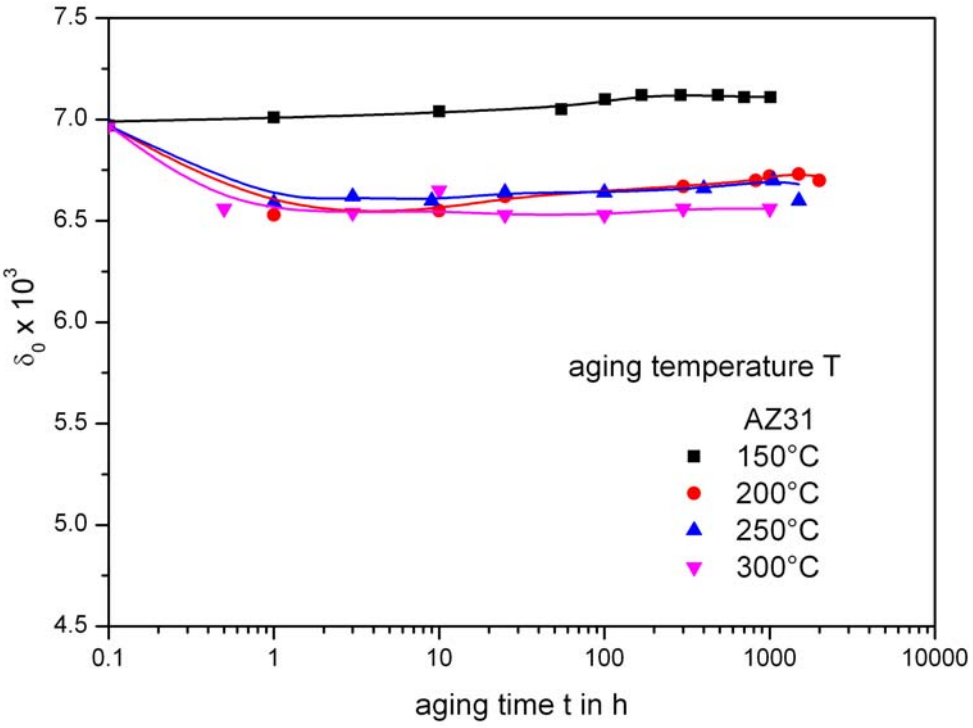

Fig. 4.31: Strain-independent damping δ_0 of extruded AZ31 as a function of time t at different aging temperatures T

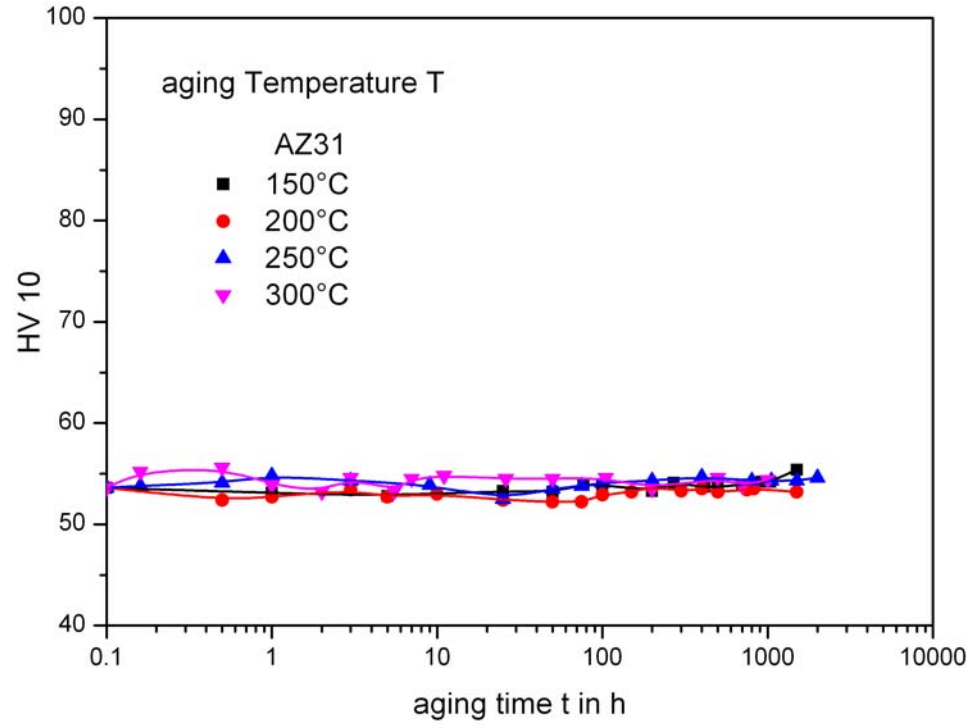

Fig. 4.32: Vickers hardness of extruded AZ31 as a function of time t at different aging temperatures T .

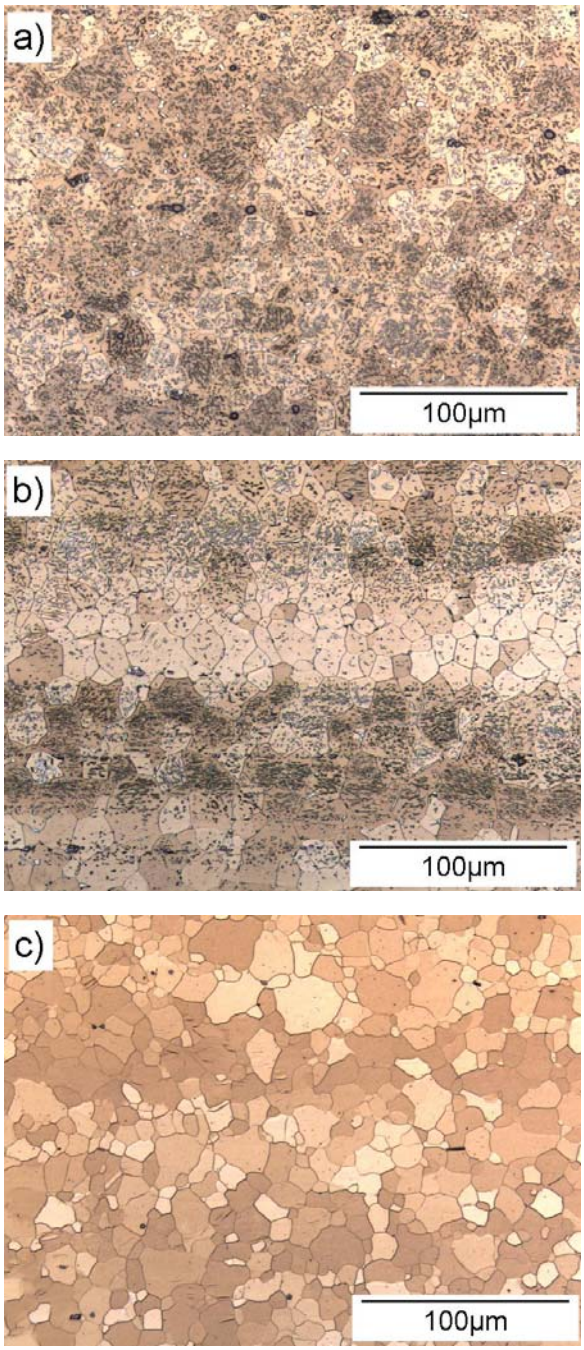

Fig. 4.33: Light micrographs of a) AZ81, b) AZ61 and c) AZ31 after indirect extrusion and aging at 300 ºC for 25 h

Fig. 4.34 shows SEM micrographs of the microstructures of the extruded AZ81, AZ61 and AZ31 alloys after aging for 25 h at 250 ºC.

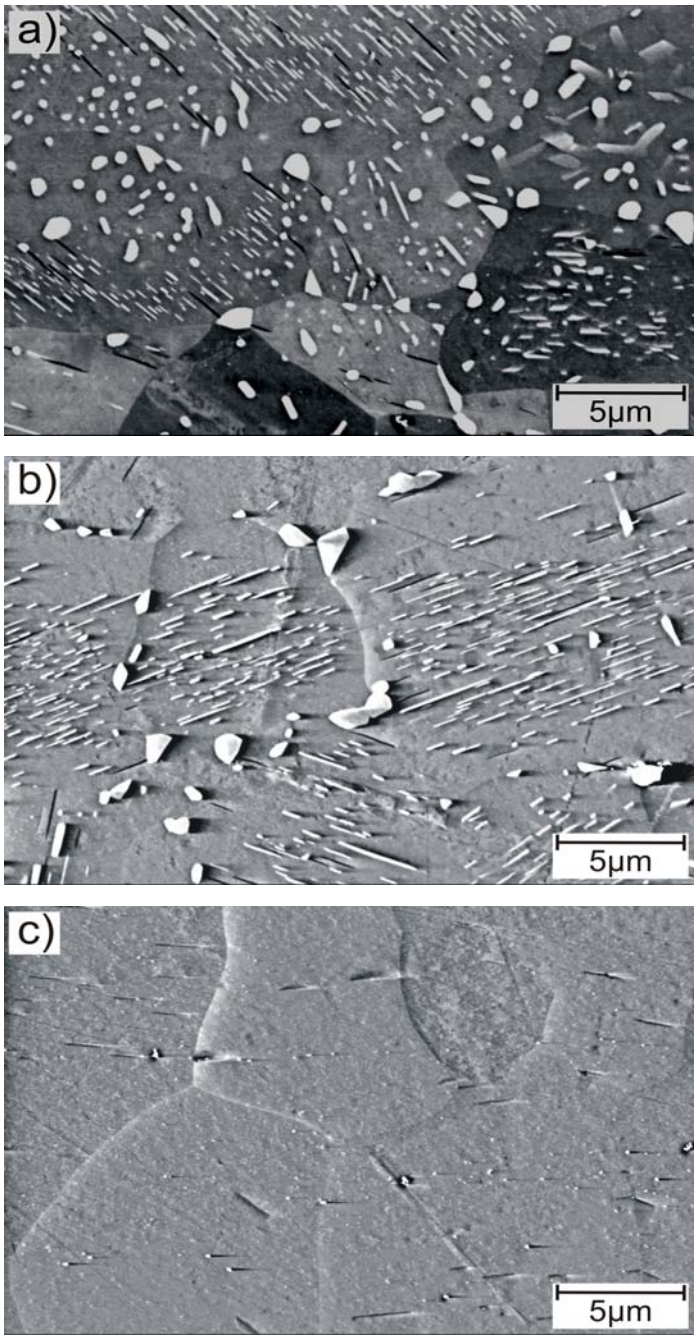

Fig. 4.34. SEM micrographs of a) AZ81, b) AZ61 and c) AZ31 after indirect extrusion and aging at 250ºC for 25h

In previous work on precipitation in AZ alloys overaging has not usually been observed [Cel00, Cla08]. However, the extruded AZ81 alloy specimens showed a drop in hardness after extended aging times that is more clearly observed at higher temperatures. This drop in hardness indicates coarsening of the precipitates.

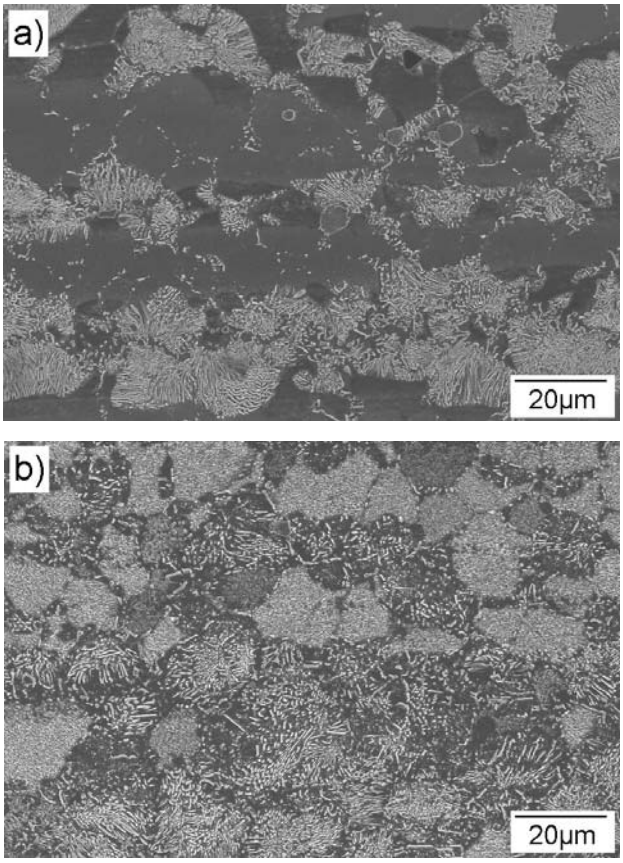

Fig. 4.35. SEM micrographs of AZ81 after indirect extrusion and aging at 150ºC for a) 50 h and b) 2000 h

Fig 4.35 shows SEM micrographs of the AZ81 alloy aged at 150 ºC for aging times of 50 and 2000 h. The evolution of microstructure with aging time at this temperature shows typical behaviour involving both continuous and discontinuous precipitation such that no noticeable drop in hardness is observed at long aging times. However at an aging temperature of 250 ºC (Fig. 4.36), coarsening of the discontinuously precipitated phase causes a change in morphology from lamellar to globular. The globular precipitates along grain boundaries coalesce and consume the discontinuous precipitates. This process leads to the observed drop in hardness after long aging times at this temperature. The hardness begins to decrease when the globular/nodular precipitation consumes the discontinuous precipitates.

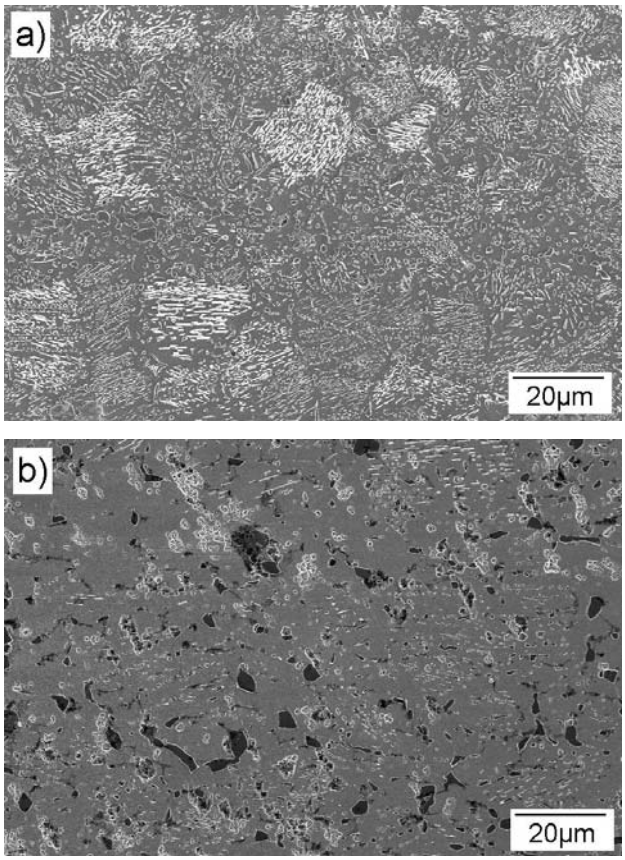

Fig. 4.36. SEM micrographs of AZ81 after indirect extrusion and aging at 250 ºC for a) 24 h and b) 2050 h

5 Discussion

The results obtained in this work suggest that both the AZ-series alloys and the binary Mg-Zn alloys show overall damping behaviour that is generally in accord with the Granato-Lücke model described in section 2.5. Before entering a discussion on the effects of aging treatments on the damping behaviour and hardness of the AZ alloys (Section 5.3), the role of alloy composition and processing on these properties is considered (Section 5.1). The effects of the alloying elements Al and Zn on the damping behaviour are discussed in more detail in Section 5.2, specifically for the regime in which the damping is independent of the strain-amplitude.

5.1 Effects of alloy composition and processing

The effects of processing history and alloying element content on the overall damping capacity of the AZ alloys can be illustrated using the measured damping curves of the alloy AZ31 as an example, Fig. 5.1. The most dramatic effects are seen in the shift of the strain-independent damping regime to higher strain amplitudes in the homogenised and extruded materials compared to the as-cast material. In the case of the extruded alloy the value of ε_{cr} is increased to such an extent that the transition to the strain-dependent damping regime is hardly detectable using the present experimental setup.

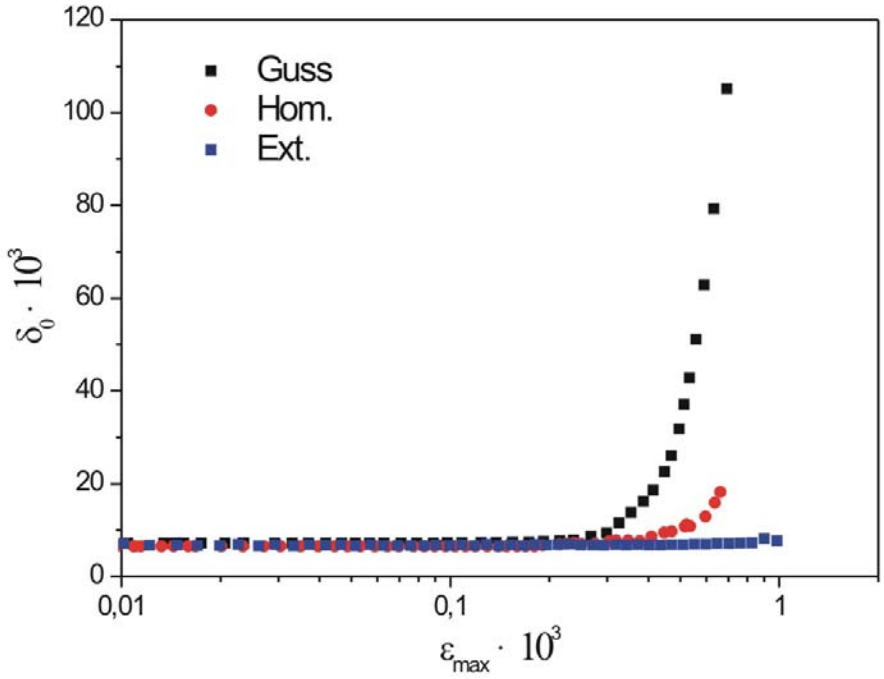

Fig. 5.1: Damping capacity of the AZ31 alloy in the as-cast, homogenised and extruded conditions

With increasing solute content of Al in the AZ alloys, the critical strains, ε_{cr}, for the transition to strain amplitude-dependent damping also increased significantly and the levels of δ_h achieved decreased substantially compared to pure Mg. These effects of the alloying elements Al and Zn are thus probably associated with solid solution strengthening, i.e. the hardening of the basal slip planes, as documented in the literature and described in section 2.2. The increase in ε_{cr} in the AZ alloys is clearly correlated with the increased Vickers hardness of the homogenised and extruded materials, as documented in Fig. 5.2, which serves to shift the onset of micro-plasticity to higher stress amplitudes. Fig. 5.2 also shows that for each of the alloys the hardness values in the as-cast and homogenised conditions are rather similar, whereas the hardness of the corresponding extruded materials is greater, probably as a result of their significantly finer grain sizes and the influence of their strong basal textures. In previous work on extruded AZ alloys similar damping behaviour was observed and was interpreted in terms of the fine grain sizes of the extruded materials [Gök05]. These initial experiments thus show that measurements at maximum strain amplitudes greater than $1 \cdot 10^3$ would be necessary if the strain amplitude-dependent damping behaviour of extruded samples were to be fully characterised.

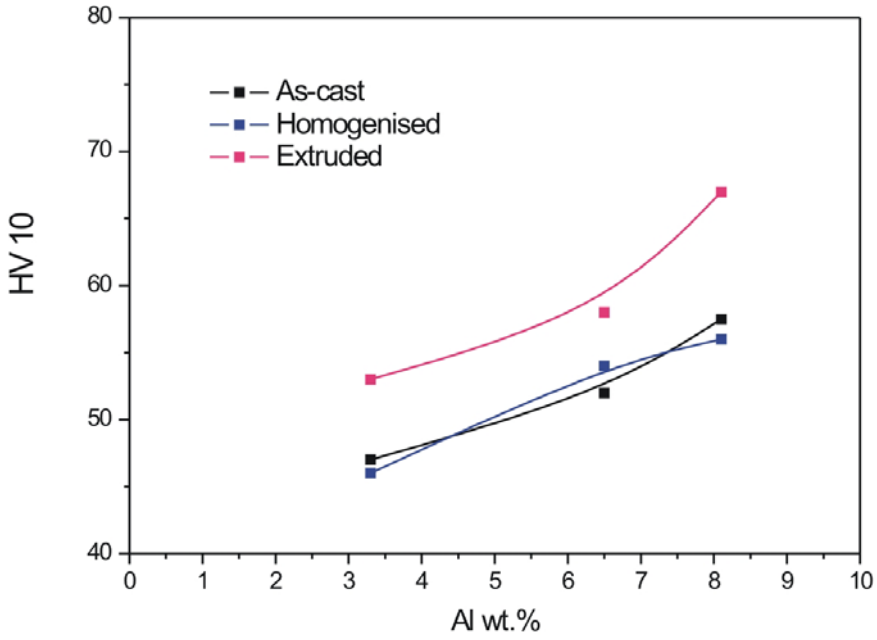

Fig. 5.2: Dependence of H_v on Al content of the AZ-alloys in the as-cast, homogenised and extruded conditions

In the case of the binary Mg-Zn alloys the damping curves of the homogenised and extruded samples showed similar characteristics, Figs. 4.8, 4.10, although the δ_0 and δ_h values measured were generally greater than in the AZ alloys. With increasing Zn content, ε_{cr} was observed to increase as a result of solid solution hardening. Again a shift of the strain-independent damping regime to higher strain amplitudes was observed in the extruded alloys compared to the homogenised material. However, the increase in ε_{cr} was not as great as in the AZ alloys so that a clear transition to a strain amplitude-dependent regime could be observed. Within this regime the extruded Mg-Zn alloys showed lower values of δ_h compared to the homogenised materials. These effects are again clearly correlated with the Vickers hardness of the homogenised and extruded materials, as documented in Fig. 5.3.

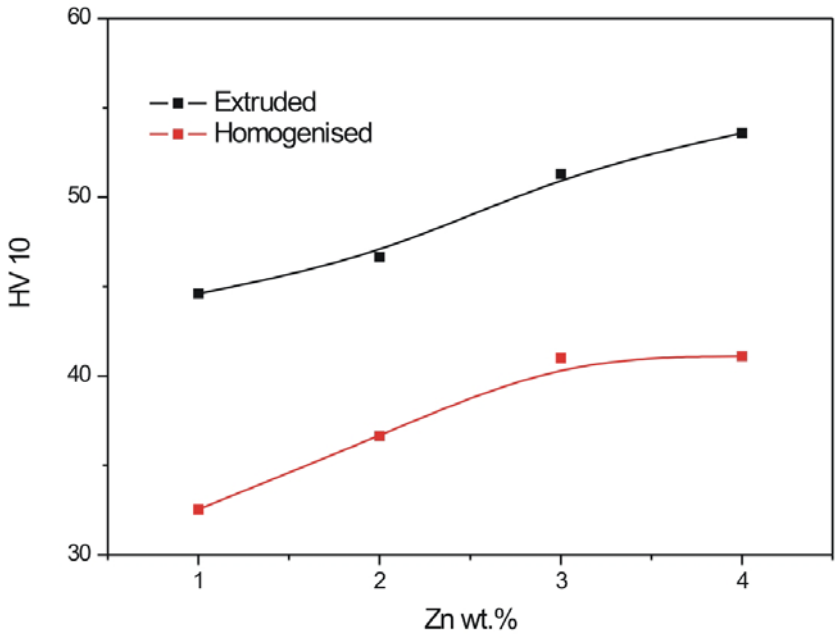

Fig. 5.3: Dependence of H_v on the Zn content of the alloys Z1, Z2, Z3 and Z4 in the homogenised and extruded conditions

The damping behaviour within the strain amplitude-independent regime is expected to depend only on the spacing of weak pinning points (solute atoms) and the dislocation density and other factors such as grain size and the presence of second phases should play a minor or secondary role. The effects of alloying additions of Al (2-8 wt. %) and/or Zn (1-4 wt. %) in solid solution on δ_0 are considerable. For comparison, unalloyed Mg samples measured under identical conditions showed δ_0 values of ~ 120 $\cdot 10^3$, i.e. a factor of around 10 times greater than the AZ or Mg-Zn alloys.

In Fig. 5.4, the results of the corresponding δ_0 measurements on the AZ alloys in the three starting conditions (as-cast, homogenised and extruded) are plotted as a function of the bulk Al content. Whereas the hardness increases with increasing Al content, δ_0 is seen to decrease.

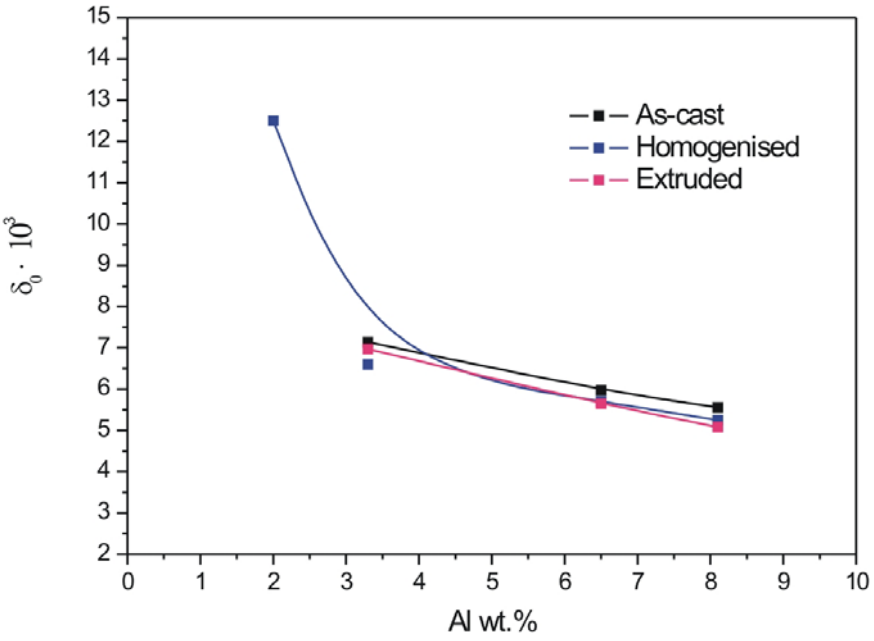

Fig. 5.4: Dependence of δ_0 on Al content of the AZ-alloys in the as-cast, homogenised and extruded conditions

The data points for the homogenised, single phase AZ alloys provide an empirical calibration curve which should enable δ_0 values to be converted to solute concentrations. The small deviations from this curve exhibited by the as-cast materials are assumed to arise from the fact that these samples are highly segregated and already contain some β-phase. However, the composition dependence of the δ_0 values is rather similar for the as-cast, homogenised and extruded materials.

In Fig. 5.5 the corresponding plot for the binary Mg-Zn alloys is shown. The results show that δ_0 decreases quite sharply with increasing Zn concentration in the homogenised alloys whereas the extruded materials have δ_0 values which are relatively independent of Zn content over the range 1-4 wt. % investigated.

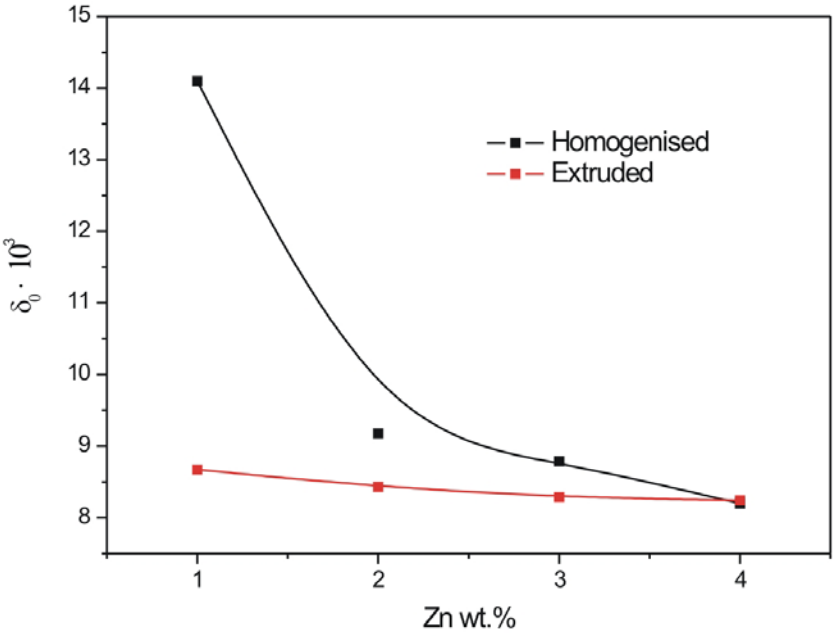

Fig. 5.5: Dependence of δ_0 on Zn content of the alloys Z1, Z2, Z3 and Z4 in the homogenised and extruded conditions

On the basis of this empirical correlation between δ_0 and alloy element concentration in solid solution it should therefore be possible to track the changes in the solute concentrations of Al and Zn in the matrix during the course of solid state precipitation of the β-phase in the AZ alloys.

5.2 Assessment of the factors responsible for the damping behaviour

It is generally assumed that the damping properties of Mg and its alloys at room temperature are mainly a consequence of dislocation damping and that the damping behaviour may therefore be interpreted qualitatively within the framework of the vibrating string model developed by Granato & Lücke. The value of the strain-independent logarithmic decrement δ_0 under these conditions is proportional to the product of the dislocation density ρ and the distance between weak pinning points (e.g. impurity atoms, clusters of atoms) on dislocations raised to the fourth power, l^4. As the strain amplitude increases beyond a critical value ε_{cr} dislocations are able to break away from the weak pinning points and the damping behaviour is characterised by an amplitude-dependent component δ_h. The overall form of all the damping curves measured in this work matches this expectation and the variations in δ_0, δ_h, and ε_{cr} as a function of alloy composition in both the AZ and binary Mg-Zn alloys would suggest that the Al and Zn atoms in solid solution are identifiable as the weak pinning points.

The known solid solution hardening effects of these elements, especially with regard to basal slip (section 2.3) would support this assumption as would the measured variation of hardness with solute element concentration (Figs. 5.2, 5.4). Compared to the magnesium sample of commercial purity referred to in section 5.1, the concentrations of pinning points in the alloys studied are orders of magnitude greater, being typically > 10^{20} per cm^3, so that it is not surprising that the δ_0, δ_h, and ε_{cr} values are changed dramatically. In general, it is thus concluded that the values of δ_h, and ε_{cr} measured can be qualitatively interpreted in terms of the breakaway and movement of dislocations foreseen by the Granato-Lücke model. However, the main emphasis in this work has been placed on measurements of δ_0 at strain amplitudes up to a maximum of ~ $1 \cdot 10^{-3}$ and before entering a discussion on the effects of aging it is necessary to examine more closely the factors determining the strain amplitude-independent damping in these alloys under the measurement conditions used.

The logarithmic decrement δ_0 measured is the sum of contributions from the following mechanisms:

δ_d – dislocation damping

δ_{th} – thermoelastic damping

δ_b – a background contribution from the measurement system

The purpose of the following calculations is to establish the magnitude of the thermoelastic damping contribution to δ_0 and how it is affected by alloy composition under the experimental conditions used for the measurements (sample thickness 2 mm and frequency ~ 38 Hz). Using the equations 2.8-2.11 presented in section 2.2.2 and literature data [Kam00, Bec39, Ave99] for the thermal conductivities and specific heats, the damping due to thermoelastic effects in the Mg and the Mg-Al-Zn alloys investigated in this work for a sample thickness of 2 mm can be calculated. It should be noted that there are uncertainties in the published data, especially with regard to the thermal conductivities so that the calculations are rather approximate in some cases. Therefore the thermal properties values in Table 5.1 have to be listed.

Table 5.1: Physical properties and calculated thermoelastic damping contributions for as-cast samples with 2 mm thickness and measurement frequency of 37 Hz

Alloy	Mg	AZ31	AZ61	AZ81	AZ91
κ (W m^{-1} K^{-1})	156	110	79.5	75.4	72
$C_{v.}$ (J m^{-3} K^{-1})	$1.78 \cdot 10^{6}$	$1.85 \cdot 10^{6}$	$1.89 \cdot 10^{6}$	$1.81 \cdot 10^{6}$	$1.81 \cdot 10^{6}$
α (° K^{-1})	$24.8 \cdot 10^{-6}$	$26.8\ 10^{-6}$	$27.3 \cdot 10^{-6}$	$27.2 \cdot 10^{-6}$	$27 \cdot 10^{-6}$
E (Pa)	$45 \cdot 10^{9}$	$45 \cdot 10^{9}$	$44 \cdot 10^{9}$	$44 \cdot 10^{9}$	$44 \cdot 10^{9}$
δ_{thmax}	$7.14 \cdot 10^{-3}$	$8.04\ 10^{-3}$	$7.98\ 10^{-3}$	$8.09\ 10^{-3}$	$7.98\ 10^{-3}$
f_0 (s^{-1})	34.32	23.3	16.5	15.99	15.27
$\delta\ th_f$	$7.12 \cdot 10^{-3}$	$7.16\ 10^{-3}$	$5.83 \cdot 10^{-3}$	$5.78\ 10^{-3}$	$5.6\ 10^{-3}$

For the AZ alloys, the results (see Table 5.1) indicate that the maximum thermoelastic damping δ_{thmax}, is slightly higher compared to unalloyed magnesium, mainly as a consequence of their slightly higher thermal expansion coefficients. However, the maximum thermoelastic damping is practically independent of alloy composition. In the case of the binary Mg-Zn alloys the calculations show that the thermoelastic damping behaviour is rather similar. The maximum thermoelastic damping corresponds to ~ $8.12 \cdot 10^{-3}$.

On the other hand, the frequency f_0 at which the thermoelastic damping has its maximum decreases significantly as the Al content is raised. The f_0 value of unalloyed magnesium – 34 Hz - is reduced progressively to 15-16 Hz in AZ91. This is a result of the strong influence of aluminium in solid solution on the thermal conductivity of magnesium as shown schematically in Fig. 5.5 [Bec39]. The data also reveal a significant effect of the amount of aluminium in solid solution on the thermal conductivity. As-cast materials have higher thermal conductivities than annealed (homogenised) materials. Fig. 5.6 also indicates that the effect of Zn on the thermal conductivity of Mg is less strong than that of Al. Using published data for the commercial alloy ZK60 (4.8-6.2 wt. % Zn, 0.45 wt. % Zr), an f_0 value of 25.2 Hz and a thermoelastic damping contribution of ~ $7.5 \cdot 10^{-3}$ can be estimated for the Mg-4 wt. % Zn alloy investigated in this work

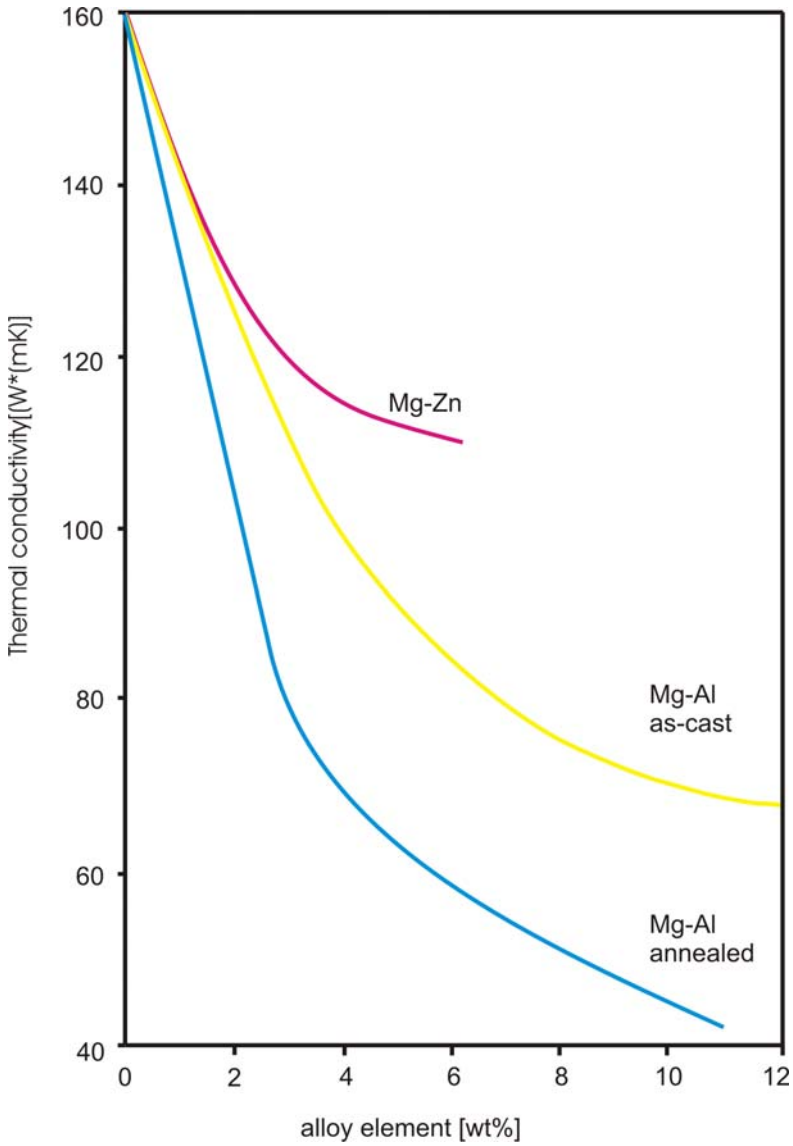

Fig. 5.6: Effect of aluminium and zinc on the thermal conductivity of magnesium [Bec39]

If we now compare the measured values of δ_0 with the calculated values of the thermoelastic damping, the following conclusions can be drawn:

In unalloyed, as-cast magnesium, the measured value of δ_0 ($120 \cdot 10^{-3}$) is far greater than the calculated thermoelastic damping contribution of $\approx 7 \cdot 10^{-3}$ (see Table 5.1). In this case, it is clear that the strain amplitude-independent damping is predominantly a result of dislocation damping and can be interpreted in terms of the Granato-Lücke model. In the as-cast AZ31, AZ61 and AZ81 alloys the measured values of δ_0 (see Table 4.2) are comparable with the calculated thermoelastic damping contributions and dislocation damping effects are effectively masked. In the as-cast alloys AZ21 and the Mg-Zn series with lower solute contents the measured values of δ_0 suggest that dislocation damping plays a measurable role.

In the case of the homogenised AZ alloys 31, 61 and 81, the values of δ_0 measured on samples with 2 mm thickness and frequencies 37-38 Hz range between 5.25 and $6.6 \cdot 10^{-3}$ (Table 4.3). The calculated values of the thermoelastic damping contribution shown in Table 5.2 indicate that again the main contribution to the measured values of δ_0 is due to thermoelastic damping.

Table 5.2: Calculated thermoelastic damping contributions for homogenised samples with 2 mm thickness and measurement frequency of 37 Hz

Alloy	**Mg**	**AZ31**	**AZ61**	**AZ81**	**AZ91**
κ (W m^{-1} K^{-1})	156	80	59	52	48
f_0 (s^{-1})	34.32	16.97	12.25	11.28	10.41
$\delta\ th_f$	$7.12 \cdot 10^{-3}$	$5.99 \cdot 10^{-3}$	$4.66 \cdot 10^{-3}$	$4.41 \cdot 10^{-3}$	$4.06 \cdot 10^{-3}$

Some additional experiments were made on samples of AZ31 and AZ80 with other thicknesses (2.5 or 3 mm) and measurement frequencies of 52 and 67 Hz.

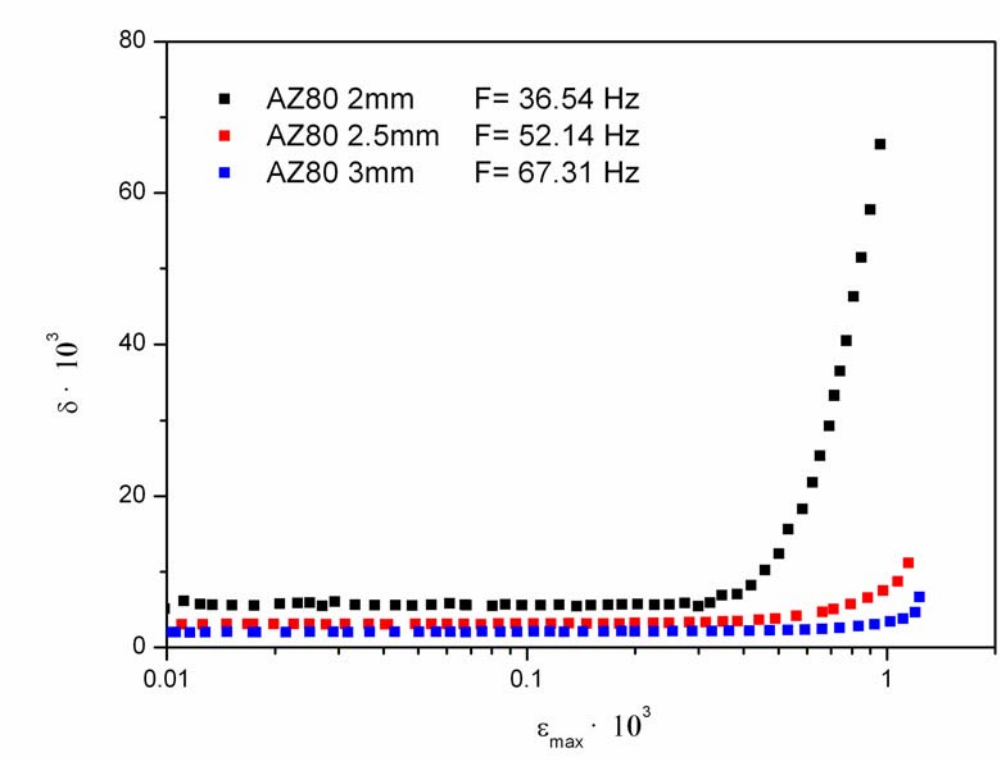

Fig. 5.7: Damping curves for samples of AZ80 with different thicknesses and measurement frequencies

Under these experimental conditions, we would expect the thermoelastic damping contribution to be lower as the measurement frequency is further away from f_0 (the frequency at which the thermoelastic damping has its maximum). The damping curves shown in Fig. 5.7 for the alloy AZ80 indeed demonstrate that δ_0 decreases significantly with increasing sample thickness and measurement frequency.

Göken and Riehemann made an extensive study of the role of thermoelastic effects in the damping behaviour of the alloy AZ91 [Gök02b]. Measurements of δ_0 were made over a wide range of frequencies with different sample thicknesses and this enabled the characteristic Debye curve to be established in a plot of δ_0 against the product of the measurement frequency and the square of the sample thickness (see Fig. 5.7).

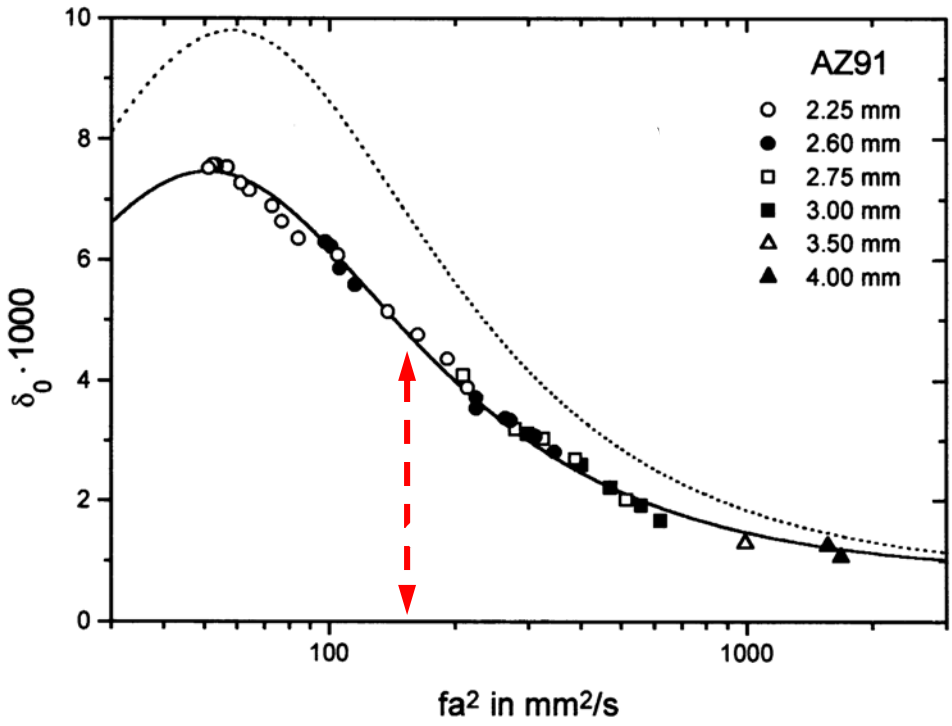

Fig. 5.8: δ_0 as a function of fa^2 for the alloy AZ91 [Gök02b]

In this plot, the full line describes the measured values and the dotted line the calculated thermoelastic damping based on physical property data [Ave99]. On the basis that δ_0 is the sum of all possible damping contributions these authors thus concluded that after subtracting δ_{th} and $\delta_{background}$ (estimated to be of the order of $0.5 \cdot 10^{-3}$), the contribution due to dislocation damping would correspond to $\sim 0.8 \cdot 10^{-3}$. In a previous investigation on the same alloy [Buc92] an even smaller value of

~$0.2 \cdot 10^{-3}$ was reported. These results thus support the conclusion that the present measurements on the AZ alloys were performed in the regime where thermoelastic effects are dominant (included in Fig. 5.7 is a red arrow indicating the value of fa^2 used in the present work). Within the limits of uncertainty of the thermo-physical data for f=37Hz and d=2mm of the AZ alloys, certain trends can be identified, e.g. the thermoelastic damping decreases with increasing Al content as a result of the decrease in thermal conductivity (see Table 5.1) and this trend is seen in the values of δ_0 measured for AZ21, AZ31, AZ61 and AZ81. In contrast, removal of Al from solid solution as a result of precipitation during casting, thermo-mechanical treatment or aging will lead to an increase in thermal conductivity κ of the matrix. As a consequence, the frequency f_0 at which the thermoelastic damping has its maximum effect will be increased. The position of the Debye peak will therefore be shifted to higher frequencies closer to the measurement frequency used and the magnitude of the thermoelastic damping will increase. The calculations show that such changes in the thermoelastic damping make a major contribution to the effects of aging on the δ_0 values measured. Changes in δ_0 will also result from a decrease in the number of weak pinning points (solute atoms) according to the Granato-Lücke model but under these circumstances, these changes cannot be accurately quantified. If it is assumed that the thermal conductivity is only dependent on the concentration of Al (and Zn) in the matrix and is largely unaffected by the formation of the β-phase, then the measured values of δ_0 can be used to follow the time dependency of the solute content of the matrix during the course of the precipitation reaction, as will be discussed in the next section. In this context, the use of 2 mm thick samples for the measurements is advantageous as the following example shows. An AZ80 sample with thickness 2 mm and a measurement frequency of 37.5 Hz has a δ_0 value of $4.9 \cdot 10^{-3}$ in the homogenised condition. After aging for 18 h at 250 ºC the δ_0 value increases to $6.3 \cdot 10^{-3}$. The corresponding values for a 3.07 mm sample and a measurement frequency of 71 Hz are $1.83 \cdot 10^{-3}$ and $2.4 \cdot 10^{-3}$ respectively. Measurements of δ_0 made on 2 mm samples are thus more sensitive to the effects of aging because with the change of δ_0 mainly the change of the thermal conductivity is measured.

The recognition that thermoelastic effects can be important in the determination of the strain-independent damping of the AZ alloys has consequences when comparing the measured values of δ_0 reported in the literature by various authors [Wat04, Liu07].

The absolute values of δ_0 are clearly dependent on the experimental setup used in terms of sample thickness and measurement frequency only for vibration beams on transversal (a) heat flow. For example, in the (sample thickness 1 mm, and f = 1 Hz a δ_0 value of ~ $2 \cdot 10^{-3}$ has been reported for as-cast AZ31 [Wan09]. This compares with a value of $7.14 \cdot 10^{-3}$ measured in the present work (Table 4.2).

5.3 Effects of aging on the damping and hardness of AZ alloys

In the following discussion, the precipitation reaction in the AZ alloys after solution treatment and aging (T6) is first considered, subsection 5.3.1. The effects of aging on the damping behaviour and hardness of as-cast and extruded materials will be discussed in the next subsection 5.3.2.

5.3.1 Aging of solution treated AZ alloys

Precipitation hardening is obtained by a fine dispersion of precipitates which are able to obstruct the movement of matrix dislocations. As a consequence, the dislocation mobility is modified by precipitation [Mar68]. Previous work on the age hardening of Mg-Al alloys has been mainly concentrated on the behaviour of the AZ91 alloy and binary alloys with 6-9 wt. % Al [Cel97 Celo00, Cel01]. The focus of these studies was on the effect of continuous precipitation on the mechanical properties so that most work has been carried out using a maximum aging temperature of 200 ºC. At this aging temperature and lower temperatures the nucleation rate of the continuous precipitates in the AZ91 alloy with its high solute supersaturation is high enough for the precipitation reaction to be dominated by the formation of continuous precipitates and the growth of colonies of discontinuous precipitates at grain boundaries ceases at an early stage of the reaction. Under these conditions, aging generates precipitation hardening effects [Cel00] with increments in peak hardness in the range 25-45 (Vickers). However, at aging temperatures greater than 200 ºC the supersaturation is lower and cannot maintain the necessary nucleation rate for continuous precipitation so that the discontinuous precipitation process begins to dominate, as shown by the precipitate morphology diagram (Fig. 2.11).

In the case of the alloys AZ81 and AZ61, the aluminium supersaturation is lower than in AZ91 so that the aging temperature at which the discontinuous precipitation

reaction begins to dominate will be lower. Close inspection of Fig. 2.11 reveals that for the alloy AZ81 and the aging temperatures used between 200-300 ºC, the discontinuous reaction dominates. Only at 150 ºC is some degree of continuous precipitation expected. Moreover for the alloy AZ61 the diagram indicates that discontinuous precipitation will predominate over the range of aging temperatures 150-250 °C. Only at the highest aging temperature of 300 ºC is a small contribution from heterogeneously nucleated, continuous precipitation anticipated. Fig. 2.11 also suggests that the low volume fraction of precipitates formed in the alloy AZ31 at an aging temperature of 150 ºC may originate from both discontinuous and continuous precipitation mechanisms. Although predictions made on the basis of Fig. 2.11 apply to binary Mg-Al alloys it appears that the 1 wt. % Zn addition in these AZ alloys has no significant effect.

It is therefore concluded that the changes in δ_0 and Vickers hardness of the solution treated AZ61 and AZ81 alloys measured as a function of aging time and temperature in this work are generally associated with the precipitation of the β-phase. The hardening produced by the formation of precipitates is offset by the loss in solid solution hardening as aluminium atoms are removed from the matrix during aging. As discussed in the previous section, the increases in δ_0 are associated with the removal of Al (and Zn) atoms from solid solution. In the case of the AZ81 and AZ61 alloys, the solute supersaturation controls the time and temperature dependencies of the changes in hardness and δ_0. The greatest changes in these properties are therefore achieved at the lowest aging temperatures and the longest times, for which the volume fraction of β precipitates is greatest and the residual Al content of the matrix is lowest. This is consistent with the phase diagram which indicates that the solid solubility of aluminium decreases substantially from ~ 5.4 wt. % at 300 ºC to ~ 1.75 wt. % at 150 ºC. As noted, the hardness and δ_0 remain largely unchanged in the AZ31 alloy except for some minor effects after aging at 150 ºC. The aluminium supersaturation at this temperature is low and the resulting precipitate volume fraction is low.

The activation energy for the precipitation reaction can be calculated if the time to reach a fixed amount of transformation, X, at various temperatures can be measured, as reported in section 4.3.3. Implicit in this analysis is the assumption that the property measured has a linear relationship with the precipitate volume fraction (or

alternatively the residual solute concentration in the matrix). For example, the time to reach peak hardness is usually taken as the time required for 100 % precipitation. For continuous precipitation at 200 ºC in binary Mg-Al alloys and AZ91, Celotto et al. [Cel97] have shown using NMR techniques that only ~ 50 % of the available aluminium atoms have precipitated by the time peak hardness is achieved. This is a consequence of the fact that peak hardness represents a balance between a gain due to precipitation hardening and a loss in solid solution hardening as aluminium is removed from solid solution. On the basis of transmission electron microscopy work by Celotto [Cel00], Hutchinson et al [Hut05] have modelled the kinetics of continuous precipitation in AZ91 at 200 ºC and were able to show that volume diffusion (self-diffusion energy of magnesium 134 kJ / mol [Sch56]) is rate controlling. It should be noted that application of the usual Arrhenius analysis of the temperature dependence of the kinetics is not a simple matter in this situation because already at 220 ºC the precipitation reaction becomes predominantly discontinuous in nature and at lower temperatures than 200 ºC the times to completion of the continuous precipitation reaction are prohibitively long.

In the AZ61 and AZ81 alloys studied, the discontinuous precipitation reaction predominates in the range of aging temperatures used and the Arrhenius analysis enabled an activation energy of ~ 40 kJ/mol to be determined (section 4.3.3) for the process. This value is less than a third of the self-diffusion energy of magnesium and is physically unreasonable. It is therefore necessary to question the assumptions made in this analysis. The determination of the kinetics of a discontinuous reaction can be complicated by the fact that the changes in macroscopic properties measured represent average values obtained from a mixture of transformed regions (the growing colonies of α + $Mg_{17}Al_{12}$ and the untransformed matrix. In the case of Vickers hardness measurements this is usually not a problem providing the hardness indents are large enough to sample both transformed and untransformed regions. The observation that the time and temperature dependence of the measured changes in both the hardness and δ_0 are correlated suggests that the aging curves do provide a valid representation of the changes in volume fraction and residual Al content of the alloys investigated. A similar conclusion was reached by Duly [Dul92] in a study of the macroscopic kinetics of the discontinuous precipitation in a Mg-8.5 wt. % Al alloy with regard to hardness and lattice parameter measurements. The analysis described in section 4.3.3 is also based on the assumption that the aging

time required to reach a saturation in the property measured is an indication of the time needed to achieve 100 % transformation. This assumption can be critically evaluated with the help of the information contained in Fig. 5.4 which provides an empirical relationship between the measured value of δ_0 and the aluminium content of the matrix. For example, aging of the alloy AZ61 at 200 ºC gives rise to a maximum value of δ_0 which corresponds to an aluminium content in the matrix of ~3.4 wt. %. However, according to the phase diagram (Fig. 2.9) the equilibrium aluminium content in the matrix following completion of the discontinuous precipitation reaction should be ~2.5 wt. %. This discrepancy indicates that in this case only 77.5 % of the equilibrium volume fraction of the β-phase has formed. Comparisons made on this basis for all the data used in the analysis of the kinetics indicate that on average the aging curves represent a discontinuous reaction which generates ~ 80 % of the equilibrium volume fraction of the β-phase. The main consequence of this is that the calculated activation energy for the process is increased from ~ 40 kJ / mol to ~ 60 kJ / mol, a value which is approximately half of the self diffusion energy of magnesium, i.e. a value which would correspond to the energy for grain boundary diffusion. This is entirely consistent with the generally well established mechanism of discontinuous precipitation in which the diffusion process occurs at the moving colony interface in the absence of volume diffusion in the untransformed matrix [Dul92, Por77]. Furthermore these authors provided direct evidence using TEM-based microanalytical techniques that the matrix phase in the discontinuous two-phase aggregates in Mg-Al alloys remains supersaturated in aluminium in support of the conclusions made above.

5.3.2 Aging of as-cast and extruded AZ alloys

One of the main objectives of this work was to compare the behaviour of as-cast, homogenised and extruded AZ alloys with regard to the effects of aging on the damping capacity and hardness.

As far as the overall damping behaviour is concerned, some insight into the effects of aging on the damping in the strain-independent regime could be obtained in the case of the as-cast AZ61 alloy. For example, the curves presented in Fig. 4.12 for the as-cast AZ61 alloy after isochronal aging reveal damping behaviour in the strain-dependent regime that suggests that δ_h depends on two mechanisms. The first

mechanism has already been discussed and interpreted as the mechanical unpinning of dislocation segments as foreseen by the Granato-Lücke model. It results in an approximately exponential curve (δ_h) as is observed for the as-cast material and the samples aged in the temperature range 50–200 ºC. After aging treatments at 250 and 300 ºC a drastic decrease in damping is observed. This suggests that the mobility of the newly generated dislocations is restricted by the precipitates formed during aging. Zhang et al. [Zha05] determined that if precipitation takes place, precipitates of $Mg_{17}Al_{12}$ will form new strong pinning points. This corresponds to a decrease in the mean distance L causing a decrease in the strain-dependent damping δ_h. In the case of aging at 350 and 400 ºC the measurements show a "hump" at larger strain amplitudes, which may be related to a measurement error.

The results shown in Fig. 4.13, which compare measurements of the strain-independent damping δ_0 using two different starting maximum strain amplitudes, demonstrate that the increased dislocation density due to this plastic strain leads to a measurable increase in the δ_0 values. The measurements performed with a starting amplitude of $1 \cdot 10^{-3}$ give δ_0 values which are consistently ~ $0.2 \cdot 10^{-3}$ higher, regardless of the aging treatment used.

However, after aging treatments in the temperature range 250-400 ºC the measurements show a "hump" at larger strain amplitudes, which may be related to a measurement error.

The strain-independent damping of AZ61 after short 1 h heat treatments between 150 °C and around 250 °C was observed to increase. This can be explained by the impoverishment of foreign atoms (Al and Zn) in the matrix as a consequence of precipitate formation. The mean distance l between weak pinning points becomes larger and dislocation segments can bow out more easily. In addition, the thermoelastic damping contribution increases as a result of the change in thermal conductivity. At temperatures > 250 ºC, the solubility of Al in the matrix increases to > 4 wt. % and the driving force for precipitation is reduced. Diffusion of aluminium atoms from the enriched, interdendritic regions to the dendrite cores takes place and the Al content of the matrix increases. This results in a decrease in δ_0. This trend continues as the aging temperature is increased until finally after aging at 400 ºC complete dissolution of the β-phase occurs.

The direct aging experiments performed on the as-cast AZ81 alloy indicate that the changes in both δ_0 and hardness resulting from isothermal aging in the temperature range 200-300 ºC are generally smaller than those obtained during the aging of the homogenised AZ81 alloy. This is a consequence of the fact that the as-cast alloy is highly segregated and already contains β-phase precipitates in the interdendritic regions. The aging response is therefore reduced due to the lower aluminium supersaturation in this temperature range. However, at an aging temperature of 150 ºC the supersaturation is clearly high enough to generate continuous precipitates of the β-phase. At this aging temperature it was observed that both δ_0 and the hardness do not reach saturation after 2000 h and continue to increase.

The aging response of the extruded alloys compared to the homogenised materials is generally rather similar. In the more supersaturated alloys AZ61 and AZ81, the fine grain size of the extruded materials appears to accelerate the nucleation of the colonies of discontinuous precipitation during aging in the temperature range 200-300 °C in agreement with the findings of Duly et al. [Dul95]. The fine grain size and the presence of globular particles of the β-phase at grain boundaries induced overaging in the extruded materials after extended aging times, an effect not seen in the more coarse-grained, homogenised alloys. After aging at a temperature of 150 °C, the age hardening response suggests that continuous precipitation of the β-phase takes place with the extruded materials showing faster precipitation kinetics, probably as a result of heterogeneous nucleation of the β-phase at dislocations.

During the direct aging of extruded materials further examples in which dislocation density effects are thought to influence the strain-independent damping were found. As shown in Fig. 4.29, a slight decrease in δ_0 is observed during the initial stages of aging of the AZ61 alloy, which is probably related to a decrease in dislocation density as a result of recovery and recrystallisation processes. Similar effects were observed during aging of the extruded AZ31 alloy as shown in Fig. 4.31. Aging the extruded AZ31 alloy at temperatures in the range 200-300 ºC produced no changes in hardness due to precipitation, but decreases in δ_0 of the order of $0.4 \cdot 10^{-3}$ due to a decrease in dislocation density. These observations are thus consistent with the proportionality between δ_0 and ρ according to Granato & Lücke.

6 Conclusions

In this work, the ambient temperature damping behaviour of unalloyed magnesium, a series of Mg-Al-Zn alloys and a number of Mg-Zn binary alloys has been measured as a function of strain amplitude. Particular attention was given to the commercial AZ alloys with a view to characterising the effects of alloy composition and microstructure on the damping behaviour and to investigate the effects of various aging treatments of commercial interest. The aging treatments used in this work were chosen in order to cover possible aging treatments (T5, T6) performed prior to service applications. In practice, direct aging treatments (T5) can be recommendable to replace the heat treatment (T6) in order to save the costs associated with a solution treatment step. The changes in damping behaviour, hardness and microstructure of as-cast, solution treated, and extruded AZ alloys were investigated after aging for times up to 2000 h at temperatures in the range 150-300 ºC. In the case of the solution treated materials the property changes resulting from aging were used to establish the kinetics of the precipitation process.

The main conclusions of this work can be summarised as follows:

In the as-cast condition, the alloys AZ21, AZ31, AZ61 and AZ81 showed interdendritic segregation of intermetallic phase which leads to increased amounts of eutectic with increasing aluminium content and a corresponding decrease in the aluminium content of the dendrite cores. The as-cast AZ alloys therefore have greater overall damping capacities in both the strain amplitude-independent and strain amplitude-dependent regimes than the corresponding alloys in the homogenised and/or extruded states.

The changes in strain-independent damping and hardness of the AZ61 alloy following isochronal aging treatments in the temperature range 50-400 ºC are correlated and SEM investigations indicated that these changes are associated with the precipitation and dissolution of the β-phase ($Mg_{17}Al_{12}$). Aging in the temperature range 150-300 ºC leads to increases in the strain-independent damping δ_0 and hardness as a result of precipitation of $Mg_{17}Al_{12}$. In contrast, the strain-dependent damping δ_h is generally decreased by aging treatments, in particular after aging for 1

hour in the intermediate temperature range, 250-300 ºC, in which the precipitation process is most advanced.

Isothermal aging of as-cast AZ81 in the temperature range 150-300 ºC produces precipitation of the β-$Mg_{17}Al_{12}$ phase. The formation of the β-phase leads to age hardening and a continuous decrease in the Al content in the solid solution as a function of aging time. Removal of Al and Zn solute atoms from solid solution as a result of precipitation of the β-phase during aging produces an increase in the strain-independent damping. Precipitation of the β-phase occurs in the regions supersaturated in solute mainly in the form of discontinuous precipitates. At 150 ºC continuous precipitation of the β-phase takes place and the reaction is not completed after 2000 h so that the δ_0 and hardness do not reach saturation values.

Homogenisation of AZ magnesium alloys diminishes the strain-independent damping capacity as a result of the increased solute concentration in the matrix which decreases the distance between weak pinning points and reduces the thermoelastic damping contribution. Isothermal aging of the homogenised AZ alloys leads to increases in the strain-independent damping and hardness as a result of the formation of $Mg_{17}Al_{12}$ by discontinuous precipitation. The rate of change in the mechanical properties increases with increasing aging temperature and is greater for the higher solute containing alloys. The increases in δ_0 and hardness depend principally upon the volume fraction of precipitates formed that increases with decreasing temperature. Property changes in the AZ31 alloy are therefore relatively small because of its low aluminium content. Analysis of the kinetics of the discontinuous precipitation reaction indicates that the process is controlled by grain boundary diffusion.

Aging of the extruded AZ81 and AZ61 alloys in the temperature range 150-300 ºC produced precipitation hardening with typical colonies of discontinuous precipitates of the β-phase at grain boundaries and some continuous precipitates within the grains. The high dislocation density in the extruded alloys provides preferred nucleation sites for precipitation. Continuous precipitation appears to dominate at the lowest aging temperature of 150 ºC. Compared to the homogenised materials, precipitation is significantly accelerated as a result of the finer grain size and higher dislocation density, so that the time necessary to reach peak hardness peak is shortened. On

the other hand, the AZ61 magnesium alloy exhibits a slight decrease in the strain independent damping δ_0 in the first stage of aging, which can be associated with recovery of the material and a corresponding reduction in dislocation density. Such recovery effects also occur in the extruded AZ31 alloy, for which the strain-independent damping δ_0 decreased with aging time. After extended aging times the extruded AZ61 and AZ81 alloys undergo some degree of softening beyond peak hardness, an effect not seen in the case of aging after homogenisation. This softening is thought to be due to discontinuous precipitate coarsening which is induced by the fine grain sizes of the extruded alloys.

The overall effects of aging on the damping capacities of the AZ-series alloys regardless of their prior processing history can be summarised as follows:

Age hardening generally leads to an extension of the strain-amplitude independent damping regime to greater strain amplitudes (increase in ε_{cr}) as well as increases in the δ_0 values due to the removal of the solute atoms Al and Zn from the matrix. From an industrial point of view, these effects can be seen as positive. However, it should be born in mind that the increases in δ_0 measured in the present work are probably dominated by thermoelastic effects and are therefore frequency and thickness dependent. Within the regime of strain-amplitude dependent damping some evidence was found to suggest that precipitation hardening in the AZ61 alloy can cause rather dramatic decreases in δ_h. This is clearly an area where further research is required.

It is well known that the mechanical properties of AZ-series alloys, in particular the strength and ductility, may change with time when as-cast alloys are used as components at moderate service temperatures ~ 100 ºC as a result of the formation of the β-phase ($Mg_{17}Al_{12}$). The present work indicates that continuous precipitation of the β-phase would be the dominating precipitation process at temperatures below 150 °C and that this causes greater hardening than the discontinuous precipitation reaction taking place in the temperature range 200-300 ºC. Aging treatments such as performed in the present work could thus be used to reduce the aluminium supersaturation in the as-cast materials to levels that would provide more stable microstructures and properties during extended service lives at lower temperatures.

Bibliography

[Abe99] F. Abed EL-AL, Abhängigkeit der Dämpfung in Magnesium von dynamischen Vorbelastungen im elastischen Bereicht, (1999) p 18

[Akh72] Akhtar, A. and Teghtsoonian, E., Substitutional Solution Hardening of Magnesium Single Crystals, Phil. Mag., **25**, (1972), p. 897-916.

[Akh68] Akhtar, A. and Teghtsoonian, E., Solid Solution Hardening in Magnesium Alloys, Trans JIM, **9**, (1968), p. 692-697.

[Akh69] Akhtar, A. and Teghtsoonian, E., Solid Solution Strengthening of Magnesium Single Crystals-II The Effect of Solute on the Ease of Prismatic Slip, Acta Metall., **17**, (1969), p. 1351-1356.

[Ash99] M. F. Ashby, Materials Selection in Mechanical Design, 2, Auflage, Butterworth Heinemann. Oxford 1999 p. 48

[Ave99] M.M. Avedesian and H. Baker, ASM Speciality Handbook Magnesium and Magnesium Alloys, ASM (1999) p 37

[Avr39] M. Avrami, "Kinetics of Phase Change. I. General Theory" J. Chem. Phys. 7 (1939) 1103

[Avr40] M. Avrami, "Kinetics of Phase Change. II. Transformation-Time Relations for Random Distribution of Nuclei" J. Chem. Phys. 8 (1940) 212

[Bai00] Seung-Han Baik, High damping Fe–Mn martensitic alloys for engineering applications, Nucl. Eng. Des. **198** (2000) 241

[Bal07] N. Balasubramani, A. Srinivasan, U.T.S. Pillai, B.C. Pai, Effect of Pb and Sb additions on the precipitation kinetics of AZ91 magnesium alloy, Mater. Sci. Eng. A **457** (2007) 275

[Bec40] Beck, A., ed. The Technology of Magnesium and its Alloys. (London: F.A. Huges and Co. 1940)

[Bec39] A. Beck, Magnesium und seine Legierungen, Springer Verlag, Berlin (1939)

[Bet03] C.J. Bettles, The effect of gold additions on the ageing behaviour and creep properties of the magnesium alloy AZ91E, Mater. Sci. Eng. A **348** (2003) 280

[Boh04] J. Bohlen, F. Chmelík, P. Dobroň, D. Letzig, P. Lukáč, K. U. Kainer, Acoustic emission during tensile testing of magnesium AZ alloys, J. Alloys Compd. **378** (2004) 214

[Bow02] A.L. Bowles, The Effect of Moderate Temperature Ageing in High Pressure Die Cast Mg–Al Alloys, Ph.D. Thesis, School of Engineering, The University of Queensland, Brisbane, Australia, (2002)

[Böh68] H. Böhm, Einführung in die Metallkunde. Bibliographisches Institut AG, Mannheim (1968) p 200

[Buc92] P. Buchhagen, W. Riehemann, B.L. Mordike, in: B.L. Mordike, F. Hehmann (Eds.), Magnesium Alloys and their Applications, DGM, Oberursel, (1992) 229

[Bur52] E. C. Burke, and W. R. Hibbard, Plastic Deformation of Magnesium Single Crystals, Trans. AIME., **194**, (1952), p. 295-303.

[Bus50] Busk, R. S., Lattice Parameters of Magnesium Alloys, Trans. AIME., **188**, (1950), p. 1460-1464.

[Các01] C. H. Cáceres, D. M. Rovera, Solid solution strengthening in concentrated Mg–Al alloys, J. Light Met, Volume 1, Issue 3, August 2001, Pages 151-156

[Các02] C.H. Cáceres, A. Blake, The Strength of Concentrated Mg-Zn Solid Solutions, Phys. Status Solidi A, Volume 194 Issue 1,(2002)147

[Cai00] Y. Cai, M.J. Tan and W. Zhou, Effect of Long-Time aging on the microstructures and mechanical properties of AZ91 magnesium die castings: in Proceedings of the 8th Symposium on Processing and Fabrication of Advanced Materials 199, Singapore: (2000) 811

[Cai06] J. Cai, G.C. Ma, Z. Liu, H.F. Zhang, Z.Q. Hu, Influence of rapid solidification on the microstructure of AZ91 HP alloy, J. Alloys Compd. **422** (2006) 92

[Cel97] S. Celotto, T.J. Bastow, P. Humble, C. J. Bettles; Proc. 3rd Int Magnesium Conf., (ed. G.W. Lorimer, Institute of Materials, London), (1997) 391-402

[Cel00] S. Celotto, TEM Study of continuous precipitation in Mg-9Wt%Al-1Wt%Zn alloy, Acta Mater. **48** (2000) 1775

[Cel00a] S. Celotto, T. J. Bastow, P. Humble and C. J. Bettles, A study of the Kinetics of Precipitation in Binary Mg-Al Alloys and AZ91E using Nuclear Magnetic Resonance, In: G.W. Lorimer, Editor, Third International Magnesium Conference, The Institute of Materials, London (1997), pp. 391– 402.

[Cel01] S. Celotto and T. J. Bastow, Study of precipitation in aged binary Mg-Al and ternary Mg-Al-Zn alloys using ^{27}Al NMR spectroscopy, Acta Mater. **49** (2001) 41

[Cer02] E. Cerri and S. Barbagallo, The influence of high temperature exposure on aging kinetics of a die cast magnesium alloy Mater. Lett. **56** (2002) 716

[Cer05] E. Cerri, Paola Leo, Influence of severe plastic deformation on aging of Al-Mg-Si alloys, Mater. Sci. Eng. A **410-411** (2005) 226

[Cla68] J.B. Clark, Age hardening in a Mg-9Wt, %Al alloy, Acta Metall. **16** (1968) 141

[Cra74] A.F. Crawley and K.S. Milliken, Precipitate Morphology and orientation relationships in an aged Mg-9% Al-1% Zn-0.3%Mn alloy, Acta Metall. **22** (1974) 557

[Lag74] A. F. Crawley and B. Lagowski, *Effect of Two-Step Aging on the Precipitate Structure in Magnesium Alloy*. *AZ91*, Metall. Trans., 5 (1974), 949

[Din07] W. Ding, Li Jin, Dongliang Lin, Xiaoqin Zeng, Dali Mao, Effect of Second Phase on the Mechanical Properties of Mg-Al-Zn Alloy by Equal Channel Angular Extrusion, Mat. Sci. Forum **546-549** (2007) 249

[Dul94a] D. Duly and Y. Brechet, Nucleation mechanism of discontinuous precipitation in Mg-Al alloys and relation with the morphology, Acta Metall. Mater. **42** (1994) 3035

[Dul94b] D. Duly, M.C. Cheynet and Y. Brechet, Morphology and Chemical Nanoanalysis of Discontinuous Precipitation in Mg-Al Alloys-I Regular Growth, Acta Metall. Mater. **42** (1994) 3843

[Dul95] D. Duly, J.P. Simon, Y. Brechet, On the competition between continuous and discontinuous precipitations in binary Mg---Al alloys Acta Metall. Mater. **43** (1995) 101

[Dut02] J. Dutkiewicz, L. Litynska, The effect of plastic deformation on structure and properties of chose 6000 series aluminium alloys, Mater. Sci. Eng. A **324** (2002) 239

[El08] Amjad Saleh El-Amoush, Effect of aluminum content on mechanical properties of hydrogenated Mg–Al magnesium alloys, J. Alloys Compd. 4693 (2008) 475

[Eml66] E. F. Emley, Principles of Magnesium Technology, Pergamon Press Oxford (1966) p 218

[Fer02] R. Ferragut, A. Somoza, I. Torriani, Pre-precipitation study in the 7012 Al–Zn–Mg–Cu alloy by electrical resistivity, Mater. Sci. Eng A **1** (2002) 1

[Fle64] R. Fleischer, Strengthening of Metals: (Reinhold Publishing. 1964).

[Gao03] N. Gao, E. Huttunen-Saarivirta, T. Tiainen, M. Hemmilä, Influence of prior deformation on the age hardening of a phosphoruscontaining Cu-0.61wt.%Cr alloy, Mater. Sci. Eng. A **342** (2003) 270

[Gjö70] J. Gjönnes, T. Ostmoe, Precipitation and Pre-Precipitation in an Mg(Al)-Alloys, Z. Metallkde. 61 (1970) 604

[Gök02a] J. Göken, W. Riehemann, Dependence of internal friction of fibre-reinforced and unreinforced AZ91 on heat treatment, Mater. Sci. Eng. A **324** (2002) 127

[Gök02b] J. Göken, W. Riehemann, Thermoelastic damping of the low density metals AZ91 and DISPAL, Mater. Sci. Eng. A **324** (2002) 134

[Gök04a] J. Göken, W. Riehemann, Damping behaviour of AZ91 magnesium alloy with cracks, Mater. Sci. Eng. A **370** (2004) 417

[Gök04b] J. Göken, D. Letzig, K.U. Kainer, Measurement of crack induced damping of cast magnesium alloy AZ91, J. Alloys Compd. **378** (2004) 220

[Gök05] J. Göken, J. Swiostek, D. Letzig, K. U. Kainer, Damping Measurements of the Magnesium Wrought Alloys AZ31, AZ61 and AZ80 After Indirect and Hydrostatic Extrusion, Mat. Sci. Forum **482** (2005) 387

[Gon07] R. González-Martínez, J. Göken, D. Letzig, K. Steinhoff, K.U. Kainer, Influence of aging on damping of the magnesium-aluminium-zinc series, J. Alloys Compd. **437** (2007) 127

[Gra56] A. Granato, K. Lücke, Application of Dislocation Theory to Internal Friction Phenomena at High Frequencies, J. Appl. Phys. **27** (1956) 789

[Gra92] E.J. Graesser and Catherine R. Wong, The Relationship of Traditional Damping Measures for Materials with High Damping Capacity, in M3D: Mechanics and Mechanisms of Material Damping, ASTM STP 1169, eds. V.K. Kinra and A. Wolfenden, American Society for Testing and Materials, Philadelphia, (1992) p 316

[Hau55] Hauser, F. E., et al., Deformation Mechanisms in Polycrystalline Aggregates of Magnesium, Trans. ASM, **47**, (1955), p. 102-134.

[Hau56a] F. E. Hauser, Deformation and Fracture Mechanisms of Polycrystalline Magnesium at Low Temperatures, Trans ASM, **48**, (1956), p. 986-1002.

[Hau56b] F. E. Hauser, F. E, Fracture of Magnesium Alloys at Low Temperatures, Trans. AIME., **206**, (1956), p. 589-593.

[He07] S.M. He, X.Q. Zeng, L.M. Peng, X. Gao, J.F. Nie, W.J. Ding, Microstructure and strengthening mechanism of high strength Mg–10Gd–2Y–0.5Zr alloy, J. Alloys Compd. **427** (2007) 316

[Hil98] T. Hilditch, J.F. Nie, B.C. Muddle, The Effect of Cold Work on Precipitation in Alloy WE54, in B.L. Mordike, Kainer, K.U. (Eds.) Magnesium Alloys and their Applications, Hamburg, Germany, Werkstoff-informationsgesellshaft. Frankfurt, (1998) p 339

[Hil57] Reed-Hill, R. E. and Robertson, W. D., Deformation of Magnesium Single Crystals by Non-basal Slip, Trans. AIME., **209**, (1957), p. 496-502.

[Hut05] C.R. Hutchinson, J.F. Nie and S. Gorsse, “Modelling of the Precipitation Processes and Strengthening Mechanisms in Mg-Al(-Zn) Automotive Alloys”, Metall. Mater. Trans. A, Vol. 36A, (200) 2093

[Jam68] D. W. James, High Damping Metals for Engineering Applications, Mater. Sci. Eng **4** (1968) 1

[Kam00] C. Kammer, “Magnesium Taschenbuch”, Aluminium Verlag Marketing & Kommunikation, Düsseldorf 2000

[Kel68] E. W. Kelley, and W. J. Hosford, Plane-Strain Compression of Magnesium and Magnesium Alloy Crystals, Trans. AIME, **242**, (1968), p. 5-13.

[Kie97] J. Kiehn, K. U. Kainer, P. Vostrý, and I. Stulíková, Resistivity Changes Due To Precipitation Effects in Fibre Reinforced Mg-Al-Zn-Mn Alloy, Phys. Stat. Sol. **161** (1997) 85

[Koc67] F. U. Kocks, and D. G. Westlake, The Importance of Twinning for the Ductility of CPH Polycrystals, Trans. AIME., **239**, (1967), p. 1107-1109.

[Koe52] J.S. Koehler, The influence of dislocations and impurities on the damping and the elastic constants of metal single crystals, in: W. Shockley, J.H. Hollomon, R. Maurer, F. Seitz (eds.), Imperfections in nearly perfect crystals, John Wiley & Sons, Inc., New York (1952), chapter 7, pp. 197-212

[Laz68] B. J. Lazan, Damping Of Materials And Members In Structural Mechanics,Pergamon Press, Oxford 1968

[Lab70] R. A. Labusch, Statistical Theory of Solid Solution Hardening, Phys. Stat. Sol. (a), **41**, (1970), p. 659-668.

[Lai08] W. J. Lai, Yi-Yun Li, Yung-Fu Hsu, Shan Trong, Wen-Hsiung Wang, Aging behaviour and precipitate morphologies in Mg–7.7Al–0.5Zn–0.3Mn (wt.%) alloy, J. Alloys and Compd. In Press (2008)

[Lam01] O.A. Lambri, W. Riehemann, and Z. Trojanová, Mechanical spectroscopy of commercial AZ91 magnesium alloy, Scripta Mater. **45** (2001) 1365

[Lam04] O.A. Lambri, W. Riehemann, L.M. Salvatierra, J.A. García, Effects of precipitation processes on damping and elastic modulus of WE43 magnesium alloy, Mater. Sci. Eng. A **373** (2004) 146

[Lam05] O.A. Lambri, W. Riehemann, Damping due to incoherent precipitates in commercial QE22 magnesium alloy, Scripta Mater. **52** (2005) 93

[Lev59] Levine, E. D., et al., Solid-Solution Strengthening of Magnesium Single Crystals at Room Temperature, Trans. AIME., **215**, (1959), p. 521-526.

[Lia05] L. Liao, Xiuqing Zhang, Haowei Wang, Precipitation behaviour and damping characteristic of Mg-Al-Si alloy, Mater. Lett. **59** (2005) 2702

[Lih07] L. Lihua, Zhang Xiuqin, Li Xianfeng, Wang Haowei and Ma Naiheng, Effect of silicon on damping capacities of pure magnesium and magnesium alloys, Mater. Lett. **61** (2007) 231

[Liu07] C. Liu, Z. Liu, X. Zhu, B. Hu, R. Wang, M. Wang; J Cent South Univ Technol, 14, (2007) 315

[Luk92] Lukac, P., Solid Solution Hardening in Mg-Cd Single Crystals, Phys. Stat. Sol. (a), **131**, (1992), p. 377-390.

[Lun07] S. Lun Sin, D. Dubé, R. Tremblay, Characterization of Al–Mn particles in AZ91D investment castings, Mater. Charact. **58** (2007) 989

[Mar06] M. Marya, L. G. Hector, R. Verma, W. Tong, Microstructural effects of AZ31 magnesium alloy on its tensile deformation and failure behaviors, Mater. Sci. Eng. A **418** (2006) 341

[Mar68] J. W. Martin “Precipitation Hardening” Pergamon Press, Oxford 19

[Mey99] M. A, Meyers, eds. Mechanics and Materials : Fundamentals and Linkages. (New York: John Wiley and Sons. 1999), p. 532.

[Mie06] A. Mielczarek, Z. Trojanová, W. Riehemann and P. Lukáč. Influence of mechanical cycling on damping behaviour of short fibre-reinforced magnesium alloy QE22, Mater. Sci. Eng. A **442** (2006) 484

[Mor01] B.L. Mordike, T. Ebert, Magnesium Properties-applications-potential Mat. Sci. Eng. A **302** (2001) 37

[Mor76] S. Morozumi, Electron Microscope Observation in and around {1-102} Twins in Magnesium, Trans. JIM, **17**, (1976), p. 158-164.

[Mue06] S. Mueller, K. Mueller, T. Huichang, P. Wolter, W. Reimers, Extrusion of Different AZ Magnesium Alloys, Magnesium, Proceedings of the 7th International Conference Magnesium and Their Aplications, (2006) p.406

[Nas85] A.D. Nashif, D.I.G. Jones, J.P. Henderson, Vibration Damping, John Wiley & Sons Inc., New York (1985)

[Nie01] J.F. Nie, X.L. Xiao, C.P. Luo, B.C. Muddle, Characterisation of precipitate phases in magnesium alloys using electron microdiffraction, Micron **32** (2001) 857

[Nie02] J.F. Nie, Precipitation and Strengthening in selected magnesium alloys, TMS (2002)103

[Nie03] J. F. Nie. Preface to viewpoint set on: phase transformations and deformation in magnesium alloys Scripta Mater. **48** (2003) 981

[Now72] A.S. Nowick and B.S. Berry, Anelastic Relaxation in Crystalline Solids, Academic Press, New York, (1972) p 500

[Oba73] T. Obara, H. Yoshinga, and S. Morozumi, $\{1122\}\langle\bar{1}\bar{1}23\rangle$ Slip System in Magnesium, Acta Metall., **21**, (1973), 845

[Ota94] T. Otani, K. Hoshino and T. Kurosawa, Damping capacity of Zn-Al alloys sheets, J. Alloys Compd. **211/212** (1994) 514

[Par67] P. G. Partridge, The Crystallography and Deformation Modes of Hexagonal Close-Packed Metals, Metall Rev, **Review 118**, (1967), p. 169-194.

[Pol95] I. J. Polmear, Light Alloys, 3rd Edition London, U.K. Arnold, (1995)

[Por92] D. A. Porter and K.E. Easterling, Phase Transformations in Metals and Alloys, Chapman & Hall (1992) p. 263

[Por77] D.A. Porter, J.W. Edington; Proc. R. Soc. London A358, (1977)335

[Qud06] W. Qudong, P. Jianguo, S. Michel, and J. J. Blandin, Effects of aging on the microstructures and mechanical properties of extruded AM50 + xCa magnesium alloys Rare Metals, 26 (2006) 377

[Rie94] W. Riehemann, Metallische Werkstoffe mit extremer innerer Reibung und deren Messung. Papierflieger-Verlag, Clausthal-Zellerfeld (1994) p 237

[Rie98] W. Riehemann, Internal Friction in Magnesium Materials, In B. L. Mordike and K. U Kainer (Eds) Magnesium Alloys and Their Applications, Frankfurt: Werkstoff-Informationsgesellschaft. (1998) 61.

[Rie00] W. Riehemann, F. Abed El-Al, Influence of ageing on the internal friction of magnesium, J. Alloys Compd. **310** (2000) 127

[Rie10] W. Riehemann, Z. Trojanová, A. Mielczarek, Fatigue in magnesium alloy AZ91-γAlumina fiber composite studied by internal friction measurements, Procedia Engineering **2** (2010) 2151

[Sak93] D. J. Sakkinen, Mike Evans, The Effect of Aging on Magnesium Die Casting Alloys (paper T93-112). in 17th international Die Casting Congress and Exposition, (Cleveland, USA: North American Die Casting Association) (1993) 305

[Sche56] Schewmon PG. Trans Am Inst Min (Metall) Eng 1956;206:918

[Skl01] V. Sklenička, M. Svoboda, M. Pahutová, K. Kuchařová, T. G. Langdon, Microstructural processes in creep of an AZ91 magnesium-based composite and its matrix alloy, Mater. Sci. Eng. A **319-321** (2001) 741

[Son06] J.M. Song, T.S. Lui, H.W. Chang, L.H. Chen, The influence of Al content and annealing on vibration fracture properties of wrought Mg–Al–Zn alloys, Scripta Mater. **54** (2006) 399

[Sri07] A. Srinivasan, U.T.S. Pillai, B.C. Pai, Effect of Pb addition on ageing behavior of AZ91 magnesium alloy, Mater. Sci. and Eng. A **452-453** (2007) 87

[Sto72] J. F. Stohr, and J. P. Poirier, Electron Microscope Study of Pyramidal Slip {11-22}<11-23> in Magnesium, Phil. Mag., **25**, (1972), p. 1313-1329.

[Sug75] K. Sugimoto, K. Matsui, T. Okamoto and K. Kishitake, Effect of Crystal Orientation on Amplitude-Dependent Damping in Magnesium, Trans JIM 16 (1975) 647

[Sug77] K. Sugimoto, Kazunori Niiya, Taira Okamoto and Katsuhiko Kishitake, A Study of Damping Capacity in Magnesium Alloys, Trans. JIM **18** (1977), 277

[Svo02] M. Svoboda, M. Pahutová, K. Kuchařová, V. Sklenička, T.G. Langdon, The role of matrix microstructure in the creep behaviour of discontinuous fiber-reinforced AZ91 magnesium alloy, Mater. Sci. and Eng. A **324** (2002) 151

[Ton02] Tonda, H. and Ando, S., Effect of Temperature and Shear Direction on Yield Stress by {1122}<1123> Slip in hcp Metals, Metall. Trans. A, **33A**, (2002), p. 831-836.

[Tro04] Z. Trojanová, Pavel Lukáč, Hans Ferkel, Werner Riehemann, Internal friction in microcrystalline and nanocrystalline Mg. Mater. Sci. Eng. A **370** (2004) 154

[Tro08] Z. Trojanová, Z. Száraz, A. Mielczarek, P. Lukáč W. Riehemann, Plastic and fatigue behaviour of ultrafine-grained magnesium, Mater. Sci. Eng. A 483–484 (2008) 477

[Ven00] K. Venkatesan, C.J. Bettles, Ageing Behaviour and Microstructure of a Mg-9Al-3Zn Alloy, in: Magnesium Alloys and their Applications, eds. Prof. Dr.-Ing. K. U. Kainer (2000) p149

[Wan08] D. Wan, J. Wang, L. Lin, Z. Feng, G. Yang, Damping properties of Mg-Ca binary alloys, Physical B **403** (2008) 2438

[Wan09] D. Wan, J. Wang, G. Wang, L. Lin, Z. Feng; Acta Metall Sin Engl Letter, **22**, (2009) 1

[Wat04] H. Watanabe, T. Mukai, M. Sugioka, K. Ishikawa, Elastic and damping properties from room temperature to 673 K in AZ31 magnesium alloy, Scripta Mater. **51** (2004) 291

[Won67] B. C. Wonsiewicz, B. C. and Backofen, W. A., Plasticity of Magnesium Crystals, Trans. AIME., **239**, (1967), p. 1422-1431.

[Woo55] R. L. Woolley, Twining and Untwining in Polycrystalline Magnesium, J. Inst. Metals, **83**, (1954-1955), p. 57-58.

[Xie98] C.Y. Xie, R. Schaller, C. Jaquerod, High damping capacity after precipitation in some commercial aluminum alloys, Mater. Sci. Eng. A **252** (1998) 78

[Xiu06] Z. Xiuqing, Liao Lihua, Ma Naiheng, Wang Haowei, Effect of aging hardening on in situ synthesis magnesium matrix composites, Mater. Chem. Phys. **96** (2006) 9

[Yan07] Z. Yang, J.P. Li, Y.C. Guo, T. Liu, F. Xia, Z.W. Zeng, M.X. Liang, Precipitation process and effect on mechanical properties of Mg–9Gd–3Y–0.6Zn–0.5Zr alloy, Mater. Sci. Eng (2007) 274

[Yoo81] H. M. Yoo, Slip, Twining, and Fracture in Hexagonal Close-Packed Metals, Metall. Trans A, **12A**, (1981), p. 409-418.

[Zen38] C. Zener, Internal Fricton in Solids, Phys. Rev.**53** (1938) 90

[Zha94] J. Zhang, Robert J. Perez, Catherine R. Wong, Enrique J. Lavernia, Effects of secondary phases on the damping behaviour of metals, alloys and metal matrix composites. Mater. Sci. Eng. R **13** (1994) 325

[Zha03] M. X. Zhang, P.M. Kelly, Crystallography of $Mg_{17}Al_{12}$ precipitates in AZ91D alloy, Scripta Mater. **48** (2003) 647

[Zha05] Z. Zhang, Xiaoqin Zeng, Wenjiang Ding, The influence of heat treatment on damping response of AZ91D magnesium alloy, Mater. Sci. Eng. A **392** (2005) 150

[Zhe07] K. Y. Zheng, J. Dong, X.Q. Zheng, W. J. Ding, Effect of thermo-mechanical treatment on the microstructure and mechanical properties of a Mg-6Gd-2Nd-0.5Zr alloy, Mater. Sci. Eng. A **454-455** (2007) 314

[Zhe09] O. Zheng, J.P. Zhou, D.S. Zhao, J.B. Wang, R.H. Wang, J.N. Gui, D.X. Xiong, Z.F. Sun, The crystallography of continuous precipitates with a newly observed orientation relationship in an Mg–Al-based alloy, Scripta Mater. (2009)